

FUNCTIONAL CHARACTERIZATION OF
THE RIBOSOME-ASSOCIATED ZUO1/SSZ1 CHAPERONE COMPLEX

by

Kanghyun Lee

A dissertation submitted in partial fulfillment of
the requirements for the degree of

Doctor of Philosophy

(Biochemistry)

at the

UNIVERSITY OF WISCONSIN-MADISON

2018

Date of final oral examination: 11/5/2018

The dissertation is approved by the following members of the Final Oral Committee:

Elizabeth A. Craig, Professor, Biochemistry

Michael M. Cox, Professor, Biochemistry

Catherine A. Fox, Professor, Biomolecular Chemistry

Ivan Rayment, Professor, Biochemistry

David A. Wassarman, Professor, Genetics

ABSTRACT

Ribosome-associated molecular chaperones interact with nascent polypeptide chains, assisting their proper folding as they exit ribosomes. In *Saccharomyces cerevisiae*, the J-protein co-chaperone Zuo1 promotes interaction between partner Hsp70 Ssb and nascent polypeptides. Interaction of Zuo1 with the ribosome is key, but how it associates remains ill-defined. Zuo1 forms a complex with an atypical Hsp70, Ssz1, whose function is unknown. In this thesis, I report results which better define the interaction between Zuo1 and the ribosome, providing insight into the function of Zuo1. In addition, I report results which indicate direct interaction between Ssz1 and Ssb, suggesting that Ssz1 is a scaffold for Ssb on the ribosome.

In Chapter Two, I describe how Zuo1 interacts with the 60S and 40S ribosomal subunits. Based on results of site-specific crosslinking, ribosomal RNA mutagenesis experiments, and computer driven docking using available structural information, I propose a model of Zuo1's interaction with the ribosome: (1) Zuo1 Homology Domain of Zuo1 interacts with ribosomal protein eL31 and RNA H24 near the ribosomal tunnel exit; (2) the C-terminus of Zuo1 interacts with the ribosomal RNA H44, which originates at the decoding center. My results provide insight into how the dual interaction of Zuo1 with both ribosomal subunits acts to coordinate protein folding and mRNA decoding.

In Chapter Three, results of experiments conducted to elucidate the function of Ssz1 are described. Crosslinking results indicated that Ssz1 interacts with Ssb. To understand the mode of interaction, unbiased computational docking was conducted. These docking results suggested that Ssz1 and Ssb interact via their ATPase domains. I verified this mode of interaction by *in vitro* crosslinking and mass spectrometry analysis. Residues forming salt bridges mediate the

interaction in the docking model. Reverse charge substitutions of these residues in Ssb or Ssz1 destabilized the interaction *in vitro* and impaired cell growth. The presence of both variants complemented the growth defects caused by a single variant, suggesting that interaction between Ssz1 and Ssb is important *in vivo*. I hypothesize that Ssz1 positions Ssb on the ribosome, facilitating its interaction with nascent polypeptide.

ACKNOWLEDGMENTS

I would like to extend my profound gratitude to my advisor Prof. Elizabeth Craig. I remember the day that I visited her office at the first time. Probably we have talked about some potential projects that I could work on. Sometime when I looked back the day, I still wondered what made Betty decided to have me in her lab as a graduate student who barely spoke English at that time. As it was before, she has been always very patient throughout my graduate studies so that I could find better ways for not only my research but also life. Also, seeing her as one of the giants inspired me to become an independent scientist. I am very thankful for that I could learn science from her. I also would like to thank my committee members: Prof. Michael Cox, Prof. Catherine Fox, Prof. Ivan Rayment and Prof. David Wassarman for helpful suggestions and encouragement throughout my graduate research.

I also thank all of the members of the Craig lab. I extend an extra special thank you to my class and lab mate See-Yeun Ting. It was very joyful and helpful to be in the lab with him. I am very thankful to my bench mate Tom Ziegelhoffer who has been my unofficial English teacher. I bugged him to talk with me everyday, and to help me with my manuscripts. I thank Brenda Schilke – the master of experiments – who was indispensable for troubleshooting of my experimental hurdles. I also want to thank Szymon Ciesielski for our many stimulating discussions. In addition, I want to thank past lab members. Hyun Young Yu helped me to settle down not only in the lab but also in Madison. I am also thankful to Ji-Yoon Song, Peter Kuhn, Om Shrestha, Ruchika Sharma, Rajesh Kumar Kar and Tommer Ravid. It was very enjoyable to work with each of these unique and talented individuals.

I also want to thank Korean scientists, postdocs, and graduate students in the Biochemistry department. It was joyful and encouraging to have them in the same building.

Moreover, I want to thank members of Korean Scientist Association of Biology. It was pleasing to have them to talk about science and life of scientist. I would like to also thank my graduate school friends with whom I have good memories. I thank Adam Bayless who approached me without any prejudice. I also thank John Crooks. Maybe, he is the only one who treats me as a friend but not a stranger. I would like to thank my friends in Korea. They are still my good friends although they live far away.

Finally, I want to thank my family. Without my parent's support, I would never have made to this point. I am deeply grateful for their endless and unwavering support. I also want to thank my parents-in-law and sister-in-law. They helped and encouraged me to come this far. I would like to mention my older brother. I am very thankful to him for being my supporter and a good friend. I am very thankful to my wife Yeojin who has gone through all the hardship with me. I am profoundly grateful for her endless support, pure love, and unconditional belief in me. Lastly, I want to thank our son Hyun. He is the singular source of pure joy in my life.

TABLE OF CONTENT

ABSTRACT	i
ACKNOWLEDGMENTS	iii
TABLE OF CONTENT	v
CHAPTER ONE: Introduction	1
1. PROTEIN FOLDING IN TEST TUBES AND CELLS	2
1.1. <i>in vitro</i> folding of polypeptides.....	2
1.2. Folding of nascent polypeptides in cells	2
2. GENERAL ASPECTS OF MOLECULAR CHAPERONES.....	3
2.1. Identification of molecular chaperones.....	3
2.2. Types and functions of molecular chaperones.....	4
2.3. Characteristics of Hsp70	5
2.4. Characteristics of J-proteins.....	8
2.5. Characteristics of atypical Hsp70s.....	10
3. RIBOSOME-ASSOCIATED MOLECULAR CHAPERONE.....	11
3.1. Features of the ribosome.....	11
3.2. Ribosome-associated molecular chaperones in prokaryotes.....	13
3.3. Ribosome-associated molecular chaperones in eukaryotes	14
4. THESIS PLAN.....	20
5. FIGURES AND TABLES	23
CHAPTER TWO: Dual interaction of the Hsp70 J protein co-chaperone Zuotin with the 40S and 60S subunits of the ribosome	45

1. ABSTRACT.....	46
2. INTRODUCTION	46
3. METHODS	49
4. RESULTS	56
4.1. Structure of the ZHD of Zuo1	56
4.2. The ZHD-60S subunit interaction.....	57
4.3. The Zuo1-40S subunit interaction	60
4.4. Zuo1 spanning of the 40S and 60S subunits	63
5. DISCUSSION	64
6. ACKNOWLEDGMENTS	68
7. AUTHOR CONTRIBUTIONS.....	68
8. FIGURES AND TABLES	68
CHAPTER THREE: The interaction between a typical and an atypical Hsp70s by ATPase domain dimerization at the ribosome.....	92
1. ABSTRACT.....	93
2. INTRODUCTION	94
3. METHODS	97
4. RESULTS	104
4.1. Site-specific crosslinking between Ssz1 and Ssb1.....	104
4.2. The binding mode of Ssz1 to Ssb1	106
4.3. Direct interaction between Ssz1 and Ssb1	107
4.4. Cellular function of the interaction between Ssz1 and Ssb1.....	108
5. DISCUSSION	109

6. FIGURES AND TABLES	112
CHAPTER FOUR: Conclusion and future direction.....	153
1. CONCLUSION.....	154
2. FUTURE DIRECTION	156
2.1. Chapter Two: Dual interaction of the Hsp70 J-protein cochaperone Zuotin with the 40S and 60S ribosomal subunits	156
2.2. Chapter Three: The interaction between a typical and an atypical Hsp70s by ATPase domain dimerization at the ribosome.....	161
BIBLIOGRAPHY	168

CHAPTER ONE: Introduction

1. PROTEIN FOLDING IN TEST TUBES AND CELLS

1.1. *in vitro* folding of polypeptides

A linear polypeptide must fold into its native three-dimensional structure to function. The physical and chemical properties of amino acids forming a polypeptide drive folding in aqueous solution. Hydrophobic interactions are the major driving force. Hydrogen bonds, which are essential for forming secondary structures such as α -helices and β -sheets, and electrostatic interactions provide additional forces to fold a polypeptide into a three-dimensional structure.

Although many forces contribute to folding, all of these forces must comply with the intrinsic properties of the polypeptide. Despite the vast diversity of protein structures found in nature, there exist universal constraints. The linearity of the polypeptide and restrictions in peptide bond angles place fundamental physical limits on the final structure of proteins.

The results of *in vitro* ribonuclease refolding experiments led Christian Anfinsen to conclude that the sequence of a polypeptide dictates its native structure (Anfinsen, 1973). Consistent with his conclusion, the native structure of a protein often corresponds to the lowest energy state that the sequence can attain. However, it can be difficult for proteins, particularly large ones, to reach their lowest energy state. Large proteins populate multiple intermediate energy states which can hinder proper folding by increasing the chance of inappropriate intermolecular interactions that lead to misfolding and/or protein aggregation.

1.2. Folding of nascent polypeptides in cells

In addition to the intrinsically complex properties of polypeptides, proteins synthesized by the ribosomes within a cell encounter additional challenges. The interior of a cell is crowded with other macromolecules such as proteins and RNAs that can interact with nascent

polypeptides and cause misfolding. Protein synthesis by ribosomes also presents inherent folding problems. The ribosome synthesizes proteins from their N- to C-termini through the ribosome tunnel. The tunnel is narrow, about 80 Å long and 20 Å wide, sufficient to allow formation of alpha helices but no higher order structures (Voss et al., 2006; Wilson and Beckmann, 2011). This increases the chance of protein misfolding, as N-terminal hydrophobic regions are exposed to the cellular environment until the synthesis of each domain completes.

Chronic protein misfolding leads to disruption of protein homeostasis in cells and can cause various medical disorders such as neurodegenerative diseases (Knowles et al., 2014). Therefore, it is critical to protect proteins from misfolding and/or aggregation. To that end, cells contain families of proteins called molecular chaperones whose role is to maintain protein homeostasis. Within this group are specific proteins that assist in the folding of nascent polypeptides.

2. GENERAL ASPECTS OF MOLECULAR CHAPERONES

2.1. Identification of molecular chaperones

Molecular chaperones were first discovered as proteins whose expression levels increased upon heat shock stress (Tissieres et al., 1974). Heat and other types of stresses such as oxidants and toxins can partially unfold proteins, resulting in the exposure of hydrophobic amino acids that are normally buried within folded proteins (Lindquist, 1986; Morimoto, 1993). This can cause misfolding by trapping a protein in a non-native intermediate energy state that is prone to aggregation and ultimately harms the cell.

Chaperone proteins, whose expression is often induced by heat, protect other proteins from misfolding and prevent aggregate formation (Pelham, 1986). These proteins were named

heat shock proteins (HSP) to reflect this observation and were further classified on the basis of their molecular weight (Lindquist and Craig, 1988). However, molecular chaperones protect proteins not only under stress conditions but also function under normal growth conditions. Many examples of heat shock cognates, with strong homology to HSPs but constitutively expressed, have now been identified and are involved in numerous cellular processes.

2.2. Types and functions of molecular chaperones

HSPs are classified in six major families based on molecular weight: small heat shock proteins (sHSP), Hsp40, Hsp60, Hsp70, Hsp90, and Hsp100. Each class possesses a distinct range of functions and structural characteristics (Table 1-1). Small heat shock proteins oligomerize to stabilize proteins unfolded by stress, acting as a “buffer” that prevents aberrant interactions between unfolded proteins (Mogk et al., 2018). Hsp40s work with Hsp70s to facilitate *de novo* folding, translocation, refolding, or degradation of proteins. I describe Hsp40 and Hsp70 function below in detail as they are a primary focus of my graduate research. Hsp60s form double-ring complexes that function by enclosing unfolded substrates in a cavity that promotes folding (Kim et al., 2013). ATP hydrolysis by Hsp60 leads to a conformational change in the double-ring complex that induces a hydrophilic environment in the cavity that favors substrate folding (i.e. burying hydrophobic amino acids). Hsp90 dimerizes and undergoes an ATPase cycle. Hsp90 interacts with substrates, such as kinases and steroid receptors involved in signaling pathways, to promote folding (Hartl et al., 2011). Hsp100s form large cylindrical complexes that disassemble protein aggregates (Mogk et al., 2018; Saibil, 2013). Hsp100s are members of the AAA+ superfamily that use the energy of ATP hydrolysis to untangle aggregated polypeptides or to disassemble protein complexes.

2.3. Characteristics of Hsp70

2.3.1. Functions of Hsp70

As mentioned above, the main role of Hsp70 was believed to be in the protection of cells from protein misfolding or aggregation upon stress. We now appreciate that Hsp70s are far more versatile, involved in protein folding, translocation, remodeling, and degradation. For example, Hsp70 associates with the ribosome to assist folding of newly synthesized proteins (Craig et al., 2003). In addition, there are Hsp70s which assist translocation of proteins across membranes in different cellular compartments, such as the ER or mitochondrial lumen (Craig, 2018). Hsp70 also disassembles protein complexes, such as the clathrin lattice of clathrin-coated vesicles (Lemmon, 2001). Hsp70 also helps degrade misfolded proteins or aggregates to avoid potential deleterious effects (Howarth et al., 2007).

2.3.2. Structure of Hsp70

How Hsp70 performs such a diversity of tasks was an enigma until the structural and functional characteristics of Hsp70 were elucidated. The key biochemical features of Hsp70 are its ATPase activity and substrate binding ability. These are mediated by allosteric communication between two distinct domains: an ATPase domain and a substrate-binding domain (SBD) that are connected by a linker (Kampinga and Craig, 2010).

Obtaining the full-length structure of Hsp70 has been difficult because Hsp70 is an ATPase that undergoes a dramatic conformational change based on its nucleotide binding state. Also, the ATPase domain is connected to the SBD by the flexible linker, making it even harder

to obtain structural information. Despite these difficulties, the structures of the individual domains have been determined.

A structure of the ATPase domain of Hsp70 was determined by X-ray crystallography (Figure 1-1a) (Flaherty et al., 1990). The ATPase domain is similar to actin, consisting of two lobes that create an ATP-binding pocket at the base of a deep cleft. Each lobe (I, II) is further divided into two subdomains (a, b). The residues forming the ATP binding pocket are highly conserved, indicating the importance of ATP binding and hydrolysis for the function of Hsp70 (Bork et al., 1992). Adenosine binds to a hydrophobic pocket (Bukau and Horwich, 1998), while the phosphates of ATP are positioned by two loops at the base of the cleft with a Mg^{2+} bridge. The key residue involved in hydrolysis of ATP to ADP is a lysine (at position 71 in DnaK, the Hsp70 homolog in *Escherichia coli*) (Flaherty et al., 1994; O'Brien et al., 1996). This lysine hydrogen-bonds to a water molecule that attacks the gamma phosphate of ATP. In-line attack of the water molecule leads to dissociation of the gamma phosphate, resulting in ATP hydrolysis.

The structure of the SBD domain was also solved by X-ray crystallography (Figure 1-1b) (Zhu et al., 1996). The SBD is subdivided into an SBD α subunit, consisting of alpha-helical structures, and an SBD β subunit that has a beta-sheet sandwich structure. The alpha-helical structure is composed of 5 alpha helices from A to E. The alpha helices A and B span the SBD β subunit. The remaining alpha helices (C, D, and E) fold into a bundle with helix B. SBD β is composed of two beta-sheets containing 4 beta strands each. The loops that connect strands 1:2 and 3:4 together with the core of the beta-sheet structure create a hydrophobic cleft where polypeptide substrate binds. Alpha helix B also interacts with the loops via salt bridges and retains substrates in the cleft, thereby acting as a “lid” (Mayer et al., 2000).

There have been efforts to stabilize Hsp70 to obtain the full-length structure of intact protein. Cysteine residues were introduced into the ATPase and SBD domains to form a disulfide bond between them (Kityk et al., 2012). Later, the structure of an ATPase mutant of Hsp70 that locks Hsp70 in the ATP-bound state was determined (Qi et al., 2013). Both structures revealed that the ATPase domain interacts with SBD, allowing transient interaction of substrate with the cleft (Figure 1-1c).

A structure of the ADP-bound state is not available at present, most likely due to the intrinsic flexibility of the linker region. An NMR study found that the linker behaves like a dynamic random coil when Hsp70 is in the ADP-bound state (Figure 1-1d) (Bertelsen et al., 2009). Current model for the ADP-bound state is a composite based on the structures of the isolated domains in the ADP-bound conformation in addition to the unstructured linker. I will discuss the ATP- and ADP-bound states of Hsp70 and the cycle between these states in more detail in the following section.

2.3.3. Cycle of Hsp70

The interaction of Hsp70 with its substrates is modulated by an ATPase cycle where Hsp70 cycles between ATP- and ADP-bound states (Figure 1-2). Binding of ATP to the ATPase domain of Hsp70 promotes interaction between the ATPase domain and SBD (Kityk et al., 2012; Liu and Hendrickson, 2007; Qi et al., 2013). SBD β forms extensive contact with subdomain Ia of the ATPase domain. SBD α binds to subdomain Ib, opening the cleft and allowing interaction of peptide substrate with high on- and off-rate (Figure 1-1c). The hydrolysis of ATP to ADP induces a dramatic conformational change in Hsp70. SBD α and SBD β dissociate from the

ATPase domain. SBD α then interacts with SBD β , acting as a lid to trap the polypeptide substrate in the cleft and greatly reducing the rate of substrate dissociation with Hsp70 (Figure 1-1d).

The intrinsic ATPase activity of Hsp70 is low. Interaction of dedicated J-protein co-chaperones stimulate the ATPase activity of Hsp70. The J-domain of J-proteins interacts with Hsp70 at the interface between the ATPase domain and SBD together with the linker, enhancing hydrolysis of bound ATP (Kityk et al., 2018).

To complete the ATPase cycle, ADP must dissociate from Hsp70. However, the exchange of ADP for ATP is a slow process. Rapid nucleotide exchange thus requires an additional interaction with nucleotide exchange factors (NEFs). NEFs, such as Hsp110, interact with the ATPase domain of Hsp70 and accelerate ADP dissociation. Release of ADP facilitates ATP binding which initiates another round of the ATPase cycle.

Recent structural studies extend our understanding of how Hsp70 functions mechanistically. On one hand, binding of ATP triggers consecutive changes in the amino acid interaction network from the ATPase domain to the SBD, leading to substrate release (Kityk et al., 2015). On the other hand, substrate binding to the cleft in the ATP-bound state of Hsp70 promotes ATP hydrolysis mediated by J-protein that results in trapping of substrate in the SBD (Mayer et al., 2000). These illustrate allosteric communication in both directions from the ATPase domain to the SBD and vice versa.

2.4. Characteristics of J-proteins

J-proteins are dedicated co-chaperones for Hsp70 that activate ATPase activity. All J-proteins contain a so-called J-domain that interacts with Hsp70. The J-domain consists of four alpha helices forming a bundle (Figure 1-3) (Szyperski et al., 1994). The J-domain contains an

HPD motif that is highly conserved and is critical for activating the ATPase activity of Hsp70 (Tsai and Douglas, 1996). A recent co-crystal of the J-domain with Hsp70 helped to clarify the interaction mechanism. The structure showed that helix II and III of the J-domain interact with the ATPase domain, the SBD β and the linker of Hsp70 in the ATP-bound state, and places the HPD motif at the interface between the ATPase domain and SBD β . This interaction makes Hsp70 more responsive to substrate binding that triggers hydrolysis of ATP and ultimately traps the substrate in the cleft (Kityk et al., 2018).

J-proteins add functional specificity to Hsp70 (Craig and Marszalek, 2017; Kampinga and Craig, 2010). It is unlikely that Hsp70 distinguishes various substrates based only on the limited characteristics of the SBD cleft. J-proteins increase the number of specific interaction between substrates and Hsp70. There are six Hsp70 homologs (Ssa1-4 and Ssb1 and 2) and thirteen J-proteins present in the cytosol of *S. cerevisiae* that I will focus on. The four Ssa proteins share 84-99% identity and the two Ssb proteins are 99% identical. But, J-proteins are far more diverse, enabling more specific substrate interactions and driving cellular localization of Hsp70 (Figure 1-4).

Most J-proteins contain substrate-binding domains with different substrate affinities, thus providing specificity to Hsp70. For example, yeast J-proteins Ydj1 and Sis1 contain substrate-binding domains (or C-terminal domains) that interact with distinct substrates (Kampinga and Craig, 2010). The substrate-binding sites of Ydj1 and Sis1 are composed of hydrophobic amino acids that resemble each other (Li et al., 2003; Sha et al., 2000), but they preferentially binds different substrates for folding or degradation, respectively, thus broadening Hsp70 function.

J-proteins also localize to different cellular compartments or complexes, and this also defines Hsp70 specificity. Some J-proteins contain signal peptides that target them to the ER or

mitochondria where they function with Hsp70. Other J-proteins contain domains that bind to particular protein complexes to perform more specific functions. For example, Zuo1, a J-protein in *S. cerevisiae*, binds to the ribosome and coordinates an interaction between the ribosome-associated Hsp70 (Ssb in *S. cerevisiae*) and nascent polypeptides.

A recent study suggested a third mechanism to drive functional diversity of Hsp70 by J-proteins. It has been suggested that J-proteins can modulate the interaction cycle between Hsp70 and substrate to optimize function of Hsp70 in various cellular processes (Schilke et al., 2017).

2.5. Characteristics of atypical Hsp70s

Several Hsp70s are classified as atypical because they cannot perform efficiently the ATPase cycle described in the previous section. These atypical Hsp70s maintain some ATPase activity or substrate binding affinity but they function independently of J-proteins and have functions that are distinct from typical Hsp70s. Two types of atypical Hsp70s are present in the cytosol. One is Hsp110 (Sse1 in *S. cerevisiae*) which is a nucleotide exchange factor, and the other is HspA14 in humans (Ssz1 in *S. cerevisiae*) whose function is not clear.

Sse1 resembles Hsp70 in structure (Figure 1-5) (Liu and Hendrickson, 2007). Sse1 contains an ATPase domain, although its ATPase activity is only marginal and is not required for normal cell growth (Shaner et al., 2004; Shaner et al., 2005). Much like Hsp70, Sse1 also contains a cleft in the SBD β which can interact with substrate (Oh et al., 1999). It has been proposed that Sse1 interacts with substrate as a “holdase” before transferring the substrate to Hsp70, but its exact role is unclear (Oh et al., 1997). In addition, the SBD α region of Sse1 has a different function compared to that of typical Hsp70.

In fact, Sse1 is one of the NEFs for Hsp70 (Dragovic et al., 2006; Raviol et al., 2006). Sse1 interacts with the ATPase domain of Hsp70 with its ATPase domain and SBD α (Polier et al., 2008; Schuermann et al., 2008). The SBD α of Sse1 interacts with the subdomain IIb of the ATPase domain of Hsp70. This leads to 27° rotation of the subdomain IIb relative to other subdomains of the ATPase domain. Opening the ATP binding pocket of Hsp70 by Sse1 is key to facilitating dissociation of ADP from the ATPase domain.

The other atypical Hsp70 is Ssz1 which is also structurally similar to Hsp70. Ssz1 comprises an ATPase domain and a C-terminus which resembles SBD β . However, Ssz1 does not contain an SBD α region, which is critical for the function of both Hsp70 and Sse1. Consistent with the lack of SBD α , there is no evidence Ssz1 acts either as a NEF or a typical Hsp70 (Jaiswal et al., 2011). This raises questions about its cellular role. I will discuss Ssz1 in more detail below, as this protein is one of the focuses of my research.

3. RIBOSOME-ASSOCIATED MOLECULAR CHAPERONE

3.1. Features of the ribosome

3.1.1 Ribosome function and structure

The ribosome, composed of ribosomal proteins and RNAs, is the central molecular machine responsible for synthesizing proteins (Ramakrishnan, 2002; Steitz, 2008). The ribosome consists of small and large subunits named after their rate of sedimentation in density gradients. The small subunit contains the mRNA decoding center and the large subunit contains the peptidyl transferase center (Figure 1-6). Decoding and peptide-bond formation are coordinated by tRNA. The ribosome contains three tRNA binding sites related to the peptide synthesis

process (Voorhees and Ramakrishnan, 2013). In the small subunit, aminoacyl-tRNA binds to mRNA containing complementary base pairs at the A site. In the large subunit, peptide bonds are formed at the P site between the growing polypeptide and aminoacyl-tRNA coming from the A site. After peptide bond formation, free tRNA leaves the ribosome at the E site.

Nascent polypeptides transit along the ribosome tunnel as a result of peptide-bond formation at the peptidyl transferase center. (Figure 1-6). It has been shown that the ribosome tunnel can sense transiting nascent polypeptides, and signal this information to the outside of the ribosome (Wilson and Beckmann, 2011; Zhang et al., 2013). Ribosomal proteins that form the tunnel mediate this signal, controlling the rate of peptide-bond formation by the ribosome in most cases.

The ribosome tunnel exit site is a hub for proteins which are involved in nascent polypeptide maturation, folding or translocation (Kramer et al., 2009). In particular, I am focused on the molecular chaperones associated with the tunnel exit that aid folding of *de novo* proteins. Intriguingly, it has also been suggested that these chaperones are involved in maintaining translational fidelity, although the underlying mechanism is unknown.

3.1.2. Ribosome-associated molecular chaperones in prokaryotes and eukaryotes

Among various molecular chaperones in cells, there is a subset that binds directly to ribosomes and assists in folding of newly synthesized polypeptides. Interestingly, there are two structurally and evolutionarily distinct ribosome-associated chaperone systems present in prokaryotes and eukaryotes. Bacteria contain a protein, called trigger factor (TF) in *E. coli*, while eukaryotes contain an Hsp70-based molecular chaperone system. I will discuss these different ribosome-associated molecular chaperones in the following sections.

3.2. Ribosome-associated molecular chaperones in prokaryotes

3.2.1. Characteristics of trigger factor

TF was found to associate with newly synthesized nascent polypeptides in *E. coli* (Hesterkamp et al., 1996). TF consists of three domains that adopt a unique dragon-like elongated structure (Ferbitz et al., 2004; Hoffmann et al., 2010). The N-terminal domain forms a “tail” containing a ribosome binding motif (GFRxGxxP) that interacts with ribosomal protein uL23 (Ferbitz et al., 2004). This interaction is the key prerequisite for the interaction with nascent polypeptides. The middle domain of TF forms a “head” that has prolyl isomerase activity, but its functional role in folding of nascent chains is unknown. The C-terminus constitutes the “body” and “arms” of the dragon, and they contribute the main chaperone activity. The body of TF interacts with substrate regions enriched in basic and aromatic amino acids with a net positive charge (Patzelt et al., 2001).

In general, TF functions with other molecular chaperones such as DnaK (*E. coli* Hsp70) and GroEL (*E. coli* Hsp60) to accomplish complete *de novo* folding of proteins (Craig et al., 2003; Hartl and Hayer-Hartl, 2009; Kramer et al., 2009). Deletion of both TF and DnaK results in increased aggregation of cytosolic proteins but individual deletion does not (Deuerling et al., 1999). These results suggest that both TF and DnaK aid protein folding and their functions might overlap. In addition, it has been suggested that substrates that are kinetically trapped, but not aggregated, are further transferred from TF to GroEL, mediated by DnaK, to complete the folding process (Frydman et al., 1994; Hartl and Hayer-Hartl, 2009).

3.3. Ribosome-associated molecular chaperones in eukaryotes

3.3.1. Characteristics of typical Hsp70, Ssb

Eukaryotes contain an Hsp70-based molecular chaperone system, which assist folding of newly synthesized proteins. In *S. cerevisiae*, the Hsp70-based chaperone system (often called a chaperone triad) consists of Hsp70 Ssb, J-protein co-chaperone Zuo1, and atypical Hsp70 Ssz1.

Ssb carries out its functions by association with the ribosome. There are two Ssb (Ssb1 and Ssb2) in *S. cerevisiae*. The sequences of Ssb1 and Ssb2 are 99% identical, and all experimental results to date indicate that Ssb1 and Ssb2 function identically. I will refer to both homologs as Ssb unless specified otherwise. Ssb was the first chaperone that was found to associate with the ribosome, aiding folding of nascent polypeptides in yeast (Nelson et al., 1992). Later it was found that Ssb is the core of the molecular chaperone triad that interacts directly with nascent polypeptides as short as 54 amino acids as they exit the ribosome tunnel (Hundley et al., 2002).

Like other Hsp70s, the substrate binding cleft in Ssb interacts with nascent polypeptides. Many of the amino acid residues that form the cleft can be altered without disrupting Ssb function, indicating a high degree of flexibility in the substrate interaction (Pfund et al., 2001). Although Ssb can bind various substrates, Ssb prefers regions enriched with positively charged and aromatic amino acids of nascent polypeptides that cannot fold efficiently (Willmund et al., 2013). These substrates are involved in cellular processes such as aging, signaling, and ribosome biogenesis.

Interplay between the ribosome-associated and cytosolic molecular chaperones is important for substrates that require further folding as described for prokaryotes. These substrates are transferred to cytosolic molecular chaperones such as Hsp90 or Hsp60 complex

where folding process is completed (Hartl et al., 2011). Co-chaperones are often involved in such substrate transfer, and also serve to connect each molecular chaperone systems by acting as a scaffold.

It has been known for some time that association of Ssb with the ribosome is mediated by all three of its domains: ATPase domain, SBD α , and SBD β (James et al., 1997). A recent study suggested that a positively charged region in SBD α is important for ribosome-association, mediated by ribosomal proteins e119, ul29, and e139, along with ribosomal RNA expansion segments 24, 41, and possibly 39 near the ribosome tunnel exit (Gumiero et al., 2016). Another study suggested concurrently that a KRR-motif in SBD β contacts the ribosome directly (Hanebuth et al., 2016). However, it is unknown how the ATPase domain of Ssb is involved in ribosome association.

Intriguingly, Ssb also plays a role in maintaining translational fidelity of the ribosome (Peisker et al., 2010). Deleting the *SSB* gene results in sensitivity to aminoglycoside antibiotics, which target translational fidelity (Nelson et al., 1992). These antibiotics bind near the mRNA decoding center of the ribosome, increasing both nonsense and missense errors in mRNA translation. In accordance with drug sensitivity, *SSB* deletion also increases readthrough of stop codons and mis-incorporation (Rakwalska and Rospert, 2004). *SSB* deletion also inhibits -1 programmed ribosomal frameshifting, which is often used by viruses to increase genomic contents (Caliskan et al., 2015; Muldoon-Jacobs and Dinman, 2006).

Further studies showed that Ssb is also involved in protein quality control. Absence of stop codons in mRNA results in translation of poly(A) tails, generating polylysine peptides. Translation of polylysine chains is normally repressed and these peptides are quickly degraded. However, several studies found that deleting *SSB* led to increased expression of polylysine

proteins, indicating that Ssb normally helps target nascent polylysine proteins for degradation (Chiabudini et al., 2012; Chiabudini et al., 2014).

The roles of Ssb in translational fidelity/protein quality control together with the function of Ssb as a molecular chaperone suggests a possible connection between protein folding and translation that is mediated by Ssb. I will elaborate on this connection in Chapter Two.

3.3.2. Characteristics of the J-protein co-chaperone, Zuo1

Zuo1 is the cognate J-protein co-chaperone for Ssb that activates ATPase activity. Zuo1 also provides substrate specificity for Ssb by binding to ribosome directly and facilitating the interaction between nascent polypeptides and Ssb (Yan et al., 1998). Non-specific crosslinking results suggested Zuo1 might interact with ribosomal protein eL31 near the ribosome tunnel exit, but eL31 is not necessary for Zuo1 association with the ribosome (Peisker et al., 2008). A cryo-EM study later confirmed that Zuo1 contacts eL31 adjacent to rRNA H24. The cryo-EM structure also identified an additional Zuo1 binding site consisting of eL22 and rRNA H59 (Figure 1-7) (Leidig et al., 2013). These binding sites remain controversial, as more recent results did not observe density for the interaction between Zuo1 and rRNA H24 (Zhang et al., 2014). It has not been clear which regions of Zuo1 and components of the 60S subunit of the ribosome interact with each other due to low resolution (7.2 Å) of cryo-EM data and lack of structural information of the domain of Zuo1 interacting with the 60S.

Zuo1 contains two domains thought to interact with the ribosome. One domain is the Zuotin homology domain (ZHD), which has sequence similarity with another ribosome-associated J-protein, Jjj1 (Albanese et al., 2010; Meyer et al., 2007). Jjj1 functions in ribosome biogenesis through interaction with eL31, which is the same binding site ascribed to Zuo1

(Greber et al., 2012). It was shown that the ZHD of both proteins is important, not only for ribosome association, but also for their respective functions (Kaschner et al., 2015). Thus, it has been hypothesized that the ZHD of both Zuo1 and Jjj1 interacts with ribosomal protein eL31. The other domain of Zuo1 that contributes to ribosome binding is the C-terminal domain. An NMR study showed that the C-terminal domain of Zuo1 forms a four-helix bundle (Figure 1-8) (Ducett et al., 2013), and contains a basic patch that is thought to interact with rRNA. No direct evidence supported this hypothesis until a recent cryo-EM structure was published (Zhang et al., 2014).

As mentioned earlier, the cryo-EM structure could not resolve the precise interaction between Zuo1 and the 60S. However, it suggested Zuo1 interacts with not only the 60S subunit but also the 40S subunit through its C-terminal domain (Figure 1-9) (Zhang et al., 2014). The Zuo1 and Ssz1 complex spans about 190 Å through the so-called middle domain of Zuo1 that connects the density of Zuo1 on the 60S subunit near the ribosome tunnel exit with the C-terminal domain on the 40S subunit.

The interaction of Zuo1 with the ribosome is dynamic. Unfolding of the C-terminus of Zuo1 leads to dissociation of Zuo1 from the ribosome, which then induces pleiotropic drug gene activation (Ducett et al., 2013). DnaJC2 (the human ortholog of Zuo1) is also implicated in transcriptional activation by displacing polycomb-repressive complex 1 (Richly et al., 2010). Both functions require dissociation of Zuo1 from the ribosome as a prerequisite. In addition, the number of Zuo1 can be decreased to about 2% of normal level without affecting cell growth. This result implies that Zuo1 dissociates from inactive ribosome and actively engages only with translating ribosome (Hundley et al., 2002).

To better understand how Zuo1 interacts with the ribosome, which is essential for understanding its function, we initiated a structural study, together with crosslinking and mutagenesis experiments. I will discuss more about these results and their implications for Zuo1 function in Chapter Two.

3.3.3. Characteristics of the atypical Hsp70, Ssz1

The atypical Hsp70, Ssz1, forms a stable complex with Zuo1 that tethers Ssz1 to the ribosome (Gautschi et al., 2001; Michimoto et al., 2000). Ssz1 has no ATPase activity, but Ssz1 can bind ATP. The C-terminus of Ssz1 has structural similarity to SBD β , indicating that it might act as a substrate-binding domain. However, the entire C-terminus is dispensable for normal cell growth (Hundley et al., 2002). Because of these unique characteristics of Ssz1, the function of Ssz1 in the chaperone triad has not been clear.

Overexpression of Zuo1 partly rescues deletion of *SSZ1*, but Ssz1 cannot rescue the deletion of *ZUO1*. This suggests that Zuo1 plays a central role as a J-protein in the complex (Gautschi et al., 2001). However, a study revealed that Zuo1 must form a complex with Ssz1 to stimulate Ssb ATPase activity, indicating a potential structural role for Ssz1 (Huang et al., 2005). It remains unclear how the formation of the complex impacts Zuo1's function as a J-protein. Ssz1 may have a regulatory role or induce conformational changes in Zuo1 that activate the ATPase activity of Ssb as an evolutionary artifact.

3.3.4. Characteristics of the Zuo1 and Ssz1 complex

When I began my thesis work, there existed some results that suggest how Ssz1 forms a complex with Zuo1. Hydrogen exchange experiments coupled with mass spectrometry analysis

suggested that the C-terminus of Ssz1 and a N-terminal segment preceding the J-domain of Zuo1 are involved in complex formation (Fiaux et al., 2010). While I was working on this interaction between Ssz1 and Zuo1, the molecular details were revealed by a crystal structure of the core Zuo1/Ssz1 complex (Figure 1-10) (Weyer et al., 2017). The structure showed that the N-terminal segment of Zuo1 is intertwined with the ATPase domain, the C-terminus, and the linker of Ssz1. This explained the stability of the complex and the lack of ATPase activity of Ssz1. The structure also showed that the C-terminus of Ssz1 contains a SBD β region with a cleft similar to the SBD of typical Hsp70, but lacking an SBD α region.

It has been known for quite some time that deleting the ATPase domain of Ssz1 impairs cell growth, indicating its functional importance (Hundley et al., 2002). The structure of the core Zuo1/Ssz1 complex suggested that the ATPase domain and linker of Ssz1 were sufficient for complex formation, explaining previous growth phenotypes. To better understand the function of Ssz1, I performed crosslinking experiments that targeted the ATPase domain, which is key for normal cell growth. I will discuss these results and their implications for cellular function of Ssz1 in Chapter Three.

3.3.5. Characteristics of the human Zuo1/Ssz1 complex

As mentioned before, metazoans do not contain an ortholog of Ssb that can bind the ribosome directly to help fold nascent polypeptides. This lack of Ssb-type Hsp70 in metazoans leads to a question about the localization of cytosolic Hsp70s to ribosomes. Heterologous overexpression of DnaJC2 in yeast partially suppresses the deletion phenotypes of Zuo1 (Hundley et al., 2005). DnaJC2 functions together with a cytosolic Hsp70, Ssa1 (an ortholog of human Hsp70) but not with Ssb to help fold nascent polypeptides. Concurrent expression of

HspA14, the human ortholog of Ssz1, and DnaJC2 further suppresses the deletion phenotypes of Zuo1, suggesting a role for HspA14 in Ssa1 activation (Jaiswal et al., 2011). Consistent with these results, the DnaJC2 and HspA14 complex promotes an interaction between cytosolic Hsp70 and nascent polypeptides on the ribosome in human cells (Jaiswal et al., 2011; Otto et al., 2005). My results in Chapter Three show that Ssz1 binds to Ssb and positions Ssb on the ribosome. The interaction between Ssz1 and Ssb has important implications for metazoans, including humans, that lack Ssb-type Hsp70. We think that HspA14 recruits cytosolic Hsp70 to the ribosome, similar to the interaction between Ssz1 and Ssb, and facilitates the interaction between cytosolic Hsp70 and nascent polypeptides. I will discuss this model in Chapter Three.

4. THESIS PLAN

A wealth of knowledge exists for the molecular chaperone triad that assists folding of nascent polypeptides as they exit the ribosome. However, new functions are emerging for the chaperone triad that extend beyond the simple Hsp70 and J-protein paradigm. When I began work on the Zuo1/Ssz1 complex, it was unknown how Zuo1 interacts with the ribosome. But in the last few years, low-resolution structures showed that Zuo1 spans both subunits of the ribosome. Together with Zuo1's general function, these results suggested that Zuo1 might coordinate mRNA decoding with the folding state of nascent polypeptide. However, the mechanism of such coordination was unknown because key details of the interaction between Zuo1 and the ribosome remained unclear. Although the Zuo1/Ssz1 complex is highly conserved in eukaryotes, the function of Ssz1 was unknown. Elucidating Ssz1 function has been difficult because it is an atypical Hsp70 that forms a stable complex with Zuo1, unlike any other known interactions between J-proteins and Hsp70s.

To better understand the function of Zuo1, I teamed up with two other people in the lab and performed experiments whose results are described in Chapter Two. Om Shrestha solved the ZHD structure at the start of the project. I performed site-specific crosslinking experiments to understand how the ZHD interacts with the 60S subunit of the ribosome. I found that the ZHD interacts with ribosomal protein eL31, which is consistent with two cryo-EM structures of Zuo1 bound to the ribosome. My crosslinking results and the cryo-EM density maps allowed us to create a computational docking model between the ZHD and ribosome, with eL31 as a fixed contact site. However, it was difficult to precisely dock the ZHD because of low resolution of cryo-EM structures. These cryo-EM structures also suggested that different components of ribosome act as contact sites (one is ribosomal RNA H24 and the other is eL22/H59). Thus, I conducted ribosomal RNA mutagenesis to examine these interactions directly. My experiments showed that the deletion of a single RNA base pair in H24, unlike H59, destabilizes the interaction, indicating that the ZHD interacts with ribosomal RNA H24 near the ribosome tunnel exit. My results also showed no crosslinking products when crosslinking was performed with eL22, supporting H24 as a contact site. The ZHD structure also contains a middle domain that positions the C-terminal domain of Zuo1 on ES12 of the 40S subunit. ES12 is part of helix44, which originates at the decoding center, suggesting a potential role for Zuo1 in maintaining translational fidelity. Ruchika Sharma verified the interaction between the C-terminus and ES12, and further showed that the interaction is critical for correct function of the ribosome in translation. Taken together, our results provide insight into the function of Zuo1 by mapping the interactions between Zuo1 and the ribosome. We speculate that Zuo1 not only helps fold nascent polypeptides, but also coordinates mRNA decoding with the folding state of nascent peptides by its dual interactions with both subunits of the ribosome.

When I began my research, it was not clear how Zuo1 forms a complex with Ssz1. To better understand this interaction, I conducted site-specific crosslinking experiments. My results showed that the N-terminus of Zuo1 interacts with the interface between the ATPase domain and SBD of Ssz1. A later crystal structure of the core Zuo1/Ssz1 complex confirmed my results. This structure advanced our understanding of the interaction, but it was unable to provide insight into the function of Ssz1. It has been known for some time that deletion of the ATPase domain of Ssz1 impairs normal growth of yeast cells, which contrasts with the lack of obvious phenotypes for deletion of the C-terminus. This result was the key to initiating experiments that focused on the ATPase domain of Ssz1. I describe these results in Chapter Three. Surprisingly, I was able to obtain crosslinking products between the ATPase domains of Ssz1 and Ssb1. Unbiased docking results suggested that they interact through ATPase domain dimerization. The interaction model was verified by *in vitro* crosslinking coupled with mass spectrometry analysis. Furthermore, I showed that highly conserved and charged residues, which might form salt bridges at the interface, are important for the interaction. Destabilizing the interaction by reverse charge substitutions of those residues impaired growth of yeast cells. Presence of both Ssz1 and Ssb1 variants complemented the growth defect caused by individual variants, suggesting that the interaction is important *in vivo*. Since Ssz1 is tethered to the ribosome by Zuo1, we speculate that Ssz1 positions Ssb on the ribosome through ATPase domain dimerization, facilitating the interaction between Ssb and nascent polypeptide.

In Chapter Four, I have summarized my results in Chapters Two and Three together with their implications for the functions of the Zuo1/Ssz1 complex. In addition, I have provided future directions that may help us better understand the Zuo1/Ssz1 complex.

5. FIGURES AND TABLES

Figure 1-1. (a) Ribbon diagram of the ATPase domain of Hsp70. The ATPase domain is composed of four subdomain Ia, IIa, Ib, and IIb. ATP analog phosphoaminophosphonic acid-adenylate ester (ANP), in stick representation, is present at the base between two lobes of Hsp70. PDB ID: 1NGJ (b) Ribbon diagram of the substrate-binding domain (SBD) of Hsp70. The SBD α trap a substrate in the cleft of the SBD β , acting as a “lid”. SBD α , green; SBD β , blue; Substrate, magenta. PDB ID: 1DKX (c & d) Ribbon diagram of the ATP-bound (PDB ID: 4B9Q) and ADP-bound (PDB ID: 2KHO) structures of Hsp70 with their cartoon representation at the bottom, respectively. In the ATP-bound state, the SBD interacts with the ATPase domain, “opening” the cleft for substrate interaction with high on- and off- rate. In the ADP-bound states, the SBD dissociates from the ATPase domain and tethered only by the linker. ATPase domain, bright orange; SBD α , green; SBD β , blue; Linker, red.

Figure 1-1

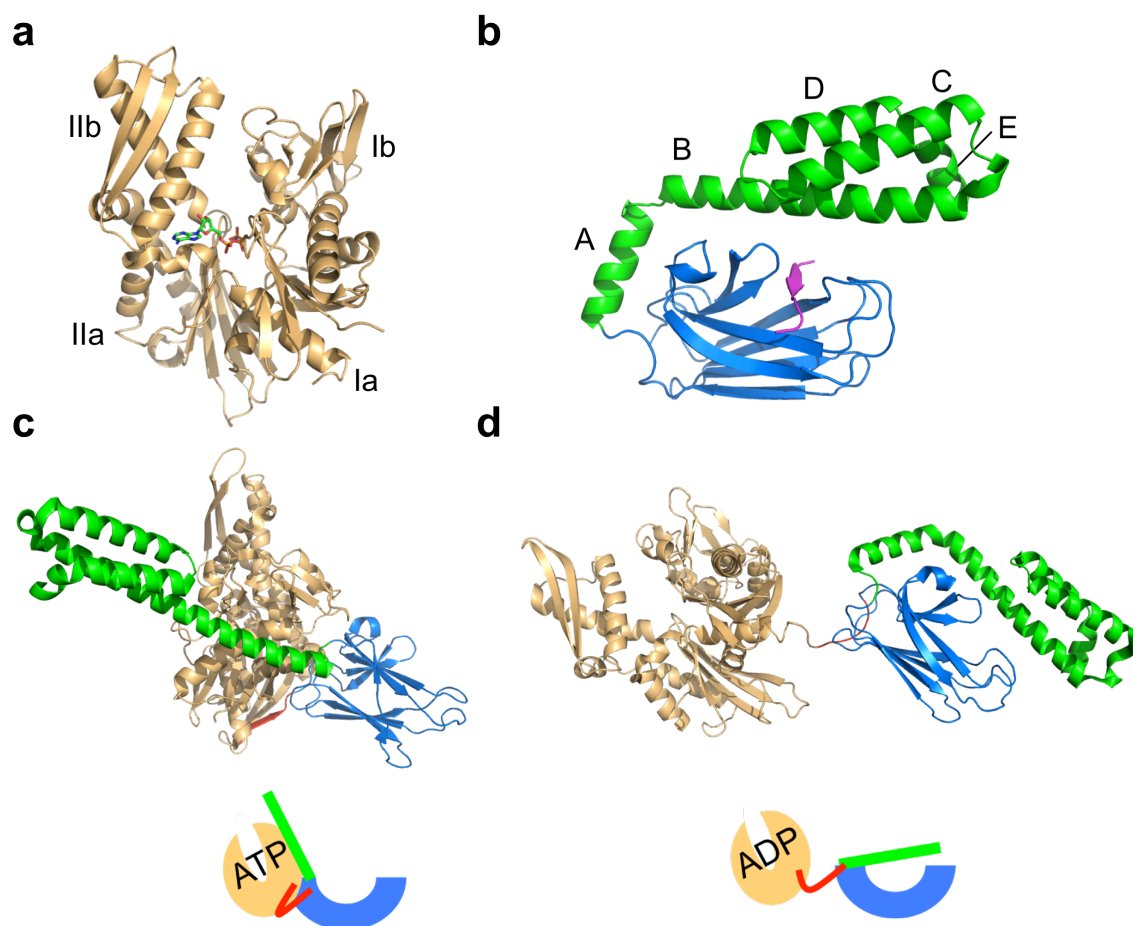


Figure 1-2. Schematic diagram of the ATPase cycle of Hsp70 associated with the ribosome in yeast. (1) The ATP-bound state of Ssb is recruited to the ribosome. (2) J-protein co-chaperone Zuo1 activates the ATPase activity of Ssb, promoting interaction with nascent chains. (3) Nucleotide exchange factor exchange ADP in the ATPase domain of Ssb to ATP, allowing another round of interaction of Ssb with nascent polypeptide. Color scheme for domains of Ssb: ATPase domain, bright orange; SBD α , green; SBD β , blue; Linker, red.

Figure 1-2

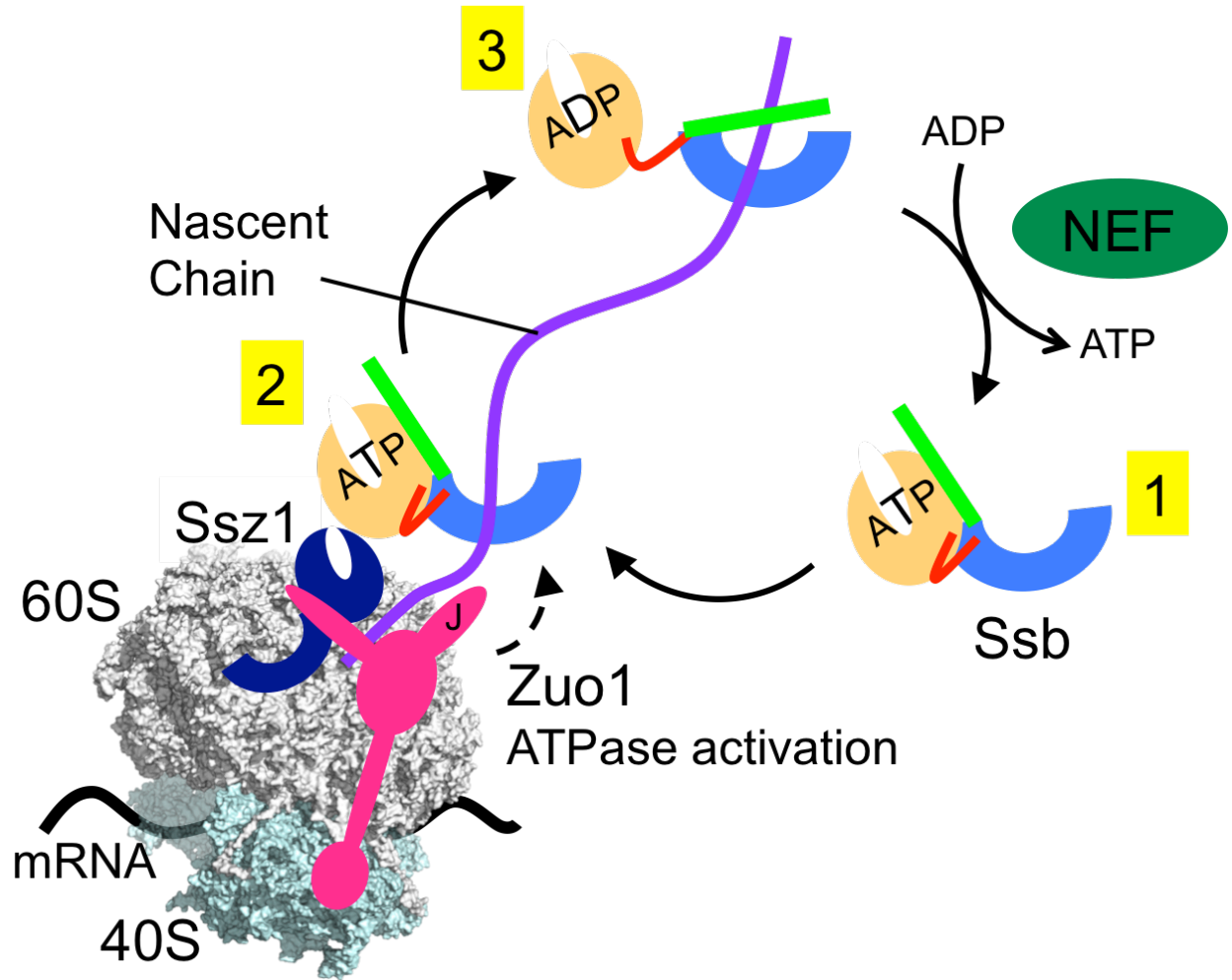


Figure 1-3. Ribbon diagram of the J-domain. Three helices are held together by hydrophobic interaction among them. The HPD motif between helix II and III is highlighted with green stick representation. PDB ID: 1XBL

Figure 1-3

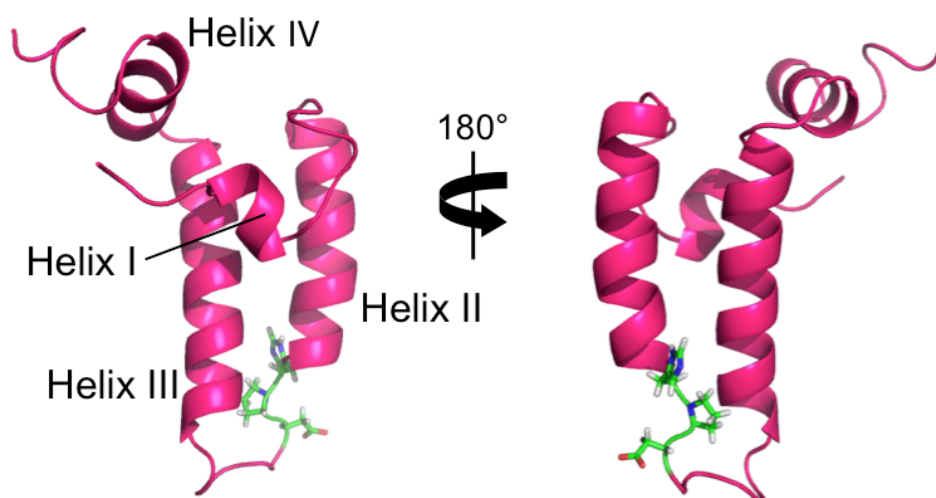


Figure 1-4. J-proteins in the cytosol of *Saccharomyces cerevisiae*. All J-proteins contain the J-domain where they interact with Hsp70. J-proteins provide specificity to Hsp70 with domains other than the J-domain. These domains are for substrate binding and localization to specific complexes or compartments. GF: Glycine-phenylalanine-rich region; CTD: C-terminal domain; DD: Dimerization domain; SID: Spliceosome-interaction domain; T: Transmembrane domain; ZHD: Zuotin homology domain; Z: Zinc finger domain; RBD: Rei1 binding domain; CBD: Clathrin-binding domain; UBA: Ubiquitin-associated domain; TPR: Tetrapeptide repeat.

Figure 1-4






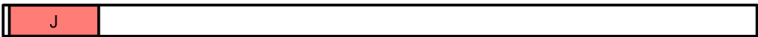


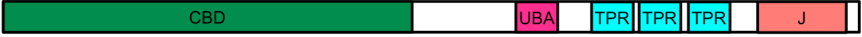


J-proteins	Function	Domain Structure
Apj1	SUMO-mediated protein degradation	
Caj1	Unknown	
Cwc23	pre-mRNA splicing	
Djp1	Peroxisomal protein import	
Hlj1	ER-associated protein degradation	
Jjj1	Ribosome biogenesis	
Jjj2	Unknown	
Jjj3	Diphthamide biosynthesis	
Sis1	Proteasomal degradation	
Swa2	Uncoating of clathrin-coated vesicles	
Xdj1	Mitochondrial protein import	
Ydj1	Protein folding and translocation	
Zuo1	Nascent polypeptide folding	

Figure 1-5. Ribbon diagram of the structure of Hsp110. Note that the linker of Hsp110 is not conserved to define, unlike typical Hsp70. ATPase domain, bright orange; SBD β , blue; SBD α , green; PDB ID: 2QXL

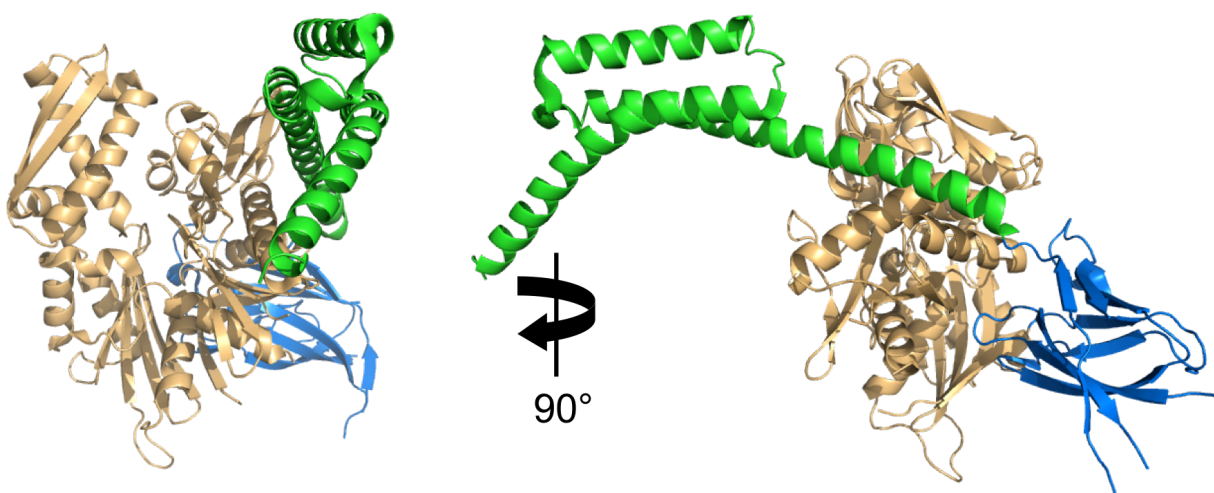
Figure 1-5

Figure 1-6. Schematic diagram of the eukaryotic ribosome. tRNA mediates decoding of mRNA at the decoding center in the 40S subunit and peptide-bond formation at the peptidyl transferase center in the 60S subunit. Nascent polypeptide exit the ribosome through the ribosome tunnel.

PTC: Peptidyl transferase center.

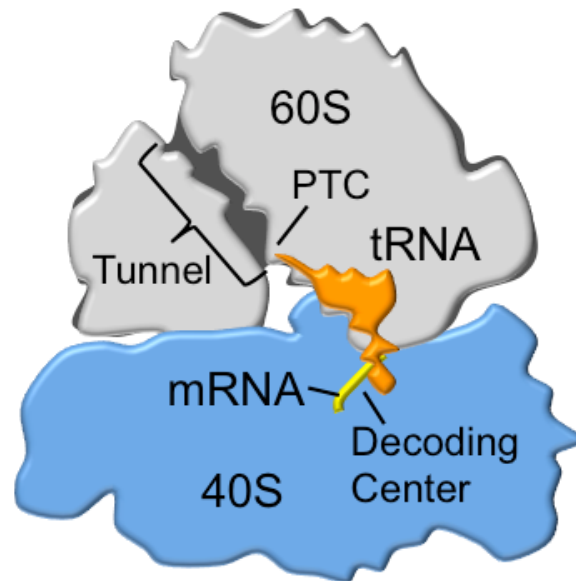
Figure 1-6

Figure 1-7. Previously suggested binding sites for Zuo1 near the polypeptide tunnel exit (PTE) of the 60S subunit. Ribosomal proteins eL31 and eL22 and ribosomal RNA H24 and H59 were implicated as contact sites for the Zuotin homology domain of Zuo1.

Figure 1-7

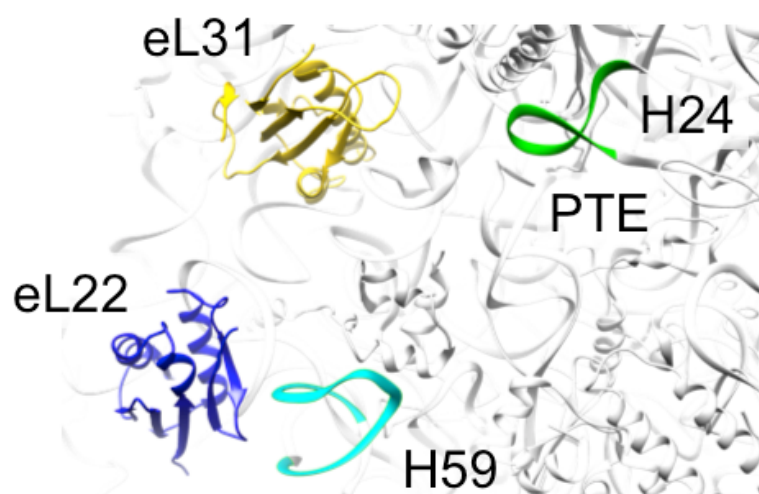


Figure 1-8. Ribbon diagram of the C-terminal four helix bundle structure of Zuo1 with surface charge density showing the distribution of basic (blue) and acidic (red) residues. Helix I contains positively charged residues (K348, K352 and K353), highlighted with sphere representation, that were indicated to interact with ribosomal RNA.

Figure 1-8

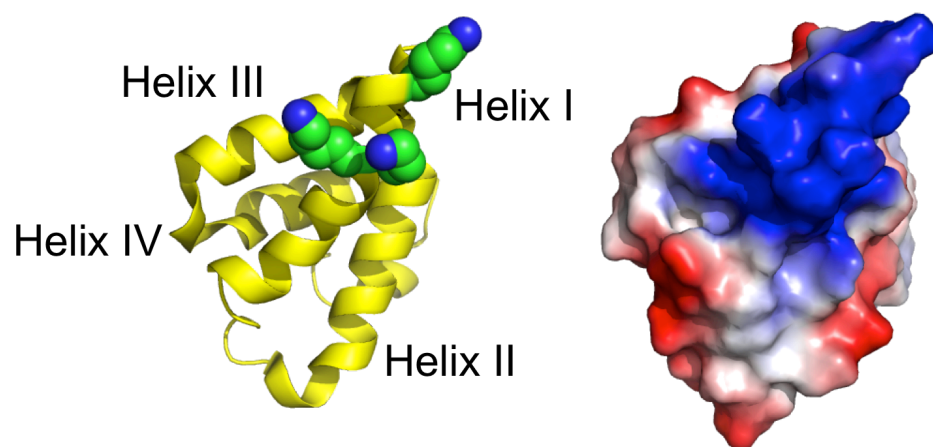


Figure 1-9. Electron density map of the Zuo1 and ribosome complex, suggesting Zuo1 interacts with both 60S and 40S subunits. 60S subunit, cyan; 40S subunit, yellow; Zuo1, red. ZHD: Zuotin homology domain

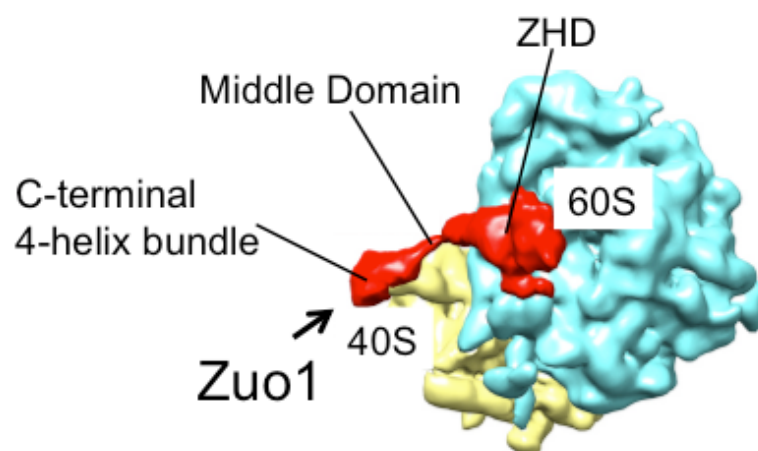
Figure 1-9

Figure 1-10. Ribbon diagram of the crystal structure of the N-terminus of Zuo1 and Ssz1 complex. The ATPase domain and the C-terminus of Ssz1 intertwined the N-terminus of Zuo1 at the interface. N-terminus of Zuo1, magenta; Ssz1, green.

Figure 1-10

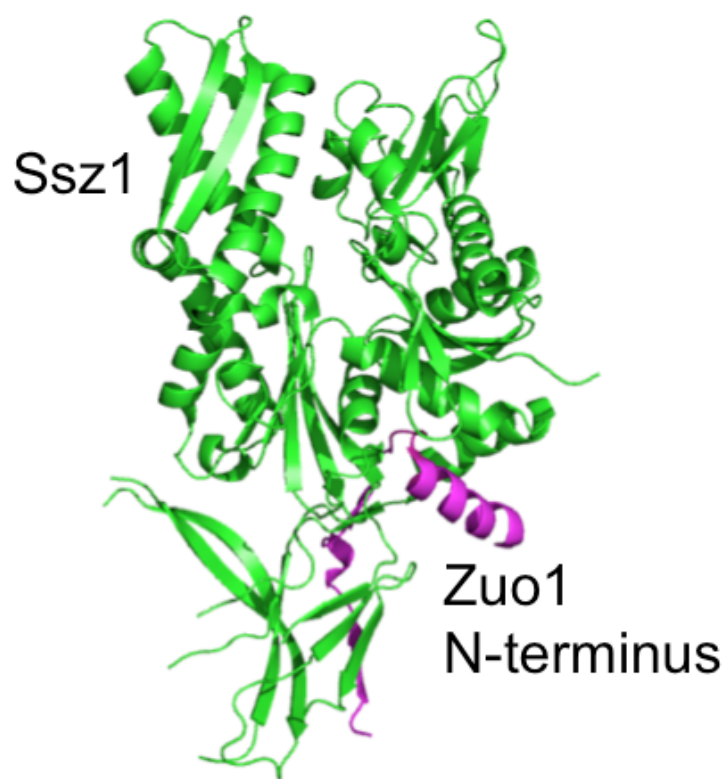


Table 1-1. Types and functions of molecular chaperones

Types	Structural Features	Functions
Small Heat Shock Protein	Oligomer formation	Prevention of intermolecular interaction among unfolded proteins caused by stress
Hsp40	J-domain of Hsp40 interacts with Hsp70	<i>de novo</i> folding, translocation, refolding or degradation of substrates
Hsp60	Double-ring complexes, exchanging hydrophobicity of the cavity based on nucleotide-bound states	<i>de novo</i> folding or refolding of substrates
Hsp70	Consisting of a N-terminal ATPase domain and a C-terminal substrate-binding domain connected by a linker	<i>de novo</i> folding, translocation, refolding or degradation of substrates
Hsp90	Consisting of three domain: An N-terminal ATPase domain, a middle domain where substrate interacts and a C-terminal domain for dimerization	<i>de novo</i> folding or refolding of substrates involved in signaling pathways
Hsp100	Cylindrical complex containing a narrow pore where substrate passes through	Disaggregate aggregates

CHAPTER TWO: Dual interaction of the Hsp70 J protein co-chaperone Zuotin with the 40S and 60S subunits of the ribosome

Adapted from:

Lee, K., Sharma, R., Shrestha, O.K., Bingman, C.A., and Craig, E.A. (2016). Dual interaction of the Hsp70 J-protein cochaperone Zuotin with the 40S and 60S ribosomal subunits. *Nat Struct Mol Biol* 23, 1003-1010.

Sherestha O.K. solved structure of a domain of Zuo1 (the Zuotin homology domain) important for ribosome association under the guidance of Bingman, C.A. These results are shown in Fig. 2-1 and Supplementary Fig. 2-1a,b. I performed experiments to position Zuo1 on both subunits of the ribosome in addition to docking and modeling. These results are shown in Fig. 2-2, Fig. 2-4c,d, Supplementary Fig. 2-2a-e and Supplementary Fig. 2-3. Sharma R. verified importance of the interaction between Zuo1 and the ribosome in translational fidelity. These results are shown in Fig. 2-3, Fig. 2-4a,b, Supplementary Fig. 2-1d and Supplementary Fig. 2-4. In addition, Sharma R. generated Supplementary Fig. 2-2f. Craig, E.A. oversaw all aspects of the manuscript.

1. ABSTRACT

Ribosome-associated J protein-Hsp70 chaperones promote nascent polypeptide folding and normal translational fidelity. Though known to span the ribosome subunits, understanding of J protein Zuo1 function is limited. New structural and crosslinking data allow more precise positioning of *Saccharomyces cerevisiae* Zuo1 near the 60S polypeptide exit site, pointing to interactions with ribosomal protein eL31 and 25S rRNA helix 24. The junction between the 60S-interacting and subunit-spanning helices is a hinge, positioning Zuo1 on the 40S, yet accommodating subunit rotation. Interaction between C-terminus of Zuo1 and 40S occurs via 18S rRNA expansion segment 12 (ES12) of helix 44, which originates at the decoding site. Deletions in either ES12 or C-terminus of Zuo1 alter stop codon readthrough and -1 frameshifting. Our study offers insight into how this cotranslational chaperone system may monitor decoding site activity and nascent polypeptide transit, thereby coordinating protein translation and folding.

2. INTRODUCTION

Generating a functioning proteome is a challenge faced by all cells. Particularly demanding is the generation of properly folded nascent chains as they exit the ribosome, both because of the crowded environment, and because a protein domain cannot fold properly until its synthesis is completed (Gloge et al., 2014; Kim et al., 2013). To maintain overall cellular protein homeostasis, the rate at which polypeptides are synthesized must also be optimized relative to capacity for folding in the cytosol and productive translocation across membranes, as well as for translation fidelity (Korennykh and Walter, 2012; Sherman and Qian, 2013; Wang and Chen,

2015; Wrobel et al., 2015). The exit site of the ribosome is a hub for factors that promote protein quality control. In eukaryotes these include a complex Hsp70-based system that is implicated in both protein folding and translational fidelity (Nelson et al., 1992; Preissler and Deuerling, 2012). Like all Hsp70 machines, the ribosome-based system includes a J protein (often called Zuo1, and more specifically Zuo1 and DnaJC2 in yeast and humans, respectively) (Hundley et al., 2005; Kampinga and Craig, 2010; Yan et al., 1998), which stimulates the ATPase activity of its partner Hsp70 (ribosome-associated Ssb in yeast) (Huang et al., 2005). This J protein activity is universally required for an Hsp70 to functionally interact with its client proteins (Clerico et al., 2015), including nascent chains exiting the ribosome (Willmund et al., 2013).

Zuo1 forms a stable heterodimer (often called the ribosome associated complex, RAC) with an atypical Hsp70 (called Ssz1 and HspA14 in fungi and humans, respectively), tethering it to the ribosome (Fiaux et al., 2010; Gautschi et al., 2001; Gautschi et al., 2002; Otto et al., 2005). Ssz1/HspA14 bind, but do not hydrolyze, ATP and thus cannot partner with a J protein and perform the classic client protein binding cycle (Conz et al., 2007; Huang et al., 2005; Jaiswal et al., 2011). These three proteins (Ssb, Zuo1 and Ssz1), which are often referred to as a chaperone triad, play a role together in folding of nascent polypeptides (Willmund et al., 2013). This chaperone triad has also been implicated in quality control pathways more closely tied to the process of protein synthesis. Translational readthrough of stop codons, a measure of translation fidelity, is increased in triad deletion mutants (Rakwalska and Rospert, 2004). The ability of ribosomes to shift translational reading frame, particularly -1 frameshifting, is a capacity used to produce alternative proteins from the same mRNA transcript or to regulate premature termination (Caliskan et al., 2015). -1 frameshifting is decreased in triad deletion mutants (Muldoon-Jacobs and Dinman, 2006).

It has been appreciated for some time that Zuo1 interacts with the 60S subunit close to the polypeptide exit site of the ribosome tunnel (Leidig et al., 2013; Peisker et al., 2008). Recently, cryo-electron microscopic (cryo-EM) analysis revealed interaction with the 40S subunit as well (Zhang et al., 2014). Consistent with small angle X-ray crystallographic analysis (Leidig et al., 2013), Zuo1 was found to span approximately 190 Å across the subunits (Zhang et al., 2014) (Fig. 2-1a). Based on its position on the 40S subunit, the C-terminal 4-helix bundle (residues 348-433) (Ducett et al., 2013; Leidig et al., 2013) of Zuo1 has been proposed to interact with expansion segment 12 (ES12), an extension of helix 44 (H44) of 18S rRNA (Zhang et al., 2014). A long internal alpha helix, called the middle domain (MD), is proposed to span the subunits. The remainder of RAC, that is Ssz1 and N-terminal segments of Zuo1, is in close proximity to the 60S subunit. The segment immediately adjacent to the MD, which is referred to as the Zuotin homology domain (ZHD), is most relevant to this report. Zuo1's ZHD has sequence identity to a second ribosome-associated J protein, Jjj1, which is involved in biogenesis of the 60S subunit. The ZHD is functionally important for association of both proteins with ribosomes (Albanese et al., 2010; Kaschner et al., 2015).

Although our understanding of chaperone function on the ribosome has increased significantly in the past few years, major questions remain. Due to its inherent flexibility, structural information for the bulk of Zuo1 is lacking. Thus, how Zuo1 interacts with the 60S subunit has remained an enigma, and therefore progress towards understanding the relationship between the 60S interaction at the exit tunnel and the 40S interaction has been slow. Furthermore, the recent observation that Zuo1 binds the 40S subunit raises the question of whether this interaction is important for Zuo1's role in translational fidelity (Zhang et al., 2014).

This question is particularly intriguing as the proposed Zuo1 interaction site is the tip of 18S rRNA H44, which originates at the decoding site.

3. METHODS

Protein expression and purification

DNA encoding residues 166-303 of Zuo1 was amplified by PCR, and cloned into a modified pET-28a vector that contains N-terminal His₆-tag, thioredoxin (TRX) tag and a cleavable tobacco etch virus (rTEV) protease site. Two mutations to substitute methionine for K210 and N269 were introduced into *ZUOI*₁₆₆₋₃₀₃ via QuikChange PCR mutagenesis (Stratagene). Protein was expressed in *Escherichia coli* Rosetta 2 (DE3) pLysS using LB or autoinduction medium (Blommel et al., 2007) containing L-selenomethionine (SeMet). Cells were resuspended in lysis buffer (50 mM Tris pH 7.5, 250 mM NaCl, 10 mM imidazole, 5% glycerol) with cOmplete EDTA-free Protease Inhibitor Cocktail (Roche), and then lysed using a French press at 4°C. Lysates were clarified by centrifugation. Initial protein purification was done using gravity flow nickel column chromatography. Tags were removed by proteolysis with recombinant rTEV protease overnight at 4°C. Tagged protein, cleaved His₆/TRX-tag, and His₆-tagged rTEV were separated from Zuo1 fragment by gravity flow nickel chromatography. Protein was further purified by using S-75 size exclusion chromatography column (GE Healthcare) in 5 mM HEPES pH 7.5, 100 mM NaCl and 5 mM dithiothreitol. Protein was used immediately or stored at -80°C.

Crystallization, data collection, structure determination and refinement

Crystals were obtained at 4°C by the hanging drop vapor diffusion method. One microliter of SeMet labeled K210M N269M Zuo1₁₆₆₋₃₀₃ (15 mg/ml) was mixed with one microliter of crystallization buffer (100 mM BisTris, pH 6.5, 30% PEG 3350, 30 mM MgCl₂, 5 mM dithiothreitol). The reservoir volume was 0.5 ml.

Zuo1₁₆₆₋₃₀₃ crystals were flash-frozen in liquid nitrogen after cryo-protecting the crystals in cryo-solution containing mother liquor and 5% ethylene glycol. X-ray diffraction data were collected at 100 K at the Advanced Photon Source beamline 23-ID-D at a wavelength of 0.95372 Å. Data were processed using XDS (Kabsch, 2010). Phenix, AutoSol (Adams et al., 2010) was used to identify the selenium atoms, and generate the electron density map and initial model. A final model was obtained after several rounds of model building using Coot (Emsley and Cowtan, 2004) and refining with Phenix.refine (Adams et al., 2010). Ramachandran plot analysis was carried out using MolProbity (Chen et al., 2010). 99.6% of the residues were in favored regions; 100% were in allowed regions.

Molecular modeling and docking

For modeling of ZHD homologs, sequences were first aligned by Clustal Omega (Sievers et al., 2011). Then, using the *S. cerevisiae* Zuo1 ZHD structure as a template, model structures were generated using Modeller (Webb and Sali, 2014). All dockings were performed by initially positioning structures to the cryo-EM map of Zuo1/Ssz1 bound nonrotated ribosome and then optimizing by rigid-body docking using Chimera (Pettersen et al., 2004). To model Zuo1 binding to the ribosome in the nonrotated state, ribosome (PDB 3J78), Zuo1 4-helix bundle (PDB 2LWX), Zuo1 MD and Zuo1 ZHD were sequentially fitted to the cryo-EM map of Zuo1/Ssz1 bound nonrotated ribosome and joined together. Since the structure of only a small portion of the

MD has been experimentally determined, I-TASSER was used for modeling (Roy et al., 2010). First, residues 284-365 were modeled using the α -helical keratin 14 (PDB 3TNU) as a template. The model was fit to the cryo-EM map, and then overlapping residues between the N- and C-termini portions of the model (284-300 and 348-365) and the experimental structures of Zuo1 ZHD and Zuo1 4-helix bundle were deleted for sequential docking. Zuo1 bound to the rotated state was modeled by rotating the modeled MD/4-helix bundle structure (285-433) by 11 degrees perpendicular to the plane of rotation of the tip of ES12 centered at the alpha carbon of R285, to mimic the ratchet-like motion. To examine the capability of the ZHD:MD hinge to accommodate such ratchet-like movement of ribosome, the minimum energy state of the amino acids forming the hinge (283-285 and 221) was generated, after rotation of 11 degrees, using Chimera.

Yeast strains and plasmids

Unless otherwise stated strains used were of the W303 genetic background. A list of yeast plasmids used in this study is shown in Supplementary Table 1-1. Mutagenesis was carried out by QuikChange PCR mutagenesis (Stratagene), using the standard protocol.

A previously described *zuo1::HIS3* deletion (James et al., 1997; Yan et al., 1998), was used for analysis of *ZUO1* mutants. Strains were passaged thrice on rich medium containing 1 mM GuHCl to ensure the absence of prions, as the [*PSI*⁺] prion is known to affect stop codon readthrough. All plasmids used containing wild-type and mutant forms of *ZUO1* were centromeric, based on the pRS plasmid series (Mumberg et al., 1995; Sikorski and Hieter, 1989). Reduced expression level of Zuo1 was achieved by growing cells expressing Zuo1 under the control of the *MET3* promoter (Mountain, 1991) on selective minimal glucose media containing 400 μ g/ml methionine.

For analysis of rDNA mutants, KAY488 (Nemoto et al., 2010), which has a deletion of the ~150 repeats of ribosomal DNA (RDN) encoding 5S, 5.8S, 18S and 25S rRNA, and harbors the plasmid pRDN-hyg1, was used. pNOY373, a 2 μ plasmid containing the *LEU2* gene and a RDN repeat, was used to construct variants of 18S and 25S rRNA. For ease of mutant creation, segments of RDN were subcloned, and then transferred back into pNOY373 after construction by QuikChange PCR mutagenesis (Stratagene). For construction of ES12 and H24 mutants, a Nde1-Mlu1 fragment was used; for the H59 mutant a Mlu1 and Xho1 fragment was used. KAY488 transformed with pNOY373 or derivatives were plated on 5-FOA to select against the original plasmid, which contains the *URA3* gene. After selection, plasmids were rescued from KAY488 and sequenced to ensure the presence of the mutation prior to carrying out experiments.

Crosslinking

p-benzoyl-L-phenylalanine (Bpa) cross-linking was fundamentally carried out as previously described, using plasmid ptRNA-Bpa, which encodes a variant tRNA synthetase and tRNA_{CUA} for Bpa incorporation (Krishnamurthy et al., 2011; Ting et al., 2014). An amber stop codon (TAG) was introduced into the open reading frames of *ZUO1*, *RPL31A* or *RPL22A* on the plasmids pRS315-Zuo1, pRS416TEF-Rpl31A-HA or pRS316-Rpl22A-HA. Cells were grown in the presence of 2 mM Bpa at 30°C in 50 ml of minimal media overnight in the dark, with a starting OD₆₀₀ of 0.06. Approximately 25 OD₆₀₀ of cells treated with 100 μ g/ml of cycloheximide were exposed to 365 nm UV (Stratalinker 1800 UV irradiator) for 1 hr at 4°C to activate Bpa, while the same amount of cells was kept at 4°C as a control. Cells were lysed via agitation for 5 min at 4°C in lysis buffer (300 mM sorbitol, 20 mM HEPES-KOH pH 7.4, 1 mM EGTA, 5 mM MgCl₂, 10 mM KCl, 10% glycerol, 2 mM β -mercaptoethanol, RNasin

Ribonuclease Inhibitor (Promega) at a dilution of 1:1000) with glass beads. 5 OD₂₆₀ units of cell lysates were loaded onto a 2 ml sucrose cushion containing lysis buffer with 0.5 M sucrose instead of sorbitol. Ribosomes were pelleted by centrifugation for 3 hr at 50,000 rpm in a TLA 100.3 rotor (Beckman Coulter) at 4°C. The ribosome-containing pellet was suspended in SDS sample buffer (0.124 M Tris-HCl buffer pH 6.8 containing 4% SDS, 10% glycerol, 0.02% bromophenol blue and 4.5% β-mercaptoethanol) and used for immunoblotting. HA tag-specific antibody (Covance, no longer available and Abcam, catalog number: ab91110) was used to detect HA-tagged eL31a and eL22a. A rabbit polyclonal antibody generated using a fusion between Zuo1₁₆₆₋₂₈₄ and glutathione-S-transferase (GST) was used to detect Zuo1 (see Supplementary Fig. 2-3e). To detect Ssz1, a rabbit polyclonal antibody to a GST fusion of the ATPase domain (residues 1-401) of Ssz1 was used (Eisenman and Craig, 2004). Crosslinking was carried out with cells of the DS10 strain background (Stone and Craig, 1990). For eL31a and eL22a crosslinking, *rpl31aΔ::KanMX* and *rpl22a::TRP1* strains, respectively, were used. For Zuo1 crosslinking, a *zuo1Δ rpl31aΔ* strain carrying the pRS416TEF-Rpl31a-HA plasmid was constructed.

Ribosome sedimentation analysis

For preparation of yeast cell lysates, cells were grown at 30°C, to mid-log phase in selective minimal medium, 100 μg/ml of cycloheximide was added and cells immediately harvested by centrifugation at 4°C. Cells were washed and resuspended in ice-cold buffer A (20 mM Tris-HCl pH 7.5, 50 mM KCl and 5 mM MgCl₂) plus 1.5 mM pepstatin, cOmplete Mini EDTA-free Protease Inhibitor Cocktail (Roche) and 20 units of Recombinant RNasin Ribonuclease Inhibitor (Promega). Cells were lysed using a Retsch MM400 mixer mill, after freezing in liquid nitrogen. After lysis, 0.2 ml of ice-cold buffer A was added and the cell lysate

was clarified by centrifugation. To separate ribosomes from soluble proteins, 5 OD₂₆₀ units of lysates were applied to the top of a 2 ml sucrose cushion (buffer A containing 0.5 M sucrose) and centrifuged for 3 hrs at 50,000 rpm at 4°C in a TLA100.3 rotor (Beckman Coulter). The supernatant was removed and precipitated with 86% acetone overnight at -20°C. The ribosome and precipitated protein pellets were resuspended in SDS sample buffer by shaking at 4°C. Equivalent amounts of total lysate, supernatant and ribosome fractions were analyzed by SDS-PAGE and immunoblot analysis. Antibodies used: Ssa, rabbit polyclonal using segment containing residues 239-589 fused to GST as an immunogen (Halladay and Craig, 1995); uL3, mouse monoclonal made to *S. cerevisiae* uL3 (Vilardell and Warner, 1997) (kind gift of Jonathan Warner); Zuo1, rabbit polyclonal made using a segment containing residues 1-68 fused to GST as an immunogen (Yan et al., 1998).

Comparison of protein expression levels using immunoblot analysis was done as described previously (Kaschner et al., 2015). Briefly, equivalent numbers of cells were harvested by centrifugation, and lysed by incubation in 0.1 M NaOH for 5 min at room temperature. The lysate was centrifuged and the pellet was resuspended in 50 µl of SDS sample buffer and boiled for 5 min. Equal amounts of extracts were subjected to SDS-PAGE and immunoblot analysis.

Stop codon readthrough and -1 frameshifting analyses

Reporter plasmids for monitoring readthrough are based on pDB688 (Kramer et al., 2010; Salas-Marco and Bedwell, 2005), which has a translational fusion of the Renilla and firefly luciferase genes. To quantitatively study readthrough, an amber stop codon (TAG) flanked by CAA codons was introduced in the linker region between Renilla and firefly luciferase genes, because CAA codons flanking a stop codon have been shown to increase readthrough (Namy et

al., 2001). As a control, another plasmid was generated that has a sense codon with CAA codons on either side. Plasmids used for assessing frameshift frequencies having the firefly luciferase gene in the 0 frame (control) or -1 frame relative to the Renilla luciferase gene were a gift of J. Dinman (Muldoon-Jacobs and Dinman, 2006).

Luciferase assays were performed in a 96-well format using BioTek SynergyTM 2 multi-mode microplate reader and the Dual-Luciferase Reporter 1000 Assay System (Promega) as described previously (Salas-Marco and Bedwell, 2005). An equivalent number of cells were harvested and lysed using Passive Lysis Buffer according to the manufacturer's protocol. 5 µl of each of the lysates was taken in Lumitrac 200 96-well microplate (Greiner Bio-One) and firefly and Renilla luciferase activities were measured by sequential injection of 25 µl each of Luciferase Assay Reagent II and Stop & Glo buffer as described by the manufacturer. For each yeast strain tested, three individual transformants were assayed. An extract was made from each and assayed in duplicate. Negative controls that contained only Passive Lysis Buffer were used to determine the background and deducted from all the experimental values. The firefly/Renilla activity ratio generated for each of the reporter plasmids was divided by that for the respective control plasmids to obtain readthrough and frameshift efficiencies, which are reported as mean \pm standard error.

Phylogenetic tree analysis

Amino acid sequences of *S. cerevisiae* Zuo1 and Jjj1, *A. thaliana* ZRF1 and human DNAJC2p and DNAJC21p were used to identify the Zuo1 and Jjj1 orthologs used in this study by protein BLAST. The protein sequences were aligned using ClustalW conducted in MEGA7

(Kumar, 2016) and trees were constructed using the Maximum Likelihood (ML) method based on the JTT matrix-based model (Jones et al., 1992).

4. RESULTS

4.1. Structure of the ZHD of Zuo1

We pursued structural analysis of the region of Zuo1 that interacts with the 60S subunit by crystallizing the Zuo1 segment spanning residues 166-303. This segment extends through the ZHD and includes a segment of the MD domain (Fig. 2-1a). Initial attempts to solve the structure of the selenomethionine (SeMet) labeled wild type protein resulted in poorly diffracting crystals, and inadequate anomalous diffraction due to low methionine content. We therefore substituted codons Lys210 and Asn269 with methionine codons to enable additional SeMet incorporation. These sites were chosen for substitution based on the observation that methionine is present at these positions in some Zuo1 orthologs, including human DnaJC2. We determined the structure of the selenomethionine-substituted variant to a resolution of 1.85 Å using the single-wavelength anomalous diffraction (SAD) method (Fig. 2-1b; Table 1). Two molecules are present in the asymmetric unit (Supplementary Fig. 2-1a). Both contain four helices (Fig. 2-1b). Helices I-III form a three helix bundle, with helix IV positioned at a 120-degree angle relative to helix III. The major difference between the monomers of the asymmetric unit occurs in the long flexible loop between helices II and III (residues 230-247) (Supplementary Fig. 2-1a). Helix IV in the structure presented here is the N-terminal portion of the MD that spans the subunits. We note that throughout, we refer to residues 184-285 of the structure presented here as the ZHD. Previously, however, the segment encompassing residues 205-285, which does not include helix

I, were referred to as the ZHD (Albanese et al., 2010; Kaschner et al., 2015). See Supplementary Fig. 2-1c for further explanation.

Helix I, helix II and the extreme C-terminal 11 residues of helix III (272-282) form the hydrophobic core of the ZHD three helix bundle. Residues Phe184, Phe192, Val217, Phe220, Tyr221, Trp224, and Val276 within this hydrophobic pocket are highly conserved among Zuo1 orthologs. The later 4 are highly conserved in Jjj1 and its orthologs as well (Fig. 2-1b). The 37 residue helix III is continuous and extended in both monomers of the asymmetric unit (Supplementary Fig. 2-1a). At its tip are two conserved arginines (Arg247, Arg251), which we previously reported to be important for ribosome association and function of both Zuo1 and Jjj1 (Kaschner et al., 2015) (Fig. 2-1b). The 120-degree angle kink between helices III and IV is centered on proline 284, and is stabilized primarily by interactions involving the side chains of Asp283 and Arg285, which are invariant in both Zuo1 and Jjj1 orthologs (Supplementary Fig. 2-1b, d). Pro284 is not as highly conserved. Although most Zuo1 orthologs have a proline at this position, some insects and plants have lysine, glutamic acid or alanine. On the other hand, although several fungi have a proline at this position, *Saccharomyces cerevisiae* Jjj1 and most of its orthologs have a positively charged residue. Modeling of the ZHD region of Zuo1 and Jjj1 human orthologs using *S. cerevisiae* ZHD as a template generated similar structures of the ZHD and junction with helix IV (Supplementary Fig. 2-1c), consistent with the possibility that ZHD domains are structurally similar in both Jjj1 and Zuo1 orthologs.

4.2. The ZHD-60S subunit interaction

Using this new structural information as a guide, we performed *in vivo* site-specific cross-linking to probe the interaction of Zuo1 with two previously implicated surface exposed

ribosomal proteins near the polypeptide exit site, eL22 and eL31 (Leidig et al., 2013; Peisker et al., 2008; Zhang et al., 2014) (Fig. 2-2a). The nonnatural, photo-activable amino acid p-benzoyl-L-phenylalanine (Bpa) was incorporated in place of endogenous, surface exposed residues by enhanced nonsense suppression at 21 positions in eL22 and 12 positions in eL31 (Supplementary Fig. 2-2a). After exposure of cells to UV, strong crosslink products migrating at approximately 90 kDa were detected for three eL31 variants, those having Bpa at positions Arg79 and Glu81 in the surface exposed loop and at position Val7, in a nearby β -strand. Each reacted with Zuo1-specific antibodies (Fig. 2-2b). Weaker, Zuo1-reacting bands were detected when Bpa was incorporated at adjacent positions on the loop (Glu82, Glu83 or Asp84) (Supplementary Fig. 2-2b). These results give strong support to the idea that eL31 interacts with Zuo1. No eL22 crosslinks to Zuo1 were detected in our analysis of 21 Bpa variants.

Bpa was also incorporated into Zuo1. We focused on the interval between residues 236 and 281, which encompasses helix III and a portion of the adjacent long loop, because it contains the most highly conserved surface exposed residues, including Arg247 and Arg251 known to be important for ribosome association (Kaschner et al., 2015). Bpa was successfully incorporated at 26 positions (Supplementary Fig. 2-2c). No crosslinks were detected when Bpa was incorporated in the segment of Zuo1 surrounding Arg247 and Arg251. However, Thr266_{Bpa} and Val273_{Bpa} generated strong crosslinks to eL31, while 6 other variants having Bpa between positions 262 to 281 crosslinked weakly to eL31 (Fig. 2-2c; Supplementary Fig. 2c-e). Earlier reports indicated that deletion of the entire eL31 gene results in only slight destabilization of the Zuo1-ribosome interaction (Peisker et al., 2008). Therefore, we anticipated that residues interacting with eL31 would not substantially affect association of Zuo1 with the ribosome. Consistent with this view, a variant altered for three residues on the exposed surface of helix III, Asp262Ala, Thr266Ala

and Val273Ala, co-migrated with ribosomes during centrifugation of cell lysates through sucrose cushions (Supplementary Fig. 2-2f).

Crosslinking of the C-terminus of helix III of Zuo1 to eL31 was key, as it allowed us to begin to position the ZHD on the 60S subunit. First, the face of the C-terminal segment of helix III having Thr266 and Val273 was manually docked to the surface-exposed loop and adjacent β -strand of eL31. The Arg247 and Arg251 residues at the N-terminal tip were pointed either towards H24 rRNA or towards H59 rRNA/eL22, as two reported cryo-EM analyses indicated these as sites of possible interaction of Zuo1 (Leidig et al., 2013; Zhang et al., 2014). The interactions for both positions were then optimized by rigid body docking within the density map of Zuo1-Ssz1 bound 60S (Zhang et al., 2014) (Supplementary Fig. 2-3). Neither model fit perfectly within the 7.2 Å density dataset used in the docking. For example, relevant to the H24 model, density is lacking near the tip of the H24 rRNA helix. In the case of the H59/eL22 model, helix IV, that is the beginning of the MD, projected away from the 40S subunit and thus away from the density ascribed to the extended MD.

Therefore, we decided to experimentally test whether H24 or H59 is important for Zuo1's interaction with the ribosome. We made use of a *S. cerevisiae* strain in which the ~150 chromosomal rDNA repeats are completely deleted and their essential function supported by rRNA transcribed from a plasmid carrying a single rDNA repeat (Wai et al., 2000). The terminal base pair of H24 or the five most terminal base pairs of H59 were removed, resulting in strains rRNA_{H24Δ1} and rRNA_{H59Δ5} (Fig. 2-2d, Supplementary Fig. 2-2g). The vast majority of Zuo1 in extracts of rRNA_{H59Δ5} cells pelleted with ribosomes through a sucrose cushion, even though the deletion of 5 base pairs removed the surface exposed portion of the helix. On the other hand, most of Zuo1 was found in the supernatant fraction when extracts of rRNA_{H24Δ1} cells were

analyzed, indicating that Zuo1's interaction with the ribosome is destabilized upon alteration of H24.

Together, these genetic, crosslinking and modeling results are consistent with the idea that H24 interacts with Arg247 and Arg251 of ZHD's helix III (Fig. 2-2e), and with the previously demonstrated importance of interactions with rRNA for association of Zuo1 with the ribosome (Peisker et al., 2008; Yan et al., 1998). As these arginines are conserved in Jjj1 (Arg221 and Arg225) and earlier cryo-EM studies pointed to interaction of Jjj1 with the exposed loop of eL31 (Greber et al., 2012; Zhang et al., 2014) the conserved segment of Jjj1 may well interact with the 60S subunit in a similar manner. We also note that although we observed no crosslink between eL22 and Zuo1, two cryo-EM studies suggest an interaction between these two proteins. It is quite possible that a region of Zuo1 not tested (e.g. the J domain) interacts with eL22 and this interaction was not detected for technical reasons in our eL22 crosslinking analysis.

4.3. The Zuo1-40S subunit interaction

Recent cryo-EM analysis suggests that Zuo1 contacts the 40S subunit via interaction with ES12 of H44 (Zhang et al., 2014). To verify this idea, we constructed a strain whose ribosomes lack the terminal 10 base pairs of ES12 (Fig. 2-3a; Supplementary Fig. 2-4a). The majority of Zuo1 remained in the supernatant after pelleting of ribosomes in extracts of rRNA_{ES12Δ10} cells (Fig. 2-3a). The Zuo1 C-terminal 4-helix bundle and the C-terminal end of the MD have been suggested to associate with the 40S subunit (Zhang et al., 2014). Both this segment of the MD and helix I of the 4-helix bundle (348-363) contain positively charged residues, which are thus candidates for interaction with ES12. We altered 6 of these, Lys341, Lys342 and Lys344 in the

MD and Lys348, Lys352 and Lys353 in helix I, individually to alanines. Interaction of each variant with the ribosome was partially destabilized, as a portion did not co-sediment with ribosomes (Fig. 2-3b). We then constructed triple mutants, combining the alanine substitutions of the MD or helix I. The vast majority of Zuo1_{Lys341/342/344Ala} and Zuo1_{Lys348/352/353Ala} did not co-sediment with ribosomes through a sucrose cushion (Fig. 2-3c, Supplementary Fig. 2-4b), indicating that most of the Zuo1-ribosome complexes were destabilized to the extent that they did not persist through the centrifugation procedure. Together, our results give strong support to the idea that ES12 of H44 of the 18S rRNA interacts with the C-terminal portion of the MD and helix I of Zuo1's C-terminal 4-helix bundle.

The base of H44 is in close proximity to the decoding center. Thus, binding of Zuo1 to ES12 raises the question as to the importance of the Zuo1-40S subunit interaction to Zuo1's known effect on translational fidelity (i.e. readthrough and -1 frameshifting). To address this issue, we constructed a C-terminal deletion mutant, *zuo1*₁₋₃₁₀, which removes the segment of *ZUO1* that encodes the 4-helix bundle and a portion of the MD helix, eliminating the possibility of interaction with ES12. As a control, we analyzed cells carrying wild type Zuo1 expressed under the control of the repressible promoter *MET3* (called *ZUO1*_{Low}); in the presence of high methionine Zuo1 is expressed at less than 5% of normal levels (Supplementary Fig. 2-4c). As previously reported (Hundley et al., 2002), such low levels of Zuo1 substantially suppressed the slow growth and cation-sensitive phenotypes of *zuo1*Δ cells, as do Zuo1₁₋₃₁₀ and Zuo1_{Lys348/352/353Ala} (Supplementary Fig. 2-4d).

Translational readthrough and -1 frameshifting were assessed using a dual luciferase system in which reporter plasmids have a translational fusion between the sea pansy luciferase (RLuc) gene and the downstream firefly luciferase (Fluc) gene. As test sequences are located

within the linker between the genes (Fig. 2-3d), Fluc serves as the reporter and Rluc as the internal control. To measure readthrough the test plasmid contained a TAG stop codon in the linker region. Wild type cells having this plasmid had 2.6% of the Fluc activity of cells harboring the control plasmid with a sense codon at that position (Fig. 2-3d). Readthrough in *zuo1_{Lys348/352/353Ala}* and *zuo1₁₋₃₁₀* cells was 160% and 210% of that in wild type cells, respectively. In *ZUO1_{Low}* cells readthrough was only 110% of the wild type level. For assessing -1 frameshifting, the reporter plasmid, previously used to demonstrate a ~50% reduction in -1 frameshifting of a *zuo1Δ* strain (Muldoon-Jacobs and Dinman, 2006), which contains a -1 shift in reading frame and a viral sequence programmed for -1 frameshifting, was used (Fig. 2-3d). -1 frameshifting in *zuo1_{Lys348/352/353Ala}* and *zuo1₁₋₃₁₀* cells was 50% and 61% of that in *ZUO1* cells, respectively, while that in *ZUO1_{Low}* cells approached wild type levels at 88%. We also tested *rRNA_{ES12Δ10}* cells in which the 40S Zuo1 binding site is deleted. Readthrough was increased (150% of wild type) and -1 frameshifting decreased (52% of wild type) in *rRNA_{ES12Δ10}* (Fig. 2-3d). Together, these results are consistent with the idea that Zuo1's interaction with the 40S subunit, more specifically with the tip of H44 (i.e. ES12) of 18S rRNA, is important for Zuo1 function in translational fidelity. In addition, consistent with a previous report (Rakwalska and Rospert, 2004), the J domain, and thus functional interaction with Hsp70, is also required for Zuo1 function in translation fidelity, as alteration of the conserved HisProAsp motif of the J domain resulted in increased readthrough and decreased -1 frameshifting (Supplementary Fig. 2-4e).

4.4. Zuo1 spanning of the 40S and 60S subunits

The 40S subunit rotates on the order of 11° relative to the 60S subunit during a round of peptide bond formation (Svidritskiy et al., 2014). Zuo1 is able to bind to ribosomes that are in both the nonrotated and rotated states (Zhang et al., 2014). But, how Zuo1 accommodates such movement is not known. Recent results (Zhang et al., 2014) indicate that the rigidity of the MD helix, which links the ribosome interacting domains, is functionally important. Therefore, we more thoroughly analyzed the junction between the ZHD and the MD as a candidate for playing a role in orienting the C-terminal 4-helix bundle for interaction with the 40S subunit and for accommodating rotation of the subunits. The helix III-helix IV 120° angled junction is centered on Pro284 and stabilized by several interactions (Fig. 2-4a, Supplementary Fig. 2-1b): (1) the salt bridge between the side chains of Asp283 and Arg285, (2) a hydrogen bond between Asp283 and Tyr221 and (3) interaction of Asp283 with the amide backbone between Pro284 and Arg285. Residues Asp283, Arg285 and Tyr221 are all well resolved in the electron density maps with the side chain B-factor of 24.46 \AA^2 , 20.67 \AA^2 , and 22.91 \AA^2 , respectively. We experimentally assessed the importance of this junction, altering Tyr221, Asp283, Pro284 and Arg285, each to alanine. Single alterations had minimal effects on cell growth even in the presence of cations (Supplementary Fig. 2-4f). The majority of all variants co-migrated with ribosomes through a sucrose cushion, but a portion of Zuo1_{Asp283Ala} was present in the supernatant, suggesting an alteration in ribosome association (Fig. 2-4b). Cells expressing Zuo1_{Asp283Ala}, but not other variants, were defective in translational readthrough and -1 frameshifting, having 176% higher readthrough and only 40% the level of frameshifting compared to wild type cells (Fig 2-4b). This *in vivo* effect of altering Asp283, the predominant interacting component of the junction,

indicates that this junction is functionally important and is consistent with a role in orienting the interaction of Zuo1 with the 40S subunit.

We next addressed the possible involvement of the ZHD-MD junction in accommodating subunit rotation. We modeled the entire ZHD-MD-4 helix bundle segment of Zuo1 (residues 169-433) using existing structural information. The entire segment was then positioned within the cryo-EM density of ribosome-bound Zuo1-Ssz1 in the nonrotated state (Zhang et al., 2014) (Fig. 2-4c), based on the positioning of the ZHD on the 60S subunit discussed in the previous section (Fig. 2-2e). The MD and 4 helix bundle segment of Zuo1 was then rotated 11 degrees relative to the ZHD. Upon this single change, the 4-helix bundle became positioned at the tip of ES12 in the rotated state, in a manner similar to that in the non-rotated state (Fig. 2-4c). To assess whether such movement could be accommodated by the junction without disrupting noncovalent interactions, the 11 degrees restraint was released for the Zuo1 ZHD-MD segment (169-303) through energy minimization. The distances between atoms forming the salt bridge and hydrogen bond at the junction changed minimally upon release, suggesting that the interactions could remain intact during subunit rotation (Fig. 2-4d). These results suggest a model in which a restrained flexibility of the ZHD-MD (i.e. helix III-helix IV) junction, which essentially forms a hinge, is important for accommodating subunit rotation, allowing Zuo1 interaction with both subunits during rounds of translation.

5. DISCUSSION

There is a growing appreciation of the importance of cellular strategies that ensure both the fidelity of the translation process itself and the productive folding of the protein synthesized (Hilal and Spahn, 2015; Pechmann et al., 2013; Shen et al., 2015). Data, both presented here and

previously published (Zhang et al., 2014), points to how Zuo1's dual interaction with the 40S and the 60S ribosomal subunits may enable it to play a key role in such protein quality control (Fig. 2-5). It is tempting to speculate that Zuo1 serves a unique role as it is positioned to monitor and/or fine tune codon-anticodon interactions and thus peptide bond formation, as well as nascent polypeptide chain folding/transit within the tunnel.

A picture of Zuo1's bipartite ribosome interaction is emerging. As suggested earlier (Zhang et al., 2014), and verified here, functional connection to the decoding center of the 40S subunit occurs via interaction of Zuo1's C-terminal 4-helix bundle with ES12 of H44. Disruption of this interaction, either by altering rRNA or Zuo1 binding sites, increases translational readthrough of stop codons and decreases -1 frameshifting. Nucleotides near the base of H44 interact with codon-anticodons base pairs and release factors regulating translation rate and ensuring accuracy of translation elongation and termination (Carter et al., 2000; Youngman et al., 2006; Zaher and Green, 2009). Thus, through interaction with ES12, Zuo1 could monitor decoding or possibly affect the proofreading process itself. In regards to Zuo1 playing a signaling/monitoring role, it is also intriguing that helix III of the ZHD interacts with H24 of 25S rRNA on the surface of the 60S subunit (Fig. 2-5). Interestingly, H24 also interacts with uL22 (previously called L17 in eukaryotes). uL22 extends from the subunit surface into the subunit interior forming a patch on the wall of the exit tunnel at its constriction point, which serves as a monitoring gate for translation arrest or pausing (Fulle and Gohlke, 2009; Lin et al., 2011; Nakatogawa and Ito, 2002; Zhang et al., 2013). There is abundant evidence in both prokaryotes and eukaryotes that interaction of the nascent chain with the tunnel interior plays a signaling role (Wilson and Beckmann, 2011). In most cases this signaling is thought to affect the rate of peptide bond formation at the peptidyl transferase site. However, there is evidence that uL22 also

signals to the ribosome surface near the exit site (Pechmann et al., 2013; Pool, 2009; Wilson and Beckmann, 2011).

The positioning of Zuo1 near the exit site and its contact with H44 suggests the possibility of regulatory functions for both interactions. In addition, structural and crosslinking data point to a possible line of communication between them, with helix III of the ZHD interacting with 60S subunit, and the adjacent MD helix extending to the 40S subunit. The intramolecular interactions at the junction between the ZHD and the MD (helices III and IV of the structure reported here) are predicted to be flexible enough to accommodate ribosome movement associated with a round of peptide bond formation, that is movement between the nonrotated and rotated states. In a purified system Zuo1 binding stabilized 80S ribosomes in the nonrotated state (Zhang et al., 2014), consistent with possible influence on the rate of peptide bond formation. Since translation rate has been linked to translation fidelity (Fluitt et al., 2007; Zaher and Green, 2009), Zuo1 binding may affect fidelity in this way as well.

What role might Zuo1's dual interaction with the ribosome play? One can imagine that it could either play a sensing role(s), signaling back to its partner Hsp70 Ssb, or act as a conduit for a signal from Ssb. For example, Zuo1 could serve as a sensor of activity at the decoding center and/or from within the tunnel, providing feedback to regulate Hsp70 activity. Such feedback might result in altering the timing of its J domain activity to stimulate Hsp70's ATPase activity and thus Hsp70's interaction with the nascent chain. Alternatively, Zuo1 could be the recipient of a signal from either Ssb or the atypical Hsp70 Ssz1. Upon interaction with a nascent chain exiting the tunnel, a signal to regulate peptide bond formation might be made through Zuo1's contacts with the 40S and/or 60S subunits.

Regardless of exact mechanisms, such ideas are reminiscent of the well-established role of the multimeric RNA-protein complex, signal recognition particle (SRP) (Wild et al., 2004). To our knowledge eukaryotic SRP is the only other factor known to span ribosomal subunits, connecting such distant sites. However, SRP action is both more specific and more direct than that of Zuo1. There is no evidence that Zuo1 directly binds nascent chains. SRP not only interacts directly with a signal sequence on the nascent chain upon its exit from the tunnel, it interacts directly with the decoding center to attenuate protein synthesis until the signal sequence contacts its receptor on the endoplasmic reticulum (Elvekrog and Walter, 2015; Wild et al., 2004). Zuo1 likely has a more general function, coupling protein folding to translation rate. A connection between translation rate and both translation fidelity and productive protein folding has been noted previously (Sherman and Qian, 2013; Zaher and Green, 2009). Thus, fine tuning of coupling of these events likely plays an important role in protein homeostasis.

It is also interesting to note that Zuo1 and its orthologs have diverse regulatory functions off the ribosome, consistent with evidence that its interaction with the ribosome is marginally stable and likely dynamic (Ducett et al., 2013; Yan et al., 1998). For example, *S. cerevisiae* Zuo1 activates Pdr1, a transcription factor implicated in quorum sensing (Ducett et al., 2013; Prunuske et al., 2012). Human DnaJC2 functions as a chromatin modulator, affecting development and DNA repair (Gracheva et al., 2016; Richly et al., 2010). Thus, via both on- and off-ribosome functions, Zuo1/DnaJC2 may play a more global regulatory role than we presently appreciate, coordinating protein synthesis and folding with other aspects of gene expression and cell physiology.

Accession code: Atomic coordinates and structure factors have been deposited to the Protein Data Bank with the accession code 5DJE.

6. ACKNOWLEDGMENTS

We thank: A. Senes, J. Keck and S. Butcher for helpful discussions during the course of this work; D. Bedwell (U. Alabama), P. Farabaugh (U. Maryland Baltimore County) and J. Dinman (U. Maryland) for dual luciferase plasmids; K. Asano (Kansas State U.) for the rDNA deletion strain; J. Warner (Albert Einstein College of Medicine) for uL3 antibody.

7. AUTHOR CONTRIBUTIONS

K.L. performed *in vivo* crosslinking experiments, analyses of ribosome association, generation of mutants and other molecular biological experiments. R.S. performed *in vivo* misreading experiments, analyses of ribosome association, generation of mutants and other molecular biological experiments. O.K.S. performed crystallographic analysis, analyses of ribosome association and generation of mutants. C.B. performed crystallographic analysis. E.A.C. oversaw all aspects of the experiments and manuscript preparation. All authors participated in interpreting the data and writing the paper.

8. FIGURES AND TABLES

Figure 2-1. Structure of the Zuotin homology domain (ZHD) of Zuo1. (a) Overall architecture of Zuo1 (left) and its interaction with the ribosome (right). The N terminus (N) of Zuo1, which interacts with the atypical Hsp70 Ssz1, is adjacent to the J domain (J). The ZHD spans residues 184–285. A predicted long α -helix constituting the middle domain (MD, green) connects the ZHD and the C-terminal four-helix bundle (yellow). Zuo1 interacts with the 60S and 40S subunits via the ZHD and four-helix bundle, respectively. (b) Ribbon representation of the crystal structure of residues 169–303 of Zuo1. Purple, ZHD; green, MD. Helices I–IV are labeled. Hydrophobic amino acids constituting the hydrophobic core of the helix bundle formed by helices I–III are in stick representation (top right). Arg247 and Arg251 at the N-terminal tip of helix III, which are important for Zuo1’s interaction with the ribosome, are in stick representation (bottom right).

Figure 2-1

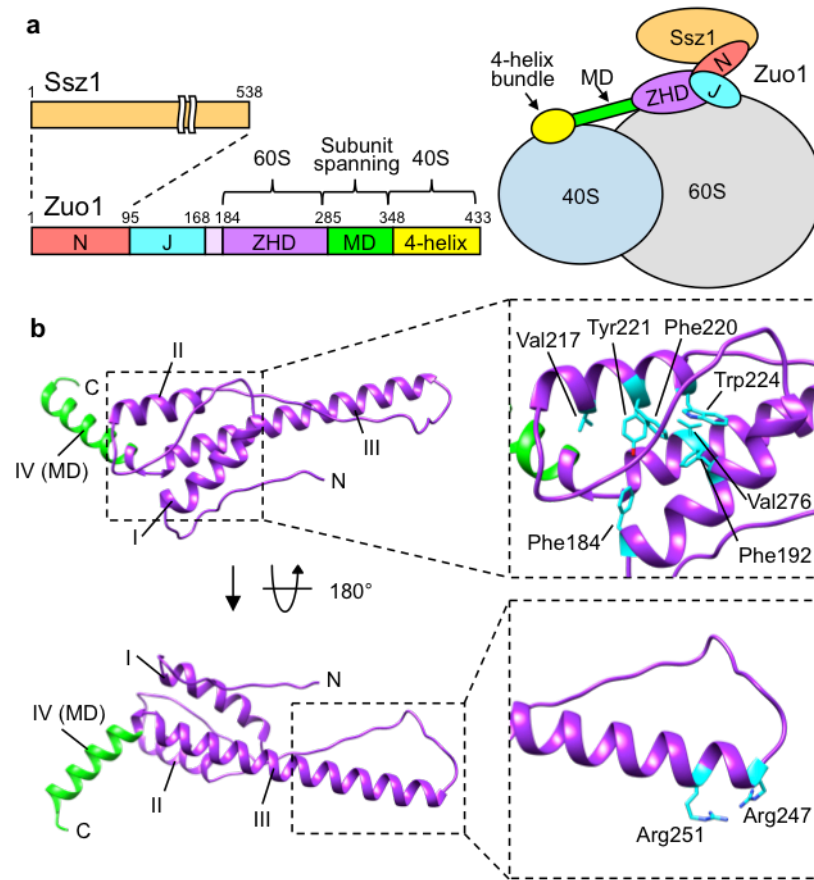


Figure 2-2. Interaction of Zuo1 with the 60S subunit. (a) Overview of previously implicated contact sites for Zuo1 near the polypeptide tunnel exit (PTE) of 60S. (b,c) Site-specific cross-linking between eL31a and Zuo1. Cells expressing variants of hemagglutinin (HA)-tagged eL31a (b) or Zuo1 (c), with Bpa incorporated at the indicated positions, were exposed to UV light (+) or left unexposed as a control (–). Cross-linking was analyzed by immunoblotting with antibodies specific for Zuo1 or the HA tag (eL31) after SDS–PAGE. MW, molecular weight. Zuo1 and HA bands are indicated with arrows. Two independent yeast strains were analyzed for each Bpa variant, with similar results. (d) Effect of 60S rRNA deletions on Zuo1 ribosome association. Lysates from cells expressing wild-type (WT) or mutant rRNAs with 1 bp of H24 (H24Δ1) or 5 bp of H59 (H59Δ5) deleted were centrifuged through a sucrose cushion. Equivalent amounts of supernatant (S) and pellet (P) fractions, as well as total lysates (T), were analyzed by immunoblotting. Antibodies specific for Zuo1, and for uL3 and Ssa (controls for ribosomes and a predominantly soluble protein, respectively) were used. One representative immunoblot (from three independent experiments, performed with different yeast cultures) is shown. (e) Docking of Zuo1 ZHD to 60S. The atomic structures of Zuo1 169–303 and ribosome (PDB 3J78) were fitted to the cryo-EM map of the Zuo1–Ssz1-bound ribosome by rigid-body docking. Residues whose cross-linking is presented in b and c are shown in sphere representation (orange, eL31; cyan, Zuo1); Zuo1 residues Arg247 and Arg251, which are known to be important for ribosome association, are also shown in sphere representation (cyan).

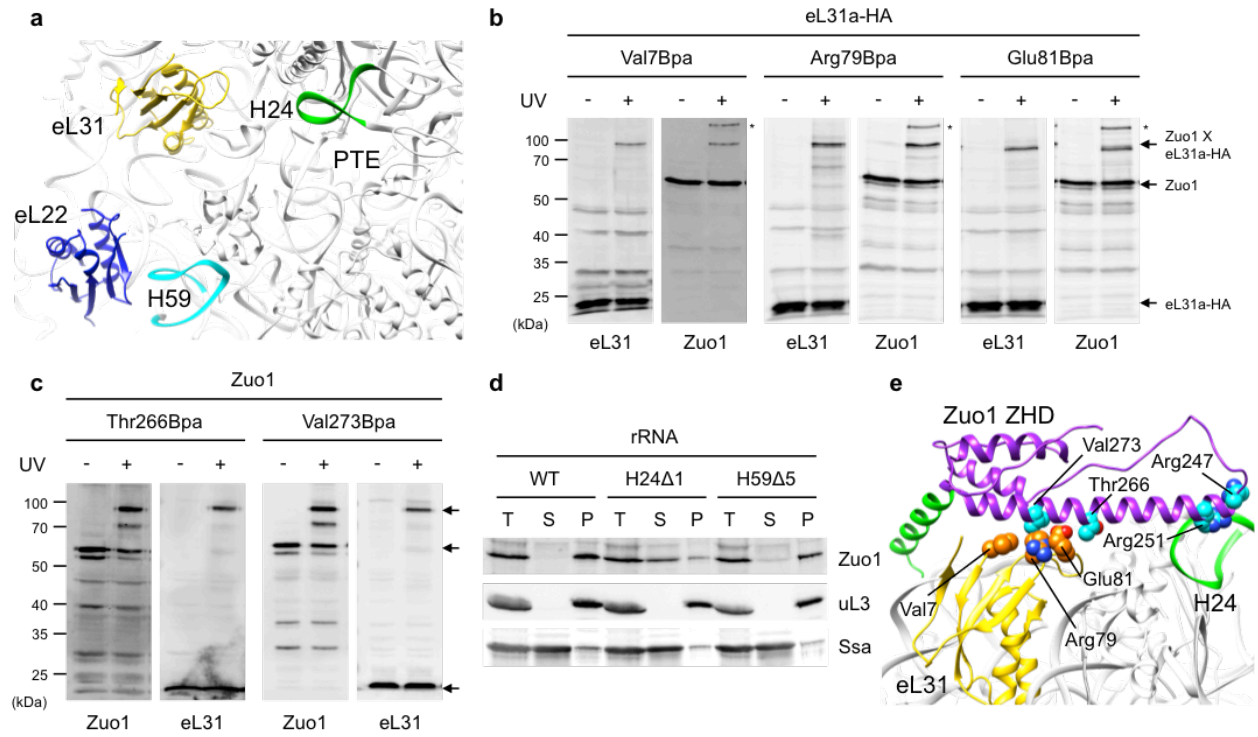
Figure 2-2

Figure 2-3. Interaction of the Zuo1 C terminus with the 40S ribosomal subunit and effect on translation fidelity. (a) Left, effect of ES12 deletion on ribosome association. Red, rRNA ES12; yellow, ES12 Δ 10 (Δ 10), which has 10 bp deleted. Right, stability of Zuo1's interaction with ribosomes in cells expressing one copy of rDNA. Lysates were centrifuged through sucrose cushions. Equivalent amounts of total lysate (T), supernatant (S) and pellet (P) fractions were subjected to electrophoresis and immunoblot analysis with antibodies specific for Zuo1, and for uL3 and Ssa (controls for ribosomes and a soluble protein, respectively). (b) Stability of the ribosome interaction of the indicated Zuo1 variants, each with an alanine substituted for a single lysine. Analysis was as in a. (c) Variants used for analysis of translational fidelity. Left, Zuo1 C-terminal four-helix bundle (residues 348–433; PDB 2LWX), with surface charge density showing the distribution of basic (blue) and acidic (red) residues. Middle, structure showing the three conserved lysine residues that were altered, highlighted as spheres. Right, *zuo1 Δ* cells expressing Zuo1 (WT), Zuo1_{K348/352/353A} (K₃A₃) or Zuo1_{1–310} (1–310), analyzed for ribosome association as in a. In a–c, one representative immunoblot (from three independent experiments, performed with different yeast cultures) is shown. (d) *In vivo* analyses of readthrough and –1 frameshifting. Top, cartoon of dual-luciferase reporters. Bottom, readthrough and –1 frameshifting in the mutants compared with control reporters in which no stop codon between genes was present, or genes were in frame. The relative changes in readthrough and frameshifting are shown; levels were set at 1 in the case of *zuo1 Δ* cells (open bars) expressing wild-type Zuo1 and in the case of rRNA_{sc}, cells carrying a single rDNA repeat (dark-gray bars) expressing wild-type rRNA. Strains are as indicated in a and c, with the addition of *ZUO1* under control of the *MET3* promoter (low) or with no Zuo1 (–). Data shown are mean and s.e.m. from three different yeast cultures, each evaluated at least twice.

Figure 2-3

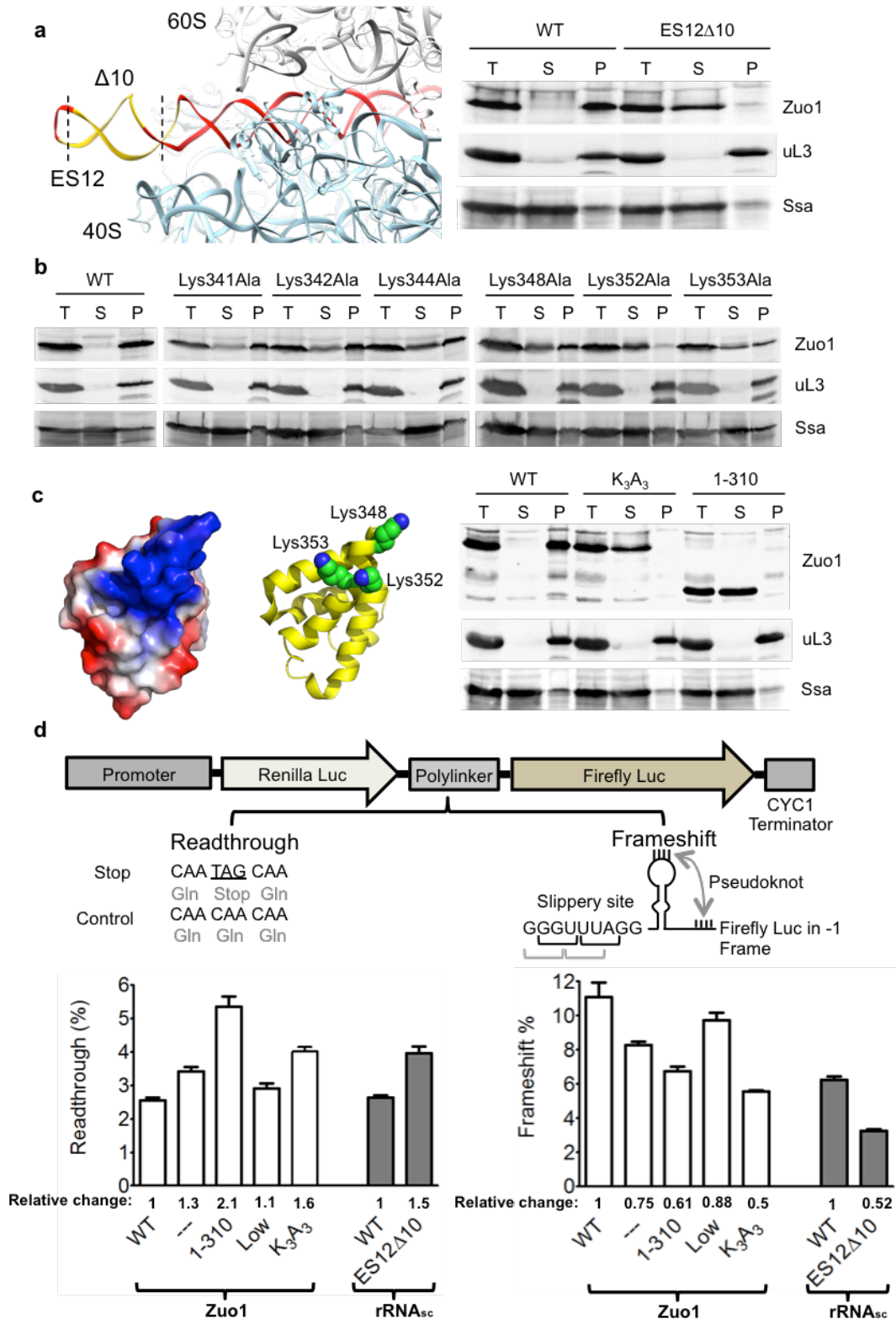


Figure 2-4. Positioning of the Zuo1 C-terminal four-helix bundle on 40S. (a) Junction between ZHD and MD. Atomic structure of ribosome (PDB 3J78) and Zuo1 residues 169–303 fitted to the cryo-EM density map of the Zuo1–Ssz1-bound ribosome by rigid-body docking. Inset, enlarged view of amino acids forming the 120°-angled hinge between helix III of ZHD and the N terminus of MD. The salt bridge and hydrogen bonds are shown as dashed lines among Tyr221, Asp283 and Arg285. (b) Effects of alteration of residues at the ZHD-MD junction. Top, stability of interaction of Zuo1 variants with ribosomes, analyzed by centrifugation of extracts through sucrose cushions; equivalent amounts of total lysate (T), supernatant (S) and pellet (P) fractions were subjected to electrophoresis and immunoblot analysis with the indicated antibodies. One representative immunoblot (from three independent experiments, performed with different yeast cultures) is shown. Bottom, analyses of *in vivo* readthrough and –1 frameshifting; relative levels in cells expressing wild-type Zuo1 are set at 1. Data shown are mean and s.e.m. from three different yeast cultures, each evaluated twice. (c) Model of Zuo1 binding to nonrotated and rotated states of the ribosome. Zuo1 residues 173–433 (ZHD–MD–four-helix bundle) and a ribosome (PDB 3J78) were sequentially fitted to a cryo-EM map of a Zuo1–Ssz1-bound nonrotated ribosome. Zuo1 bound to a ribosome in the rotated state was modeled by moving Zuo1 MD and the four-helix bundle by 11° relative to the nonrotated state to mimic the ratchet-like motion of the ribosome. (d) Accommodation of an 11° movement of the ZHD-MD hinge. The minimum-energy state of amino acids (orange) after 11° rotation of MD is superimposed on the junction shown in a (purple and green).

Figure 2-4

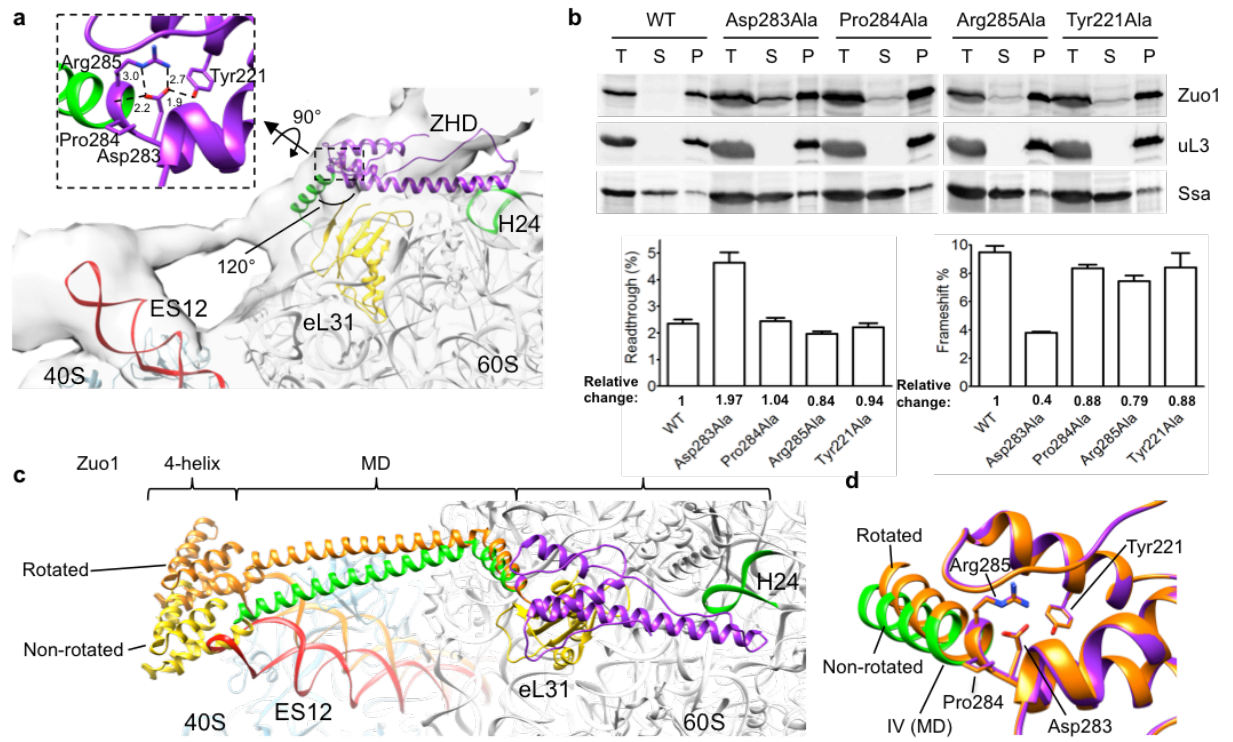


Figure 2-5. Model of the network of interaction of Zuo1 with the ribosome. (a) Proximity of H24, uL22 and the ribosome tunnel. H24 (green) on the subunit surface directly interacts with uL22 (magenta), which extends into the interior of the subunit, forming a patch on the tunnel surface. (b) Schematic diagram of Zuo1's interactions with the ribosome, implying Zuo1's function in coordinating protein translation and protein folding. Zuo1 monitors the transit of nascent polypeptide chains in the tunnel via its interaction with H24 (green), which in turn interacts with uL22 (magenta). Zuo1 monitors or regulates peptide-bond formation at the decoding center via interaction of its C-terminal four-helix bundle with ES12 of H44 (red), which originates at the decoding center. Through these interactions, Zuo1 functionally connects the two subunits of the ribosome.

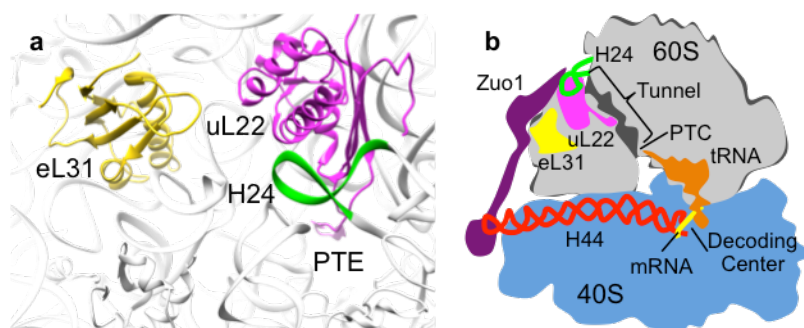
Figure 2-5

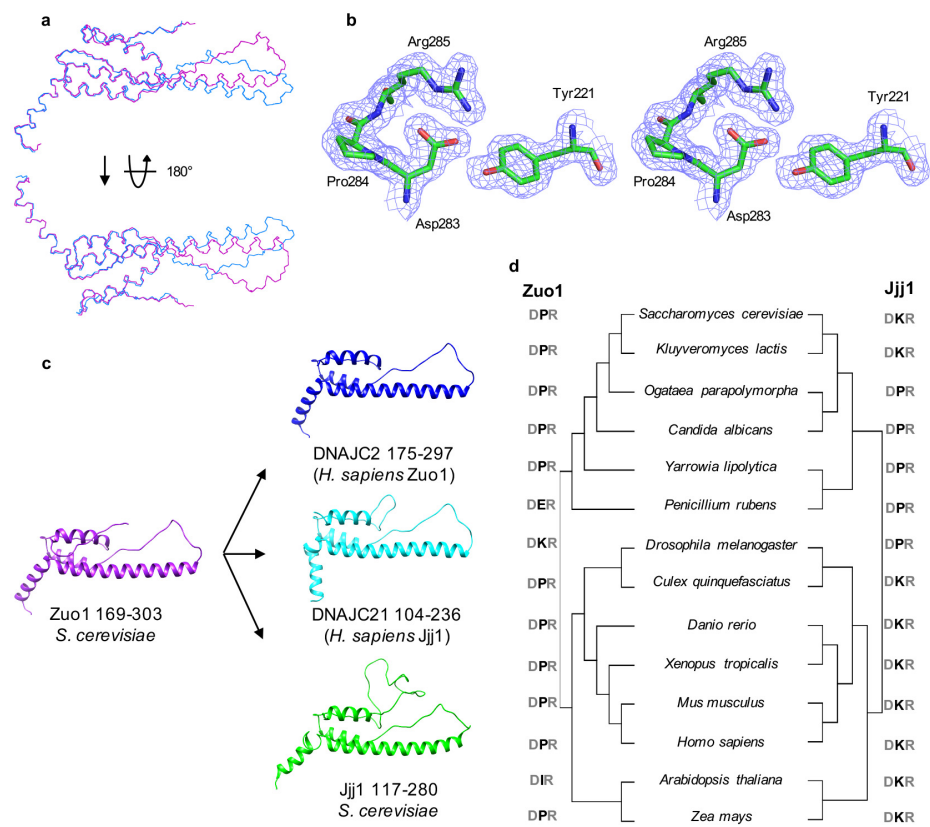
Table 1. Data collection and refinement statistics

	Zuo1 ₁₆₆₋₃₀₃ PDB 5DJE
Data collection	
Space group	P2 ₁ 2 ₁ 2 ₁
Cell dimensions	
<i>a</i> , <i>b</i> , <i>c</i> (Å)	60.33, 69.45, 95.08
<i>a</i> , <i>b</i> , <i>g</i> (°)	90, 90, 90
Resolution (Å)	47.67-1.85(1.92-1.85)
<i>R</i> _{merge}	0.1087(1.51)
<i>R</i> _{meas}	0.113
<i>CC</i> 1/2	0.999(0.636)
<i>CC</i> * ₂	1.000(0.882)
<i>I</i> / <i>sI</i>	16.76(1.77)
Completeness (%)	100(99)
Redundancy	13.2(12.8)
Refinement	
Resolution (Å)	1.85
No. reflections	35251
<i>R</i> _{work} / <i>R</i> _{free}	0.175/0.219
No. atoms	
Protein	2278
Ligand/ion	32
Water	96
<i>B</i> -factors	
Protein	38.5
Ligand/ion	52.9
Water	42.8
R.m.s. deviations	
Bond lengths (Å)	0.012
Bond angles (°)	1.23

Structure was determined from one crystal.
Values in parentheses are for highest resolution shell

Supplementary Figure 2-1. Structure and sequence analyses of the Zuotin homology domain (ZHD). (a) Superimposition of the two molecules of Zuo1 166-303 in the asymmetric unit. Chain A and B are colored blue and purple, respectively. No electron density was observed for residues 166-168 of chain A and 166-167 of chain B. The RMSD of alpha carbon positions is 2.8 Å. The major difference between chain A and B is the loop between helix II and helix III (residues 228-245). When these residues are excluded, the RMSD is 1.4 Å. Chain A and chain B have an average B-value of 35 and 40, respectively. Chain A was used throughout. Figure generated by PyMol. (b) Representative stereo image of the $2F_o - F_c$ electron density map of ZHD calculated after the final refinement contoured at 1.0 σ . Residues Tyr221, Asp283, Pro284 and Arg285 forming the hinge at the junction between ZHD and middle domain shown in stick representation. Figure generated by PyMol. (c) Model structures of the ZHD. *S. cerevisiae* and human Zuo1 and Jjj1 sequences were aligned by Clustal Omega. The resulting alignment was used for generating model structures by Modeller, employing the *S. cerevisiae* Zuo1 ZHD structure as a template. The ZHD of yeast Jjj1 contains an insertion between helix I and helix II that is not conserved in higher eukaryotes such as humans. This insertion and the lower conservation of helix I led to an initial definition of the ZHD (i.e. 205-285 of Zuo1) that lacked helix I. (d) Phylogenetic analysis of Zuo1 and Jjj1 and conservation of residues forming the hinge region in the two proteins. Amino acid sequences of Zuo1 and Jjj1 orthologs from the indicated organisms were aligned using ClustalW. The trees were constructed using the Maximum Likelihood method based on the JTT matrix-based model conducted using MEGA7. The three residues present at the hinge of Zuo1 and Jjj1 [Asp283(D), Pro284(P), Arg285(R) and Asp257(D), Lys258(K), Arg259(R), respectively] are shown indicating a high conservation of salt-bridge partners aspartic acid and arginine flanking a relatively variable residue.

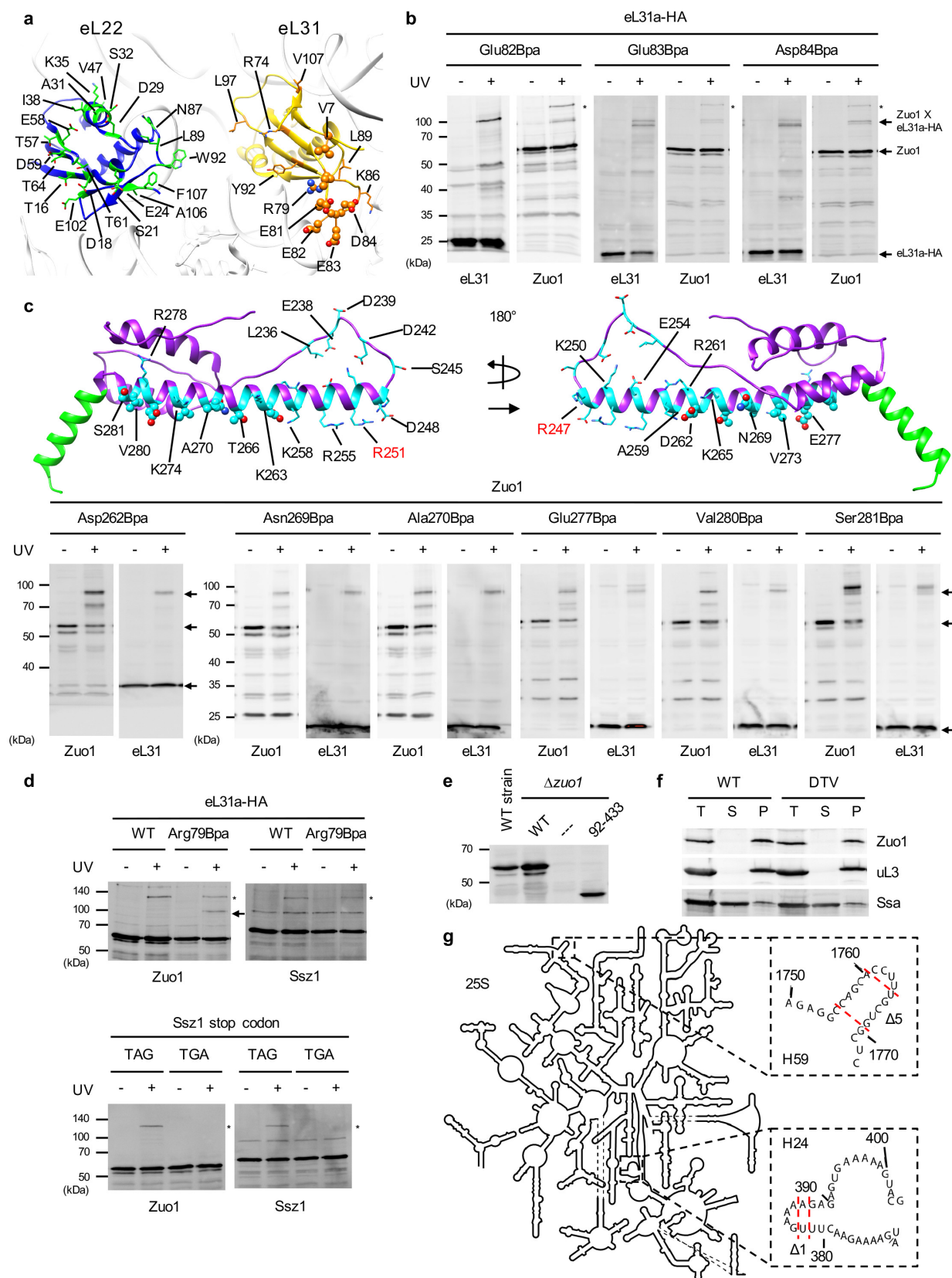
Supplementary Figure 2-1



Supplementary Figure 2-2. Interaction of Zuo1 ZHD with the 60S subunit. (a) Bpa was incorporated into eL31a-HA and eL22a-HA at positions highlighted. Sites that cross-linked shown in ball and stick representation; those that did not by stick only. (b) Site-specific cross-linking between eL31a-HA and Zuo1. Cells expressing indicated variants were grown in the presence of Bpa and exposed to UV light (+), or as a control not exposed (-), before lysis. Samples, run in parallel, were separated by gel electrophoresis and analyzed using antibodies specific for Zuo1 or HA tag (eL31a). Migration of molecular weight standards (left, in kDa) and Zuo1 and HA reactive bands (right, arrows) are indicated. Asterisk indicates crosslink between Zuo1 and Ssz1 (see panel d for explanation). Crosslinking was carried out with two independent yeast transformants, with similar results. (c) Residues of Zuo1 ZHD tested by Bpa cross-linking are highlighted (top, cyan). Sites that crosslinked are shown in ball and stick representation; those that did not, stick representation only. Cross-linking to eL31a was analyzed as in b except Zuo1-Asp262Bpa samples were electrophoresed in gels having 15%, rather than 10%, acrylamide. Crosslinking was carried out with two independent yeast transformants, with similar results. (d) Control of site-specific Bpa cross-linking experiments for unidentified band indicated by asterisks in panel b above, and in Fig. 2b. Cells expressing HA-tagged eL31a wild type (WT) and Arg79Bpa (top) and *Δssz1* cells carrying pRS315-Ssz1 or a pRS315-Ssz1 variant with stop codon altered to TGA from TAG (bottom) were grown in the presence of Bpa. Cross-linking was analyzed as in b except antibodies specific for Zuo1 or Ssz1 were used for immunoblot analysis. Band reacting with both Zuo1 and Ssz1 antibody indicated with asterisk (*). Zuo1 and eL31a cross-linked band indicated with arrow. Migration of molecular weight standards is indicated in kDa (left). (e) Validation of antibody directed against Zuo1 residues 166-284. Yeast cell lysates of wild type cells of DS10 (WT strain) or *Δzuo1* cells expressing Zuo1 (WT), no Zuo1 (---) or

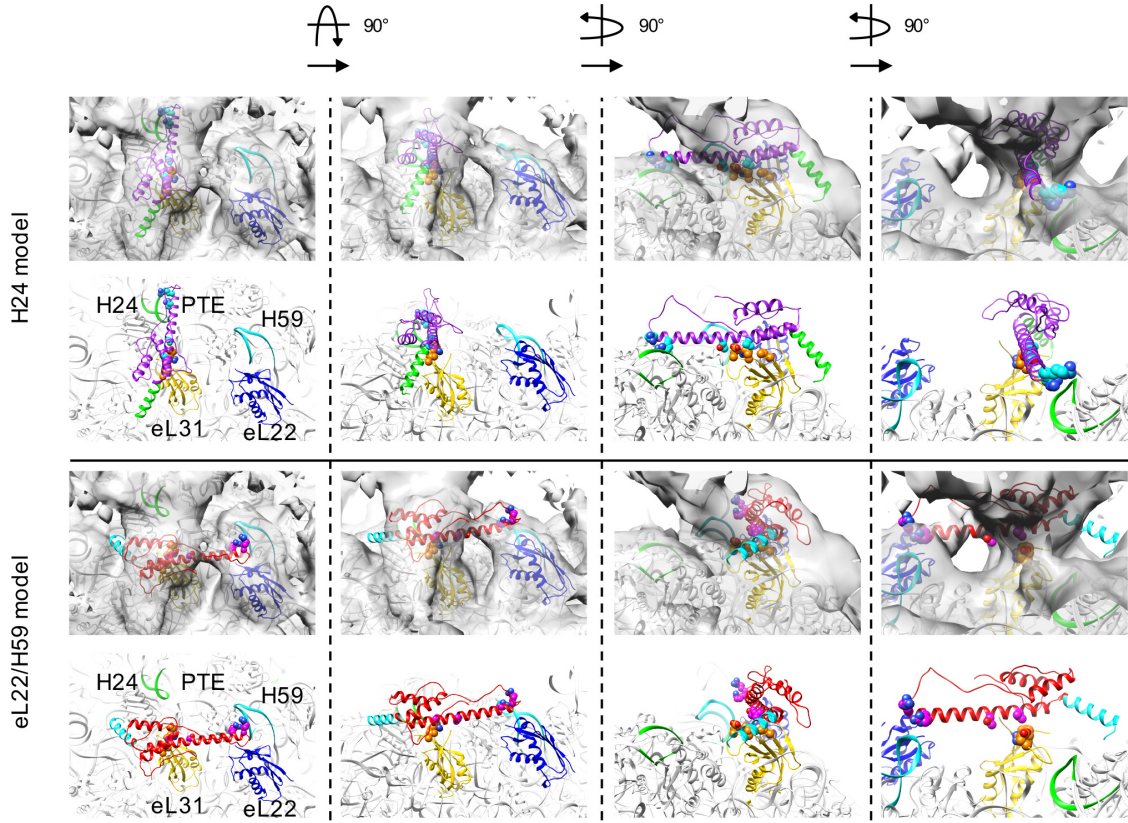
truncation Zuo1 variant lacking the N-terminal 91 residues (92-433) were subjected to electrophoresis and immunoblot analysis. Antibody raised to Zuo1 residues from 166 to 368 tagged with GST was used. (f) Lysates of cells expressing wild type (WT) or variant Zuo1 with alterations Asp262/Thr266/Val273Ala (DTV) were centrifuged through sucrose cushions. Supernatant (S) and pellet (P) fractions, as well as total lysates (T), were analyzed by immunoblotting with indicated antibodies after SDS-PAGE. One representative immunoblot (from three independent experiments, performed with different yeast cultures) is shown. (g) Secondary structure of 25S rRNA. Close-up view of H24 and H59 shown, with red dashed lines indicating deletions. Adapted from <http://apollo.chemistry.gatech.edu/RibosomeGallery>.

Supplementary Figure 2-2



Supplementary Figure 2-3. Docking of Zuo1 ZHD to the 60S subunit. The atomic structure of the ribosome (PDB 3J78) was fit to the cryo-EM map (gray surface) of Zuo1-Ssz1 bound ribosome. Zuo1 ZHD 169-303 was then manually docked to eL31, positioning the cross-linked residues (Thr266 and Val273 of Zuo1 and Val7, Arg79 and Glu81 of eL31, shown as spheres) in close proximity. After manually pointing the Arg247/Arg251 (spheres) at the tip of helix III, either towards H24 (H24 model, ZHD purple) or H59 and eL22 (eL22/H59 model, ZHD red), Zuo1 ZHD was fit to the cryo-EM map by rigid-body docking. PTE: Polypeptide tunnel exit.

Supplementary Figure 2-3



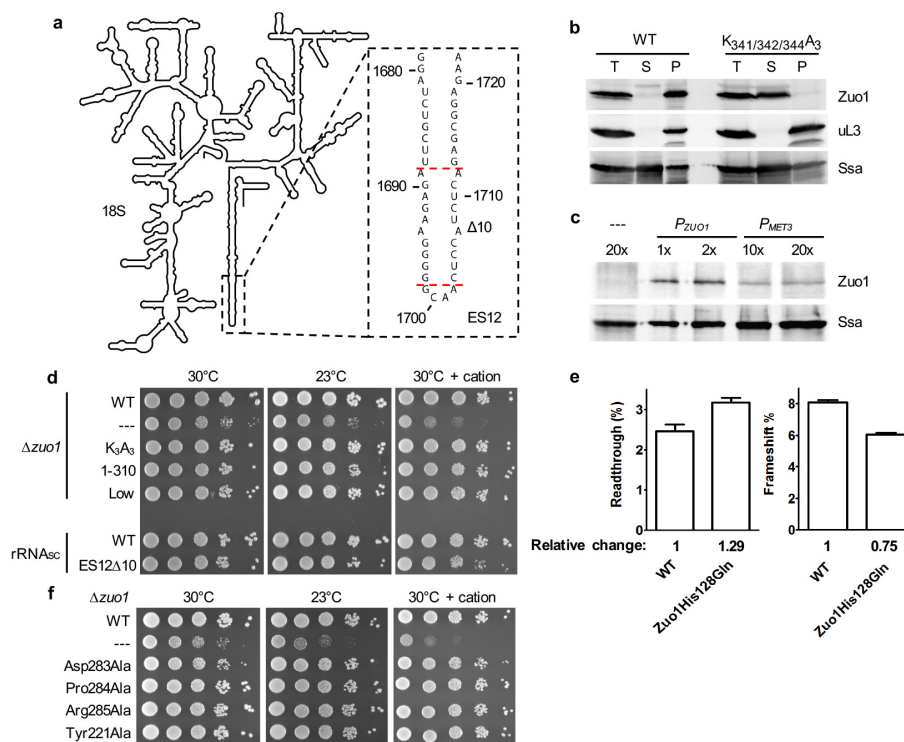
Supplementary Figure 2-4. Interaction of the C terminus of Zuo1 with the 40S subunit. (a)

Secondary structure and location of expansion segment 12 (ES12) of rRNA H44. Secondary structure of 18S rRNA was adapted from <http://apollo.chemistry.gatech.edu/RibosomeGallery>.

Deleted base pairs of ES12 are indicated with red dashed lines in the close-up view. (b) Stability of interaction of Zuo1 and MD variant with ribosomes. *Δzuo1* cells expressing either wild type Zuo1 (WT) or variant Zuo1_{Lys341/342/344Ala} (K_{341/342/344}A₃) were lysed and centrifuged through sucrose cushions. Equivalent amounts of total lysate (T), supernatant (S) and pellet (P) fractions were subjected to electrophoresis and immunoblot analysis. Antibodies specific for Zuo1, and for uL3 and Ssa, as controls for ribosomes and a soluble protein, respectively were used. One representative immunoblot from three independent experiments, performed with different yeast transformants, is shown. (c) Expression of Zuo1 from the *MET3* promoter. *Δzuo1* cells harboring a plasmid with no insert (---), Zuo1 expressed from its endogenous promoter (*P_{ZUO1}*) or from the repressible *MET3* promoter (*P_{MET3}*) were grown in selective minimal glucose medium supplemented with 400 μg/ml methionine to 0.5 OD units. Equal number of cells were harvested and indicated amounts (1x, 2x, 10x or 20x) of whole cell lysates were subjected to electrophoresis and immunoblotting with antibody specific for Zuo1 or a cytoplasmic protein, Ssa, as a control. Zuo1 levels from *P_{ZUO1}* and *P_{MET3}* were analyzed at least three times using different yeast transformants; one representative immunoblot is shown. (d) Growth analysis of strains with a deletion of *ZUO1* (*Δzuo1*) or a deletion of all chromosomal rDNA genes, and expressing only one rDNA gene from a plasmid (rRNA^{sc}). Ten-fold serial dilutions of yeast cells were spotted on selective medium plates and incubated at 30°C for 2 days or at 23°C for 3.5 days. Plates supplemented with 0.75 M NaCl (+cation) were incubated at 30°C for 3.5 days. *Δzuo1* cells contained plasmids encoding either wild-type Zuo1 (WT), no insert (---),

Zuo1_{Lys348/352/353Ala} (K₃A₃), residues 1-310 of Zuo1 (1-310) or reduced levels of Zuo1 expressed from the *MET3* promoter (Low). In the case of rRNA^{sc}, cells harboring either wild type (WT) rDNA or a copy of rDNA with a deletion of 10 base pairs from the stem of ES12 (ES12 Δ 10) are shown. One representative experiment (from three independent experiments, performed with different yeast cultures) is shown. (e) *in vivo* analyses of readthrough and -1 frameshifting of wild type Zuo1 and Zuo1_{His128Gln}, altering the conserved HPD motif of the J-domain. Relative levels in cells expressing wild type Zuo1 set at 1. Data shown are means and s.e.m. from values obtained for three independent yeast transformants each assayed in triplicate. (f) Effects of alteration of amino acids forming the ZHD-MD hinge on cell growth. *Δzuo1* cells that contained plasmids encoding either wildtype Zuo1 (WT), no insert (---), or indicated variants were used. Cell growth was analyzed as in d.

Figure 2-4



Supplementary Table 1. Yeast plasmids used in this study

Plasmid	Description	Reference
pRS315-ZUO1	pRS315 carrying <i>ZUO1</i> under control of its native promoter; used as template to generate all Zuo1 variants used in this study unless specified otherwise.	1
pRS316-ZUO1	pRS316 carrying <i>ZUO1</i> under control of its native promoter; used to construct <i>zuo1</i> _{Asp262/Thr266/Val273Ala} mutant.	1
pRS315-ZUO1 ₁₋₃₁₀	pRS315-ZUO1 with codons 311-433 deleted.	This study
pRS315-MET3-ZUO1	<i>ZUO1</i> under control of <i>MET3</i> promoter in pRS315.	This study
pRS416-TEF1-RPL31A	pRS416 carrying <i>RPL31A</i> under the control of <i>TEF1</i> promoter; used to generate pRS416-TEF1-RPL31A-HA.	This study
pRS416-TEF1-RPL31A-HA	pRS416 carrying <i>RPL31A</i> gene with HA-tag coding sequence at its 3'-end, under control of <i>TEF1</i> promoter; used to generate all Bpa <i>RPL31A</i> substitution mutations for crosslinking.	This study
pRS316-RPL22A-HA	pRS316 with <i>RPL22A-HA</i> tagged gene under the control of its native promoter; used to generate all Bpa <i>RPL22A</i> point mutations for crosslinking.	This study
ptRNA-Bpa	A 2 micron plasmid encoding a variant tRNA synthetase and tRNA _{CUA} for Bpa incorporation; plasmid with either a <i>TRP1</i> or <i>LEU2</i> marker was used.	2
pRDN-hyg1	URA3-based 2 micron plasmid carrying a hygromycin-resistant <i>rDNA</i> repeat under control of its native promoter.	3
pNOY373	A derivative of the 2 micron plasmid YEp351 (<i>LEU2</i>) carrying a single copy of <i>rDNA</i> repeat under control of its native promoter; used for generating H24Δ1, H59Δ5 and ES12Δ10.	3
pDB688	Reporter plasmid carrying a translational fusion of Renilla and firefly luciferase genes under the control of the <i>PGK</i> promoter.	4
pDB688-Stop	Test plasmid for readthrough assays; existing CAA codon replaced with TAG stop codon and flanking GAT and ACG codons with CAA in the linker region between luciferase genes in pDB688.	This study
pDB688-QQQ	Control plasmid for readthrough assay; generated by substituting CAA for GAT and ACG codons flanking the existing CAA codon in the linker region between Renilla and firefly luciferase genes in pDB688.	This study
pJD375	Control plasmid for frameshift assays with Renilla and firefly luciferase genes in frame.	5
pYDL-LA	Test plasmid for assaying -1 PRF with firefly luciferase gene in -1 frame to Renilla luciferase gene.	5

References for Supplementary Table 1

1. Yan, W., Schilke, B., Pfund, C., Walter, W., Kim, S., and Craig, E.A. (1998). Zuo1, a ribosome-associated DnaJ molecular chaperone. *EMBO J* 17, 4809-4817.

2. Krishnamurthy, M., Dugan, A., Nwokoye, A., Fung, Y.H., Lancia, J.K., Majmudar, C.Y., and Mapp, A.K. (2011). Caught in the act: covalent cross-linking captures activator-coactivator interactions in vivo. *ACS Chem Biol* 6, 1321-1326.
3. Wai, H.H., Vu, L., Oakes, M., and Nomura, M. (2000). Complete deletion of yeast chromosomal rDNA repeats and integration of a new rDNA repeat: use of rDNA deletion strains for functional analysis of rDNA promoter elements in vivo. *Nucleic Acids Res* 28, 3524-3534.
4. Salas-Marco, J., and Bedwell, D.M. (2005). Discrimination between defects in elongation fidelity and termination efficiency provides mechanistic insights into translational readthrough. *J Mol Biol* 348, 801-815.
5. Muldoon-Jacobs, K.L., and Dinman, J.D. (2006). Specific effects of ribosome-tethered molecular chaperones on programmed -1 ribosomal frameshifting. *Eukaryot Cell* 5, 762-770.

CHAPTER THREE: The interaction between a typical and an atypical Hsp70s by ATPase
domain dimerization at the ribosome

We plan to submit this chapter as a manuscript for publication authored by myself, Thomas Ziegelhoffer, Grzegorz Sabat, Michael R. Sussman and Elizabeth A. Craig. Grzegorz Sabat conducted mass spectrometry experiments under the supervision of Michael R. Sussman. I performed all other experiments, obtaining initial results. However, some of western blots presented in Fig. 3-1 & Fig. 3-2 were performed by Thomas Ziegelhoffer who is continuing the project. Elizabeth A. Craig oversaw all aspects of this chapter.

1. ABSTRACT

Eukaryotes contain a Hsp70-based molecular chaperone system associated with the ribosome to help folding of nascent chains translated by the ribosome. In *Saccharomyces cerevisiae*, the system, often called a chaperone triad, consists of typical Hsp70 Ssb, J-protein co-chaperone Zuo1 and atypical Hsp70 Ssz1. Ssb is the key Hsp70 which directly interacts with nascent chains. Ssz1 forms a complex with the ribosome-associated J-protein co-chaperone Zuo1, thus tethering it to the ribosome. The Ssz1/Zuo1 complex, by interaction of the J-domain of Zuo1, activates the ATPase activity of Ssb, driving stable interaction of Ssb with nascent chains. Although a recent structural study clarified the nature of the interaction between Ssz1 and Zuo1, the functional role of Ssz1 in the chaperone triad remains unclear. Here we present crosslinking and docking results verified with mass spectrometry analysis, suggesting binding of the ATPase domain of Ssz1 to ATPase domain and alpha-helical bundle structure of Ssb. The interaction is mediated by highly conserved amino acids forming salt bridges. Destabilizing the interaction by charge reverse mutations of the conserved residues of either Ssz1 or Ssb1 impaired growth of yeast cells, indicating functional importance of the interaction. A yeast strain expressing charge reverse variants of both Ssz1 and Ssb complemented the growth defects caused by the presence of only one variant. These results strongly support the model that Ssz1 and Ssb interact with each other as predicted by the docking model and that the interaction is important for cell growth. Our study offers insights into the functional role of Ssz1 in the chaperone triad and leads to the hypothesis that Ssz1 helps to precisely position Ssb on the ribosome, promoting interaction between Ssb and nascent chains.

2. INTRODUCTION

Correct folding of nascent chains translated by the ribosomes is fundamental for maintaining protein homeostasis in all cells (Hartl et al., 2011). However, the cellular environment is highly crowded with other macromolecules, impeding their proper folding (Hartl and Hayer-Hartl, 2009). In addition, domains of proteins often cannot form their native structures until synthesis is complete. Thus, nascent chains need to be protected during translation.

To aid folding of nascent chains, there exist a set of proteins called molecular chaperones in cells. In particular, all eukaryotes contain a Hsp70-based molecular chaperone system associated with the ribosomes. In *S. cerevisiae*, the system consists of a “typical” Hsp70 Ssb, a J-protein co-chaperone Zuo1 and an “atypical” Hsp70 Ssz1 and is often called a chaperone triad (Craig et al., 2003). Yeast cells contain two Ssb proteins Ssb1 and Ssb2. They are 99% identical in sequence and all data thus far indicate they are identical in function. They will be referred to as Ssb here unless otherwise specified. While general cytosolic Hsp70 functions with orthologs of Zuo1 and Ssz1 in metazoans, Ssb, which directly interacts with the ribosome, functions with Zuo1 and Ssz1 in fungi.

Among the chaperone triad, Ssb has a key role in folding of nascent chains. Ssb binds directly to nascent chains as they exit the ribosome, promoting their correct folding (Doring et al., 2017; Hundley et al., 2002; Peisker et al., 2010; Willmund et al., 2013). In this process, Ssb utilizes its structural and functional features as a typical Hsp70. All typical Hsp70s contain distinct two domains: an N-terminal ATPase domain and a C-terminal substrate-binding domain (SBD). The ATPase domain has ATPase activity. A highly conserved linker connects the ATPase domain with the SBD. The SBD is comprised of an alpha-helical bundle structure

(SBD α) and a beta-sheet sandwich structure (SBD β). The SBD β contains a cleft formed by hydrophobic amino acids in which substrate interacts.

Interaction of a typical Hsp70 with substrate is modulated by ATPase cycle between ATP- and ADP-bound states of typical Hsp70. In the ATP-bound state, SBD α and SBD β associate with the ATPase domain, allowing transient interaction of substrate with the “open” cleft. Hydrolysis of ATP to ADP leads to an overall conformational change of Hsp70 (Kityk et al., 2018; Kityk et al., 2015). The SBD β dissociates from the ATPase domain, remaining tethered to the SBD only by the linker. It also induces conformational change of SBD α , trapping substrate in the cleft by acting as a “lid” over the cleft. However, the ATPase activity of Hsp70 is low. A J-protein co-chaperone activates the ATPase activity of Hsp70 by transient interaction of its J-domain. To complete the ATPase cycle, Hsp70 requires interaction with a nucleotide exchange factor (NEF). Dissociation of ADP from the ATPase domain of Hsp70 allows binding of ATP, initiating another round of the ATPase cycle.

Ssb interacts directly with the ribosome (Pfund et al., 1998). Recent studies suggested that both SBD α and SBD β interact with ribosomal proteins and RNAs near the ribosome tunnel exit (Gumiero et al., 2016; Hanebuth et al., 2016). Ssb type Hsp70s that interact directly with the ribosome are found only in fungi. However, metazoans contain a ribosome-associated ortholog of Zuo1, which partners with the soluble Hsp70, the ortholog of the Ssa type Hsp70 of the yeast cytosol (Hundley et al., 2005). Metazoans also contain an ortholog of Ssz1, which forms a complex with an ortholog of Zuo1 (Otto et al., 2005).

The role of Ssz1 in the chaperone triad remains unclear. Ssz1 is an atypical Hsp70 - although it can bind ATP, the ATPase domain does not have ATPase activity, and thus cannot undergo the ATPase cycle. Though the C-terminus of Ssz1 is divergent, it forms a SBD β

subdomain with a cleft, but lacks a SBD α . Ssz1 forms a stable heterodimer with Zuo1 through an N-terminal segment next to the J-domain of Zuo1, tethering Ssz1 to the ribosomes. A recent structural study revealed the core structure of the Ssz1/Zuo1 complex which explains the extraordinary stability of the complex (Weyer et al., 2017). The ATPase domain and SBD β of Ssz1 are intertwined with the N-terminal segment of Zuo1 at the domain interface.

Yeast cells with deletion of individual genes or any combination of *SSB*, *SSZ1* or *ZUO1* display similar slow growth phenotypes that are enhanced in the cold or in the presence of aminoglycosides such as paromomycin or high salts, suggesting these chaperones function in the same pathway (Hundley et al., 2002). The amounts of Ssz1 and Zuo1, but not Ssb, can be reduced significantly (about 2% of normal level), consistent with the idea that the Ssz1/Zuo1 complex functions as a catalyst.

Ssz1 is not the only atypical Hsp70 in the cytosol. Sse1 is also an atypical Hsp70. Sse1 binds ATP but has marginal ATPase activity at most. Thus, Sse1, like Ssz1, does not undergo the typical Hsp70 ATPase cycle. Sse1 is a nucleotide exchange factor of typical Hsp70s. It binds to the ATPase domain of Hsp70 through its ATPase domain and SBD α to release ADP (Polier et al., 2008; Schuermann et al., 2008). There is no evidence Ssz1 acts as a nucleotide exchange factor (Jaiswal et al., 2011).

Ssz1 was identified as a component of the chaperone triad about two decades ago. However, the functional role of Ssz1 remains an enigma, not only because it is an atypical Hsp70 but also because it is the only Hsp70-type protein that forms a stable complex with a J-protein. The core structure of the Ssz1/Zuo1 indicates the ATPase domain of Ssz1 is critical for its function in the chaperone triad. Our results suggest that the ATPase domain of Ssz1 binds to the

ATPase domain and the SBD α of Ssb. We speculate that the interaction between Ssz1 and Ssb positions Ssb on the ribosome, promoting the interaction between Ssb and nascent chains.

3. METHODS

Yeast strains and plasmids

Strains used were of the DS10 genetic background. For Ssz1 crosslinking, a *ssz1 Δ ::LYS2* strain was used (Hundley et al., 2002). For Ssb1 crosslinking, a *ssb1 Δ ::HIS3 ssb2 Δ ::LEU2* strain was used (Pfund et al., 2001). For Zuo1 crosslinking, a *zuo1 Δ ::HIS* strain was used (Yan et al., 1998). Plasmids encoding *SSZ1*, *SSB1*, *ZUO1* or its variants in pRS315-Ssz1, pRS316k-Ssb1 (James et al., 1997), or pRS316-Zuo1 were used respectively.

For yeast growth assays, a *ssz1 Δ ::LYS2* strain and a *ssb1 Δ ::HIS3 ssb2 Δ ::LEU2* strain were used. For yeast complementary growth assays along with immunoblotting, a *ssb1 Δ ::HIS3 ssb2 Δ ::LEU2 ssz1 Δ ::LYS2* strain was used (Hundley et al., 2002). Plasmids encoding wildtype or mutant *SSZ1* or *SSB1* under endogenous promoter in pRS315-Ssz1 or pRS316k-Ssb1 or under *CYC* promoter in p414CYC-Ssz1 (Hundley et al., 2002) were used.

The mutant genes were constructed in plasmids by Quick Change PCR mutagenesis (Stratagene) unless otherwise mentioned. Mutations were verified by DNA sequencing.

in vivo crosslinking

p-benzoyl-L-phenylalanine (Bpa) crosslinking was conducted essentially as previously described (Krishnamurthy et al., 2011; Lee et al., 2016; Ting et al., 2014). The plasmid ptRNA-Bpa which encodes a variant tRNA synthetase and tRNA_{CUA} was used for Bpa incorporation. A

TAG (amber) stop codon was introduced into the open reading frames of *SSZ1* or *SSB1* in the plasmids pRS315-Ssz1 or pRS316k-Ssb1 respectively. Cells were grown in minimal medium supplemented with 2 mM of Bpa at 30°C overnight with a starting OD₆₀₀ of 0.06. Approximately 50 OD₆₀₀ units of cells treated with 100 ug/ml of cyclohexamide were split in half for 365-nm UV exposure (Stratagene, Stratalinker 1800) for 1 hour at 4°C or kept on ice as a control. Cells were lysed via agitation with glass beads for 5 min at 4°C in *in vivo* lysis buffer (300 mM sorbitol, 20 mM HEPES-KOH, pH 7.4, 1 mM EGTA, 5 mM MgCl₂, 10 mM KCl, 10% glycerol, 2 mM β-mercaptoethanol and RNasin RNase Inhibitor (Promega) at a dilution of 1:1,000). 5 OD₂₆₀ units of cell lysates were loaded onto 2 ml of sucrose cushion composed of lysis buffer with 0.5 M sucrose instead of sorbitol. Ribosomes were pelleted by centrifugation for 3 hours at 50,000 r.p.m. in a TLA100.3 rotor (Beckman Coulter) at 4°C. The pellet was suspended in SDS sample buffer (0.124 M Tris-HCl, pH 6.8, 4% SDS, 10% glycerol, 0.02% bromophenol blue and 4.5% β-mercaptoethanol) for immunoblotting. A membrane was used for immunoblotting and erased for another immunoblotting with different antibody. Antibodies specific for glutathione S-transferase (GST) fused Ssz1₁₋₄₀₁ (Eisenman and Craig, 2004), GST fused Ssb1₅₃₄₋₆₁₃ and GST fused Zuo1₁₆₆₋₂₈₈ (Lee et al., 2016) were used.

Docking and modeling

Docking was carried out using the ZDOCK server (Pierce et al., 2014). Crystal structures of Ssz1 (PDB 5MB9) and Ssb1 (PDB 5TKY) of *C. thermophilum* were used as input without contacting or blocking residue selection. To build a docking model between *S. cerevisiae* Ssz1 and Ssb1, a model structure of *S. cerevisiae* Ssz1 was generated by Modeller (Sali and Blundell, 1993) using the crystal structure of *C. thermophilum* Ssz1 (PDB 5MB9) as a template. Similarly,

a model structure of *S. cerevisiae* Ssb1 was generated by Modeller using the crystal structure of *C. thermophilum* Ssb1 (PDB 5TKY). Model structures of *S. cerevisiae* Ssz1 and Ssb1 were aligned individually to the docking model between the crystal structures of Ssz1 (PDB 5MB9) and Ssb1 (PDB 5TKY) of *C. thermophilum*, respectively, using PyMOL. To generate a model complex between *S. cerevisiae* Ssz1 and Zuo1, a model structure of *S. cerevisiae* Ssz1 was generated by Modeller using the crystal structure of *C. thermophilum* Ssz1 complexed with Zuo1 N-terminus (PDB 5MB9) as a template. Similarly, a model structure of *S. cerevisiae* Zuo1 N-terminus was generated by Modeller using the crystal structure of *C. thermophilum* Zuo1 N-terminus, complexed with Ssz1 (PDB 5MB9) as a template. Each model was aligned to its ortholog in the complex structure (PDB 5MB9), respectively, using PyMol.

Protein expression and purification

The plasmid pSmt3 encoding a N-terminal His₆-Smt3 (SUMO) tag was used for expression of Ssz1, Zuo1 and Ssb1. The open reading frame of *SSZ1*, *ZUO1* or *SSB1* was cloned into the plasmid pSmt3. The variants of *SSZ1* and *SSB1* were constructed by QuickChange PCR mutagenesis. Proteins were expressed in *E. coli* Rosetta 2 (DE3) pLysS cells. Cells were grown in LB medium supplemented with chloramphenicol and kanamycin at 37°C for 2 hours until an OD₆₀₀ reached around 0.5. Protein expression was induced by addition of 0.5 mM isopropyl-β-D-thiogalactopyranoside (IPTG) overnight at 18°C. Cell lysates in *in vitro* lysis buffer (50 mM Tris, pH 7.5, 250 mM NaCl, 10 mM imidazole and 5% glycerol) was prepared using a French press at 4°C. Proteins were purified using HisPur Ni-NTA Resin (Thermo Scientific). Purified Ulp1 (Sahi et al., 2013) from *E. coli*, containing a His-tag, was used to cleave the His₆-SUMO tag during dialysis overnight at 4°C in dialysis buffer (50 mM Tris, pH 7.5, 250 mM NaCl and

5% glycerol). Proteolytic digestion of the tag by Ulp1 left a serine at the N-terminus of proteins. Cleaved proteins were separated using HisPur Ni-NTA Resin (Thermo Scientific) from the tag and Ulp1.

Expression and purification of proteins containing His₆-SUMO-tag were carried out similarly to proteins without His₆-SUMO-tag except some modifications as follows: The Ulp1 recognition motif consisting of two glycines right before the serine at the N-terminus of proteins were altered to two alanines by Quick Change. Proteins were dialyzed without Ulp1 and used without further purification steps.

Expression and purification of proteins containing Bpa were similarly carried out with the following modifications: A TAG (amber) stop codon was introduced into the open reading frames of *SSZ1* and *ZUO1* respectively. Proteins were expressed in *E. coli* BL21 (DE3) cells harboring pSUPT/BpF (Ryu and Schultz, 2006; Winkelman et al., 2015) encoding a variant tRNA synthetase and tRNA_{CUA} for Bpa incorporation. Cells were grown in LB medium supplemented with 1 mM of Bpa and 0.02% arabinose together with chloramphenicol and kanamycin at 37°C for 2 hours until an OD₆₀₀ reached around 0.5. Purification of proteins was carried out as written above.

in vitro crosslinking

Proteins, purified from *E. coli.*, were used for *in vitro* crosslinking. For crosslinking between Ssz1 and Zuo1, approximately equal amounts of proteins were incubated in the *in vitro* lysis buffer for 10 min at 4°C, then subjected to UV exposure (Stratagene, Stratalinker 1800) for 1 hour at 4°C or left on ice as a control. Proteins were suspended in the SDS sample buffer for electrophoresis. Major crosslinking products, only present in the sample containing all proteins

upon UV exposure, were excised and digested with trypsin and Asp-N for crosslinking products between Ssz1 T217Bpa and Zuo1 or trypsin alone for crosslinking products between Zuo1 F36Bpa and Ssz1.

For crosslinking between Ssz1 and Ssb1, Ssz1 S282Bpa, Zuo1 and Ssb1 were incubated in the pull-down assay buffer (10 mM Tris, pH 7.5, 100 mM KCl, 30 mM Imidazole, 5 mM MgCl₂, 1 mM ATP and 1 mM 1,4-dithiothreitol) before UV exposure. Unique crosslinking products between Ssz1 S282Bpa and Ssb1 were excised from SDS-PAGE gel and digested with trypsin and Asp-N.

Enzymatic “in gel” digestion

Coomassie R-250 stained gel pieces were de-stained completely in MeOH/H₂O/NH₄HCO₃ (50%/50%/100 mM), dehydrated for 2 min in ACN/H₂O/NH₄HCO₃ (50%/50%/25mM) then once more for 30 sec in 100% ACN. Dried in a Speed-Vac for 1 min, reduced in 25 mM DTT (Dithiotreitol in 25 mM NH₄HCO₃) for 15 min at 56°C, alkylated with 55 mM IAA (Iodoacetamide in 25mM NH₄HCO₃) in darkness at room temperature for 15 min, washed once in H₂O, dehydrated for 2 min in ACN/H₂O/NH₄HCO₃ (50%:50%:25 mM) then once more for 30 sec in 100% ACN. Dried again and rehydrated with 20 µl of trypsin solution with 0.01% ProteaseMAX™ surfactant (10 ng/µl *Trypsin* from Promega Corp. in 25 mM NH₄HCO₃/0.01% w/v of ProteaseMAX™ from Promega Corp.). Let stand for 2 min at room temperature then additional 30 µl of overlay solution (25 mM NH₄HCO₃/0.01% w/v of ProteaseMAX™) was added to keep gel pieces immersed throughout the digestion. The digestion was conducted for 3 hrs at 42°C then peptides generated from tryptic digestion were transferred to a new Protein LoBind tubes (~50 µl volume) and secondary digestion followed by

addition of 5 μ l AspN proteinase (20 ng/ μ l endoproteinase AspN from Roche Diagnostics in 25 mM NH_4HCO_3). That digestion was conducted for 2 hrs at 37°C. Concurrently, the gel pieces post tryptic digestion were dehydrated with 10 μ l of ACN and re-hydrated with 20 μ l of secondary digestion mix composed of 5 μ l AspN proteinase (20 ng/ μ l endoproteinase AspN from Roche Diagnostics in 25 mM NH_4HCO_3), 13 μ l 25 mM NH_4HCO_3 and 2 μ l of 0.1% ProteaseMAX™ surfactant. This digestion was allowed to proceed for 2 hrs at 37°C after which the solution was pulled off and combined with the primary “in liquid” AspN digestion. Proteolysis was terminated by acidification with 2.5% TFA (Trifluoroacetic Acid) to 0.3% final (10 μ l added). Degraded ProteaseMAX™ was removed via centrifugation (max speed, 10 minutes) and the peptides solid phase extracted (Bond Elut *OMIX C18* pipette tips from Agilent). Peptides were eluted off the C18 column with 15 μ l of acetonitrile/ H_2O /TFA (70%:30%:0.1%) dried to minimum volume then brought up to 20 μ l total volume with 0.1% formic acid and 3 μ l was loaded on the instrument.

NanoLC-MS/MS

Peptides were analyzed by nanoLC-MS/MS using the Agilent 1100 nanoflow system (Agilent) connected to a hybrid linear ion trap-orbitrap mass spectrometer (LTQ-Orbitrap Elite™, Thermo Fisher Scientific) equipped with an EASY-Spray™ electrospray source. Chromatography of peptides prior to mass spectral analysis was accomplished using capillary emitter column (PepMap® C18, 3 μ M, 100 Å, 150 x 0.075 mm, Thermo Fisher Scientific) onto which 3 μ l of extracted peptides was automatically loaded. NanoHPLC system delivered solvents A: 0.1% (v/v) formic acid, and B: 99.9% (v/v) acetonitrile, 0.1% (v/v) formic acid at 0.50 μ L/min to load the peptides (over a 30 minute period) and 0.3 μ L/min to elute peptides

directly into the nano-electrospray with gradual gradient from 3% (v/v) B to 20% (v/v) B over 18 minutes and concluded with 5 minute fast gradient from 20% (v/v) B to 50% (v/v) B at which time a 4 minute flash-out from 50-95% (v/v) B took place. As peptides eluted from the HPLC-column/electrospray source survey MS scans were acquired in the Orbitrap with a resolution of 120,000 followed by MS2 for the 20 most intense peptides detected in the MS1 scan from 350 to 1800 m/z; redundancy was limited by dynamic exclusion with repeat count of 2 and 15 sec duration. CID-based MS/MS fragmentation in the Ion Trap portion of the instrument used activation time of 10 msec, normalized collision energy of 35 and isolation width of 2AMU. Monoisotopic precursor selection and charge state screening were enabled and +2 and lower charge states were rejected.

Data analysis and crosslinking assignment

To obtain identifications of un-crosslinked peptides raw MS/MS data were converted to mgf file format using MSConvert (ProteoWizard: Open Source Software for Rapid Proteomics Tools Development). Resulting mgf files were used to search against *E. coli* amino acid sequence database containing Ssz1 and Zuo1 constructs with a decoy reverse entries and a list of common contaminants (8,493 sequence entries) using our in-house *Mascot* search engine 2.2.07 [Matrix Science] with variable Methionine oxidation with Asparagine and Glutamine deamidation plus fixed cysteine Carbamidomethylation. To determine the identity of crosslinked products a targeted database search of raw mass spec data was conducted using only the sequence of proteins used in the crosslinking experiment plus common lab protein contaminants. Crosslinked candidates were generated using StavroX software (StavroX Freeware version 3.6.6. from University of Halle-Wittenberg) with BPA chosen as a cross-linker, Lysine, Arginine and

Aspartate, included only when applicable, with 3 missed cleavages as a protease sites and static Cysteine carbamidomethylation plus variable Methionie oxidation as possible modifications. Peptide mass tolerance was set at 10 ppm and fragment mass at 0.6 Da. (except for crosslinking products between Zuo1 F36Bpa and Ssz1, at 20 ppm, because of mass spectrometer calibration.) All crosslinking candidates were below 5% of the false discovery rate. Designation of crosslinking sites was based on the number of occurrence of the crosslinking sites of the candidates within top ten highest score. MS1 and MS/MS spectrum of crosslinking candidates were manually examined. Crosslinking results were crosschecked with UV unexposed or individually UV exposed proteins as controls to ensure its robustness.

Pull-down assays

Unless otherwise stated, final concentration of 5 μ M of Ssz1, Zuo1 and Ssb1 wildtype or variants proteins were used for pull-down assays. Proteins were incubated for 10 min at 4°C to allow complex formation in the pull-down assay buffer. HisPur Ni-NTA Resin (Thermo Scientific), previously washed with the pull-down assay buffer, was added to proteins mixture and incubated for 1 hour at 4°C in a rotator. Resins were washed by centrifugation with the pull-down assay buffer three times and bound proteins were eluted with 300 mM of imidazole. Eluted proteins were suspended in SDS sample buffer for electrophoresis.

4. RESULTS

4.1. Site-specific crosslinking between Ssz1 and Ssb1

To identify novel proteins interacting with the ATPase domain of Ssz1, *in vivo* site-specific crosslinking experiments were conducted. The photoactivatable amino acid analogue p-

benzoyl-L-phenylalanine (Bpa) was incorporated individually at 15 sites of the ATPase domain of Ssz1 in place of endogenous surface-exposed residues through nonsense suppression (Supplementary Fig. 3-1a). Crosslinking was observed at 6 sites (strong bands with Bpa at T217 or D284; weak bands with Bpa at K23, Y50, T221 or Y389). Crosslinking species migrated at two disparate apparent molecular weights. Crosslinking products with Ssz1 containing Bpa at position K23, Y50 or D284, on a face of the ATPase domain, migrated close to 260 kDa; Crosslinking products of Ssz1 containing Bpa at position T217, T221 or Y389, located near the groove of the ATPase domain where the linker interacts in the ATP-bound state of Hsp70, migrated close to 140 kDa (Fig. 3-1 and Supplementary Fig. 3-1).

Because Ssz1 forms a complex with Zuo1, we tested whether crosslinking products reacted with Zuo1 antibody. Consistent with the core structure of Ssz1 and Zuo1 complex which was published after we obtained these results (Weyer et al., 2017), variants having Bpa near the groove specifically reacted with Zuo1 antibody (Supplementary Fig. 3-1b).

The crosslinking products generated when Bpa was incorporated on the face of the ATPase domain of Ssz1 did not react with Zuo1 antibody. Because Ssb1 is a component of the molecular chaperone triad with Ssz1 and Zuo1, we tested Ssb1-specific antibody. In each case, reaction with Ssb1 antibody was detected (Fig. 3-1a). We incorporated Bpa at 6 additional positions (D25, Q54, N275, S282, D291 or F341) on the same face of the ATPase domain (Supplementary Fig. 3-1a). Three, those having Bpa at position Q54, S282 or D291, crosslinked to Ssb1 (Fig. 3-1).

As these results strongly suggested direct interaction between Ssz1 and Ssb1, we tested whether the ATPase domain of Ssb1 could be crosslinked to Ssz1. Bpa was incorporated at 6 Ssb1 sites (E29, Q35, L63, S279, D288 or K364) on the face of the ATPase domain not blocked

by the interaction of the SBD (Supplementary Fig. 3-2). We observed that Bpa at position Q35 crosslinked to Ssz1 (Fig. 3-2). To validate the crosslinking results, we incorporated Bpa at 6 additional sites (N37, A56, N59, K136, E286 or D295) on the same face of the ATPase domain (Supplementary Fig. 3-2). We observed specific crosslinking products between Ssb1 containing Bpa at position N59 or D295 and Ssz1 (Fig. 3-2).

4.2. The binding mode of Ssz1 to Ssb1

The crosslinking results implied direct interaction between Ssz1 and Ssb1 through the ATPase domains. To better understand the interaction, unbiased docking was performed using the ZDOCK server (Pierce et al., 2014). The results suggested the ATPase domain of Ssz1 binds both the ATPase domain and SBD α of Ssb1 (Fig. 3-3b). The interface between the ATPase domains has multiple contacts in three of the four subdomains (Ia, Ib and IIb) of both Ssz1 and Ssb1. Crosslinking results agree well with the docking model. All crosslinked sites are located at the interface between the ATPase domains of Ssz1 and Ssb1 (Fig. 3-3). Overall, the binding is reminiscent of that between Sse1 and Hsp70, although there are some clear differences because of lack of a SBD α of Ssz1. Therefore, subdomain IIb of Ssb1 interacts only with subdomains Ib and IIb of Ssz1 (Fig. 3-3b and Supplementary Fig. 3-3). Instead, the SBD α of Ssb1 interacts with the subdomain IIb of Ssz1 (Fig. 3-3b).

To verify the docking model, mass spectrometry analysis was performed on crosslinking products obtained using proteins purified from *E. coli*. First, two crosslinking products between Ssz1 and Zuo1 (Ssz1 T217Bpa:Zuo1 and Zuo1 F36Bpa:Ssz1) were analyzed to test the feasibility of the technical approach as the core structure of Ssz1 and Zuo1 complex is available (Supplementary Fig. 3-4a and 3-5a). In good agreement with the crystal structure, Bpa at

position T217 of Ssz1 crosslinked to valine at position 29 of Zuo1 (Supplementary Fig. 3-4b,c and Table 1), and Bpa at position F36 of Zuo1 crosslinked to leucine at position 398 of Ssz1 (Supplementary Fig. 3-5b,c and Table 2 and Supplementary Fig. 3-6).

After validation of the technical approach, *in vitro* crosslinking products between Ssz1 containing Bpa at position 282 and Ssb1 were analyzed by mass spectrometry (Supplementary Fig. 3-7). Bpa crosslinked to leucine at position 63 of Ssb1 (Fig. 3-4a,b). Positions 282 of Ssz1 and 63 of Ssb1 are next to each other in the docking model, strongly supporting the validity of the model of the interaction between Ssz1 and Ssb1 (Fig. 3-4c).

4.3. Direct interaction between Ssz1 and Ssb1

The crosslinking and mass spectrometry results suggest a physical interaction between Ssz1 and Ssb1. To test this idea, I conducted *in vitro* pull-down assays using purified proteins. Zuo1 was included because Ssz1 forms a stable heterodimer with it. I incubated Ssz1 and Zuo1 with Ssb1 having a N-terminal His-SUMO tag (His-Ssb) to allow complex formation, and then conducted the pull-down experiments. A fraction of Ssz1 was eluted with His-Ssb1 in a concentration-dependent manner, suggesting direct interaction between Ssz1 and Ssb1 (Fig. 3-5a,c).

To identify key residues important for the interaction between Ssz1 and Ssb1, 43 fungal Ssz1 protein sequences were aligned (Supplementary Fig. 3-8). Ssz1 contains only a few highly conserved residues. Several are located at the predicted interface between Ssz1 and Ssb1. The surface exposed charged residues R36, D291 and R300 at the predicted Ssb1 interface are highly conserved. To test whether these residues are important for the interaction between Ssz1 and Ssb1, a Ssz1 variant containing charge reverse mutations on residues R36E, D291R and R300E

(Ssz1_{RDR/ERE}) was constructed and used in the *in vitro* pull-down experiments. Compared to wildtype, only a small fraction of Ssz1_{RDR/ERE} eluted with His-Ssb, indicating the highly conserved residues of Ssz1 at the interface are important for interaction with Ssb1 (Fig. 3-5b,c).

4.4. Cellular function of the interaction between Ssz1 and Ssb1

To begin to investigate the functional importance of the interaction between Ssz1 and Ssb1 we first looked more carefully at the Ssz1:Ssb1 docking model. We noted that R36, D291 and R300 of Ssz1 form potential salt bridges with the conserved Ssb1 residues E370, R261 and E547 of Ssb1, respectively (Fig. 3-6a and Supplementary Fig. 3-8). As a means of testing functional interaction, we asked if charge reversal substitutions at the interacting positions of Ssb1 could overcome a functional defect caused by the three charge reversals in the Ssz1 variant Ssz1_{RDR/ERE}. To that end we constructed the *SSB1* variant gene encoding three substitutions E370R, R261D and E547R (Ssb1_{ERE/RDR}).

To test *in vivo* effects we expressed Ssz1 at a reduced level under *CYC1* promoter, as previous work demonstrated that only approximately 2% of the normal levels are required for robust growth (Hundley et al., 2002). Indeed, $\Delta ssb\Delta ssz1$ cells expressing wildtype Ssb1 from its endogenous promoter and wildtype Ssz1 from the *CYC1* promoter grew as well as cells expressing both wildtype genes from their endogenous promoters (Fig. 3-6b). However, cells expressing Ssz1_{RDR/ERE}, rather than wildtype Ssz1 grew poorly at 23 and 30°C, as well as in the presence of high cation concentration.

Cells expressing Ssb1_{ERE/RDR} along with low levels of wildtype Ssz1 also grew poorly (Fig. 3-6b). However, cells expressing both variants, that is Ssz1_{RDR/ERE} and Ssb1_{ERE/RDR}, grew better, approaching that of cells expressing both wildtype proteins. This enhanced growth

strongly supports the idea that Ssz1 and Ssb1 interact with each other as predicted by the docking model and that this interaction is functionally important *in vivo*.

5. DISCUSSION

Cellular localization of proteins is critical for their specific functions. Here we present evidence that Ssz1 binds directly to Ssb through ATPase domain dimerization. Ssz1 is located close to the ribosome tunnel exit by its interaction with Zuo1. Thus, the interaction between Ssz1 and Ssb may provide a guide for localization of Ssb on the ribosome, facilitating interaction between Ssb and nascent chain (Fig. 3-7).

Dimerization between Ssz1 and Ssb

There is a growing body of evidence suggesting that dimerization of ATPase domains is an intrinsic feature of Hsp70-type molecular chaperones (Malinverni et al., 2015). It was shown that DnaK, Hsp70 in *E. coli*, forms a homodimer through ATPase domain dimerization (Sarheng et al., 2015; Thompson et al., 2012). Similarly, Sse1 forms a heterodimer with Hsp70 through ATPase domain dimerization (Polier et al., 2008). In our docking model, Ssz1 also interacts with Ssb through ATPase domain dimerization. The interactions between different types of Hsp70s in different species are similar each other, suggesting that Hsp70 adapted to form homodimers at an early time point in evolution. Moreover, differentiation of Hsp70 might lead to heterodimer formations that have diverse functional roles.

There are differences in dimerization between Ssz1:Ssb, Sse1:Hsp70 and DnaKs, which depend on the nucleotide-bound states that are related to functions of the interactions

(Supplementary Fig. 3-9). Each SBD α of DnaKs in the ATP-bound state binds to the ATPase domain of partner DnaK, allowing both clefts to be available for substrate interaction (Supplementary Fig. 3-9c). The SBD α of Sse1 interacts with the subdomain IIb of the ADP-bound state of Hsp70, releasing ADP (Supplementary Fig. 3-9b). Ssz1 lacks SBD α , thus Ssz1 is unlikely to induce “opening” of the subdomain IIb of Ssb (Supplementary Fig. 3-9a). Instead, the SBD α in the ATP-bound state of Ssb interacts with subdomain IIb of Ssz1 in the docking model that might allow nascent chain interaction with the cleft of Ssb.

Importance of interaction between Ssz1 and Ssb

The functional interaction between Ssz1 and Ssb might be critical for normal cell growth, as suggested by the result showing that growth of the yeast strain containing both variants of Ssz1 (Ssz1_{RDR/ERE}) and Ssb1 (Ssb1_{ERE/RDR}) was similar to wild type. These results support the idea that the salt bridges at the interface between Ssz1 and Ssb mediate the interaction as in the docking model.

The complementary growth assays help to address possible caveats that apply to the individual variants. The mutated residues might have other functional and structural roles, impairing growth of cells for other reasons. It is possible that E547R mutation of Ssb1_{ERE/RDR} destabilizes the interaction between the SBD α and SBD β in the ADP-bound state, causing slow growth phenotypes (Fernandez-Saiz et al., 2006). In addition, R261D and E370R mutations of Ssb1_{ERE/RDR} could lead to slow growth phenotype. These mutations may constrain nucleotide exchange of Ssb1 by Sse1 because they are located at the interaction interface between the ATPase domains of Ssb and Sse1. The pull-down results between Ssz1_{RDR/ERE} and Zuo1 suggested slight reduction in Zuo1 binding (Supplementary Fig. 3-10). This result might indicate

that these mutations impair proper folding of Ssz1, important for normal cell growth. Despite of potential functional and structural impairments by the Ssz1 and Ssb1 variants, our results showed that the growth of cells is more dependent on the functional interaction between Ssz1 and Ssb. These results strongly support the idea that the key function of Ssz1 is to interact with Ssb through the ATPase domain, which is in line with the previous results that the ATPase domain of Ssz1 but not C-terminus is important for normal cell growth (Hundley et al., 2002).

The ribosome association of Ssb

Association of Ssb with the ribosome is complex because Ssb interacts not only with Ssz1 but also binds to the ribosome directly. It has been known for some time that all three domains of Ssb are involved in ribosome association (James et al., 1997). Recently, it was shown that positively charged regions in the SBD α and SBD β interact with different ribosomal proteins and RNAs near the ribosome tunnel exit (Gumiero et al., 2016; Hanebuth et al., 2016). It was particularly suggested that the C-terminal end of SBD α interacts with ES41 or ul29/el39 (previously called Rpl35/Rpl39) depending on the ATP- or ADP-bound state, respectively, of Ssb. However, interaction of Ssb with the ribosome remains ill-defined. I will discuss more about the interaction between Ssb and the ribosome in the future direction section in the Chapter Four.

Functional implication of the interaction between Ssz1 and Ssb

The potential interaction between cytosolic Hsp70 and Ssz1 ortholog in metazoans might be much more important because metazoans lack a dedicated Hsp70 which binds to the ribosome directly. Thus, HspA14, Ssz1 ortholog in humans, might be the only component interacting with

cytosolic Hsp70s on the ribosome. Notably, DnaJC2, ortholog of Zuo1 in humans, can partially activate the ATPase activity of cytosolic Hsp70s by itself (Hundley et al., 2005; Jaiswal et al., 2011). This is in contrast to Zuo1 which requires complex formation with Ssz1 (Huang et al., 2005). The Zuo1/Ssz1 complex might be more specialized because it only works with the ribosome-associated Hsp70 Ssb. But, the DnaJC2/ HspA14 complex activates cytosolic Hsp70s in that DnaJC2 remains as a more general J-protein, which can function independently from the complex formation with HspA14.

Consistent with our results implying Ssz1 might position Ssb on the ribosomes, localization of Hsp70s to particular compartments or protein complexes in the cell is important for specific functions of Hsp70s (Craig, 2018). Mitochondrial Hsp70 interacts with a protein called Tim44 in *S. cerevisiae* which binds to a translocase of the inner membrane (TIM) complex to help import of mitochondrial proteins. It has been suggested that Tim44 coordinates the interaction between the mitochondrial Hsp70 and a J-protein, Pam18 in *S. cerevisiae*, which is also associated with the TIM complex (Ting et al., 2017). Similar to Tim44, Ssz1 might coordinate the interaction between Ssb and Zuo1, activating the ATPase activity of Ssb only when nascent chain is present.

6. FIGURES AND TABLES

Figure 3-1. Crosslinking of the ATPase domain of Ssz1 to Ssb1. (a) Cells expressing Ssz1 variants containing Bpa at the indicated sites were exposed to UV (+) or unexposed (-) as a control. Immunoblotting was conducted after SDS-PAGE using Ssz1 or Ssb1 specific antibodies. Ssz1 D291Bpa sample was electrophoresed shorter time than other samples. All tested crosslinking sites and Zuo1 crosslinking results are shown in Supplementary Fig. 3-1. Mw, molecular weight. Ssz1 and Ssb1 bands are indicated with arrows. (b) Ribbon diagram of model structure of the ATPase domain of *S. cerevisiae* Ssz1 based on the crystal structure of *C. thermophilum* Ssz1 (PDB 5MB9). Sites that crosslinked to Ssb1 when having Bpa are highlighted with sphere representation in green.

Figure 3-1

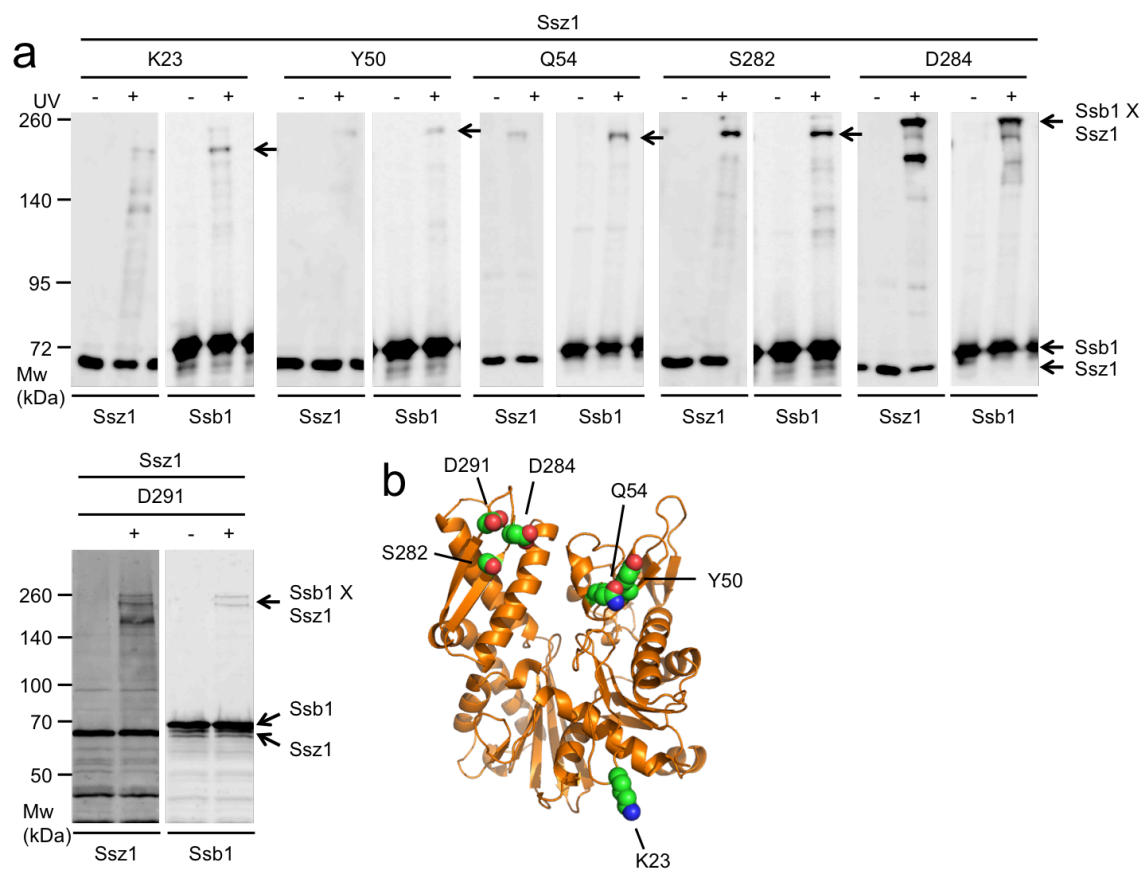


Figure 3-2. Crosslinking of the ATPase domain of Ssb1 to Ssz1. (a) Cells expressing Ssb1 variants containing Bpa at the indicated sites were exposed to UV (+) or unexposed (-) as a control. Immunoblotting was conducted after SDS-PAGE against Ssb1 or Ssz1 specific antibodies. All tested crosslinking sites are shown in Supplementary Fig. 3-2. In addition, Q35Bpa and N59Bpa of Ssb1 were immunoblotted with Sse1 specific antibody. It was found that bands with asterisk correspond to cross-linking products between Ssb1 and Sse1. (data not shown) Mw, molecular weight. Ssb1 and Ssz1 bands are indicated with arrows. (b) Ribbon diagram of model structure of the ATPase domain of *S. cerevisiae* Ssb1 based on the crystal structure of *C. thermophilum* Ssb1 (PDB 5TKY). Sites that crosslinked when having Bpa are highlighted with sphere representation.

Figure 3-2

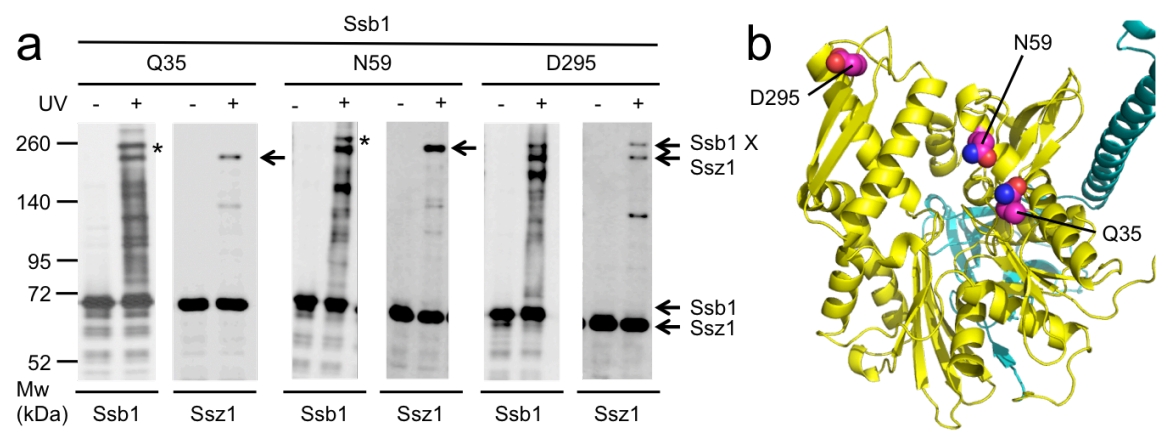


Figure 3-3. Docking between Ssz1 and Ssb1. (a) Model structures of *S. cerevisiae* Ssz1 and Ssb1 with the crosslinked sites highlighted with sphere representation. (b) Unbiased docking model between Ssz1 and Ssb1 generated by the ZDOCK server.

Figure 3-3

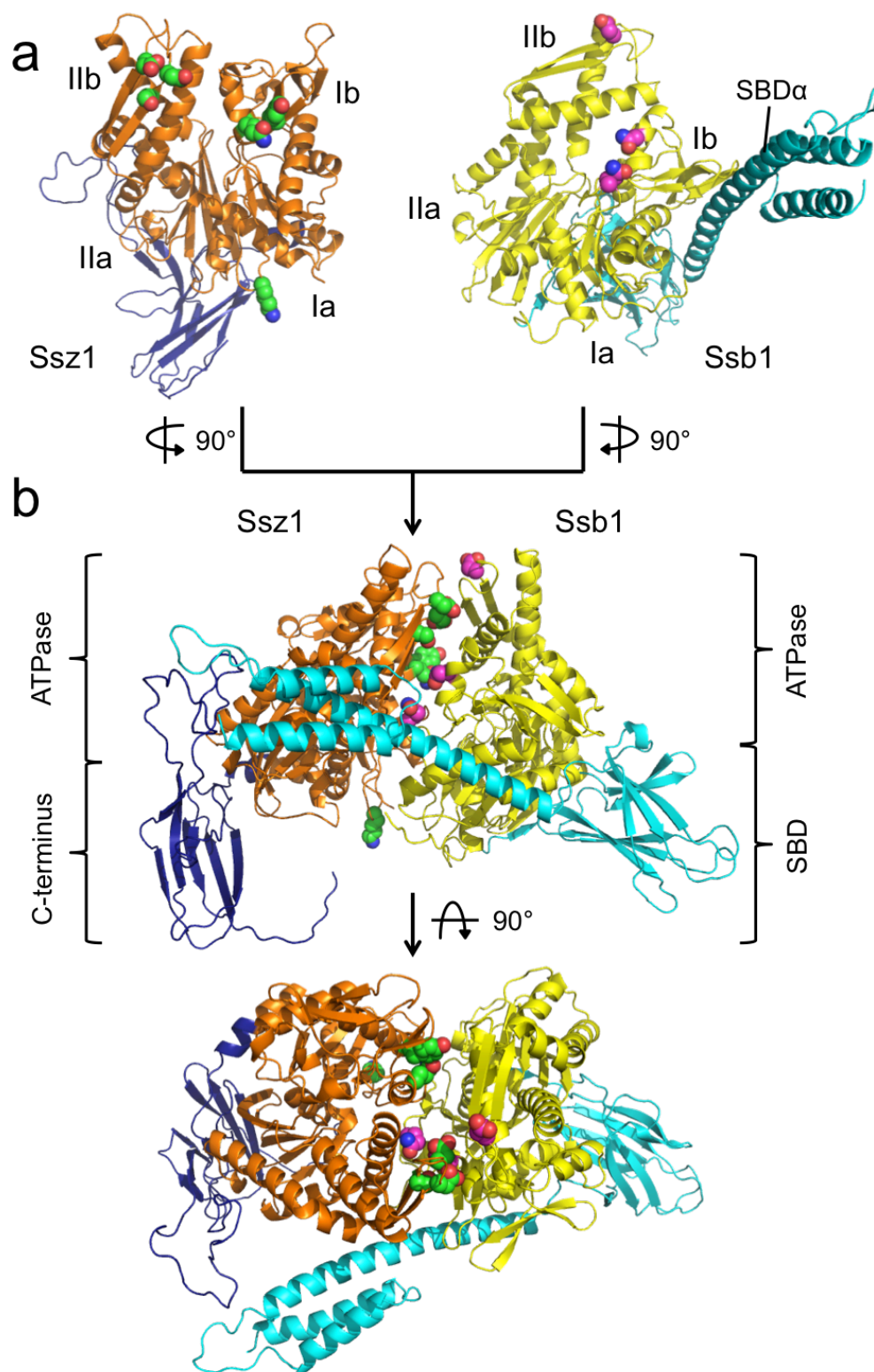


Figure 3-4. Mass spectrometry analysis of crosslinked products between Ssz1 S282Bpa and Ssb1. (a) Mass spectrum (MS) containing a 3+ charged ion at m/z 785.092 with a zoom-in view which was selected for fragmentation. (b) Fragment ion mass spectrum (MS/MS) of crosslinked peptides between Ssb1 (β peptide, in blue; amino acids 59-66) and Bpa containing Ssz1 (α peptide, in red; amino acids 271-283). Leucine at position 63 of Ssb1 was identified to be crosslinked to Bpa at position 282 of Ssz1. (c) Position of crosslinked sites in the docking model. The Bpa incorporation site of Ssz1 in green and the residue of Ssb1 crosslinked to Bpa in red were highlighted with sphere representation.

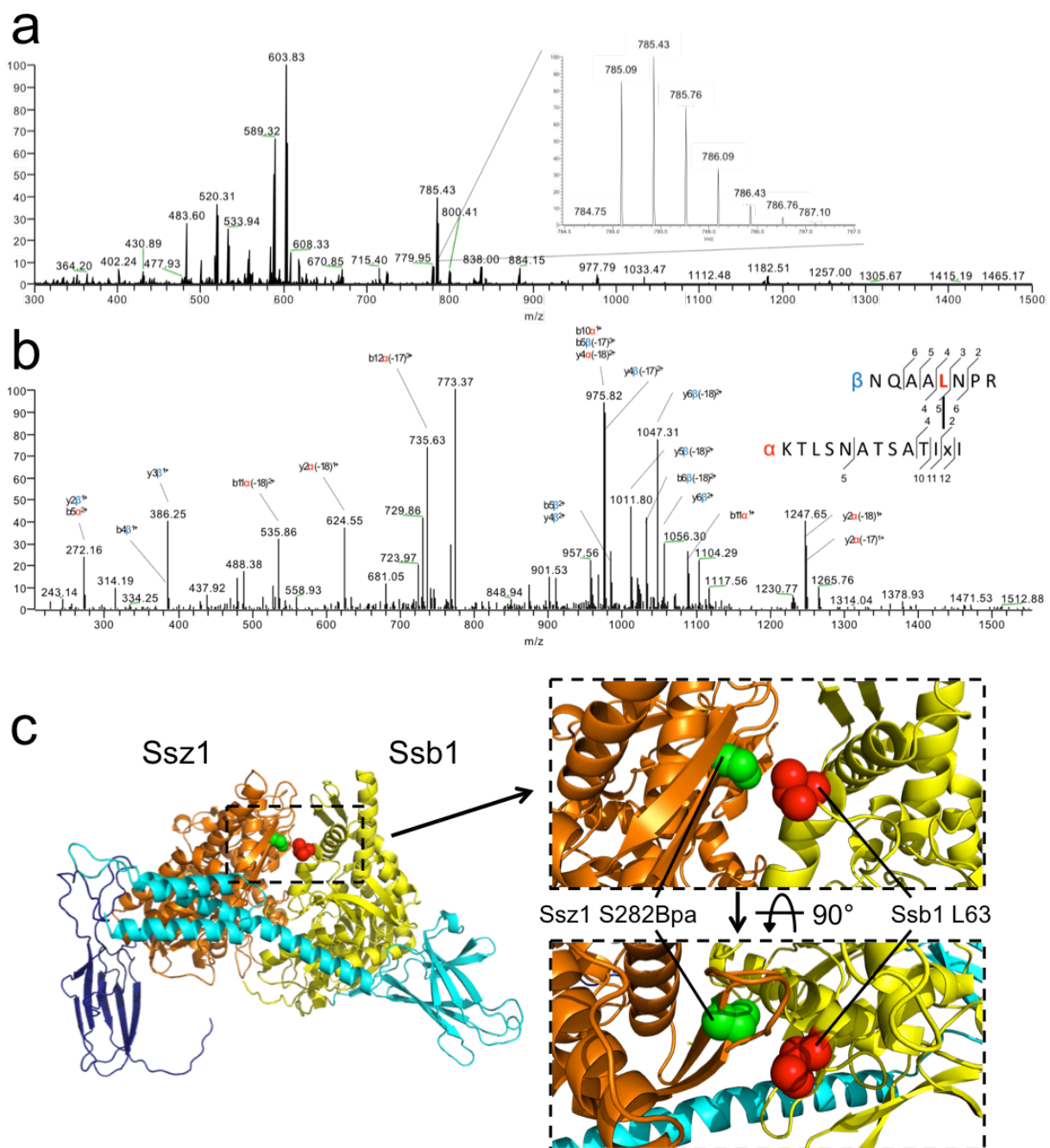


Figure 3-5. Interaction between Ssz1 and Ssb1 in the presence of Zuo1. (a) Combinations of the indicated concentrations of Ssz1, Zuo1, and/or Ssb1 containing a His-SUMO tag at the N-terminus (His-Ssb1) were incubated to allow complex formation, prior to the addition of pre-washed Ni-NTA resin. Bound proteins were eluted with imidazole and subjected to SDS-PAGE. (b) Similar pull-down experiments as in (top) were performed except a Ssz1 variant containing charge reversal substitutions at position R36, D291 and R300 (R36E, D291R and R300E) was used. (c) Amounts of Zuo1 binding were plotted as relative units (r.u.). (bottom) Proteins amounts in the gels (a and b) were quantified using FIJI and values were normalized to the amount of Zuo1 bound when 15 μ M of Zuo1 and Ssz1 were applied to wildtype His-Ssb1, which was set at 1. Zuo1 binding was used to represent Ssz1 binding because of the presence of a band that overlapped with Ssz1. Mw, molecular weight. His-Ssb1, Ssz1, Ssz1_{ERE} and Zuo1 bands are indicated with arrows.

Figure 3-5

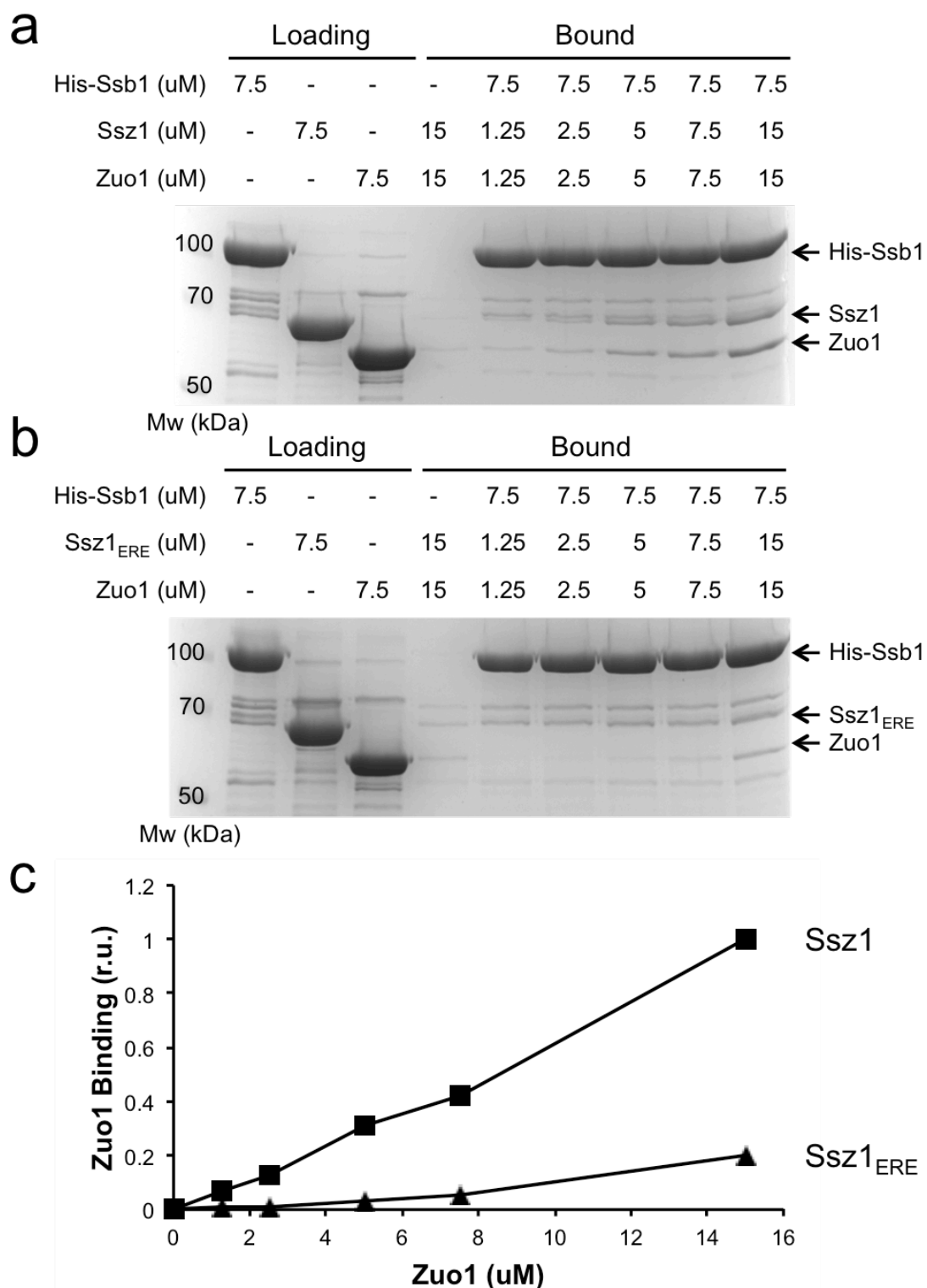


Figure 3-6. (a) Residues important for the interaction between Ssz1 (R36, D291 and R300) and Ssb1 (R261, E370 and E547) are highlighted by sphere representation in the docking model. (b) Growth of strains with deletion of *SSB* and *SSZ1* ($\Delta ssb\Delta ssz1$) harboring plasmids encoding Ssz1 and Ssb1 wildtype or their variants. Ssz1 was expressed under either its endogenous or the *CYC* promoter (indicated by LOW) to reduce the expression level; Ssb1 was expressed under its endogenous promoter. Ten-fold serial dilution of yeast strains harboring the indicated combination of plasmids were spotted on YPD plates. *SSZ1_{ERE}*, Ssz1 variant having substitutions R36E, D291R and R300E; *Ssb1_{RDR}*, Ssb1 variant having substitutions R261D, E370R and E547R. Plates supplemented with 100 ug/ml paromomycin (Paro) or 0.5 M sodium chloride (NaCl) were incubated at 30°C for 2 days. Plate supplemented with 0.1 M lithium chloride (LiCl) was incubated at 23°C for 3 days. Plates without supplement were incubated at 30°C or 23°C for 2 days. All strains were on the same plate, but irrelevant strains were cropped out.

Figure 3-6

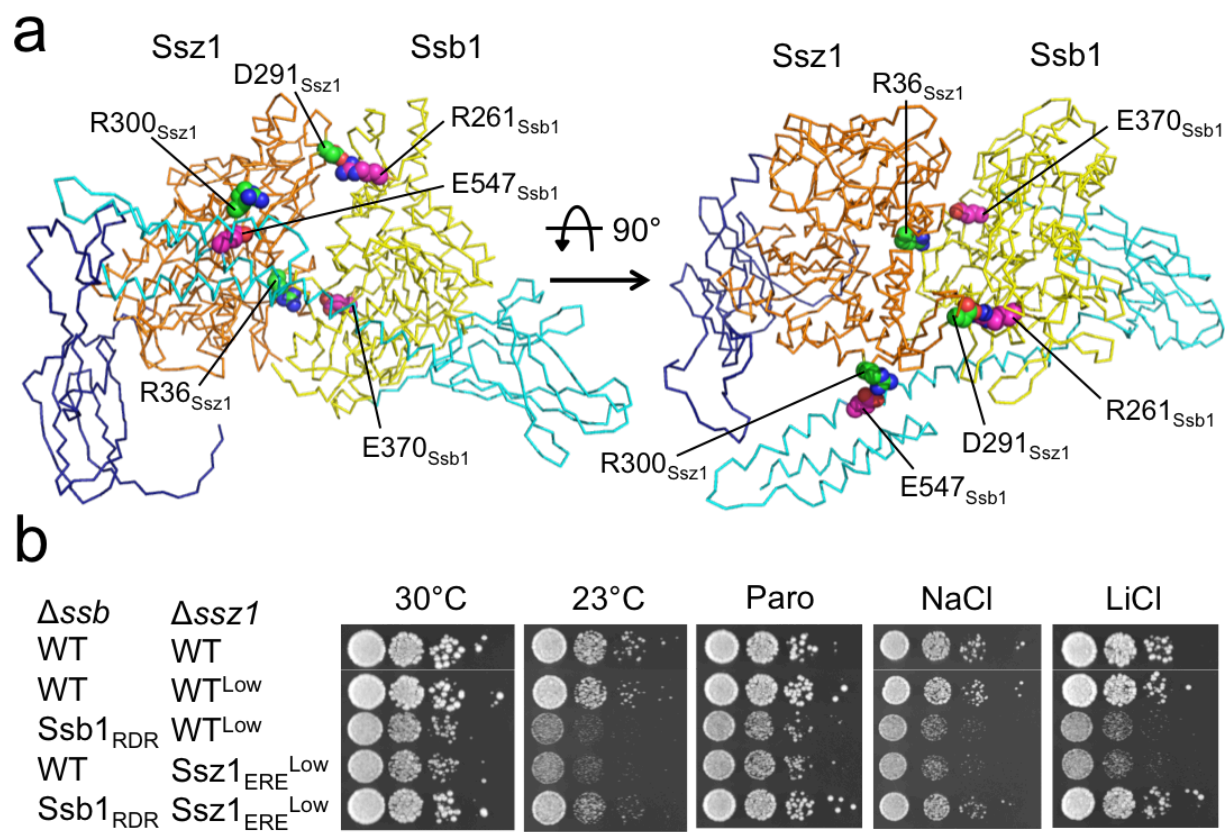
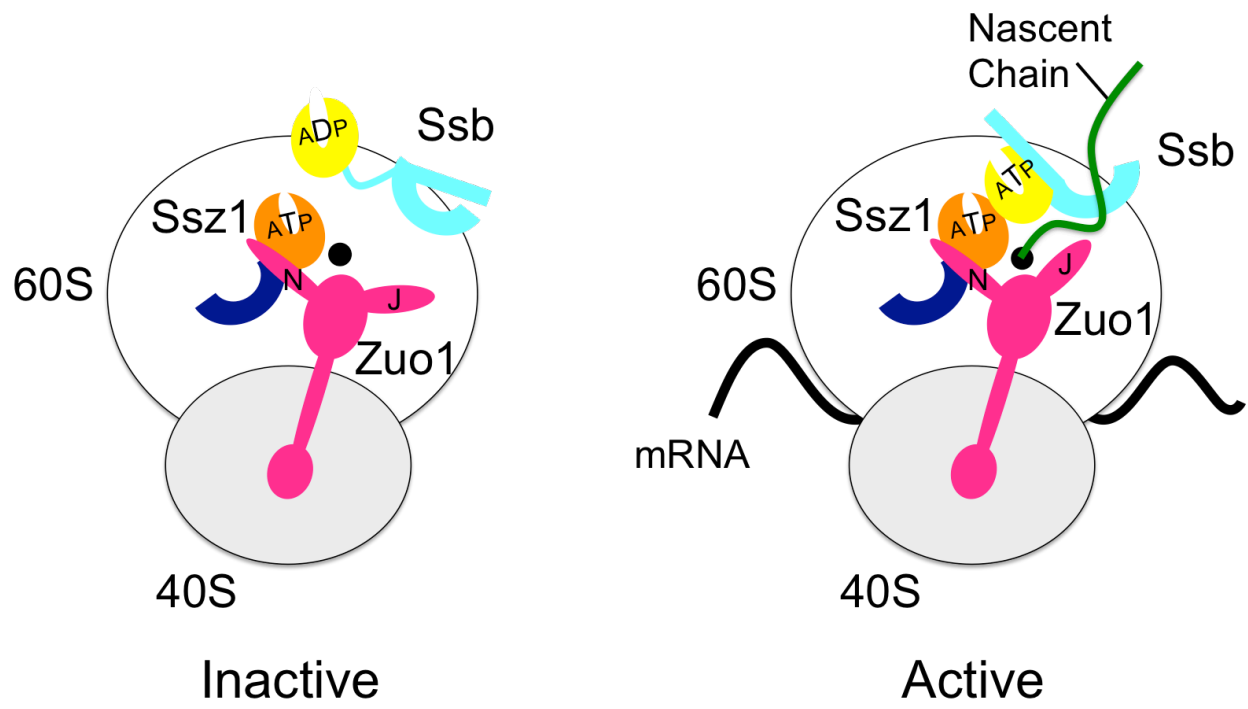


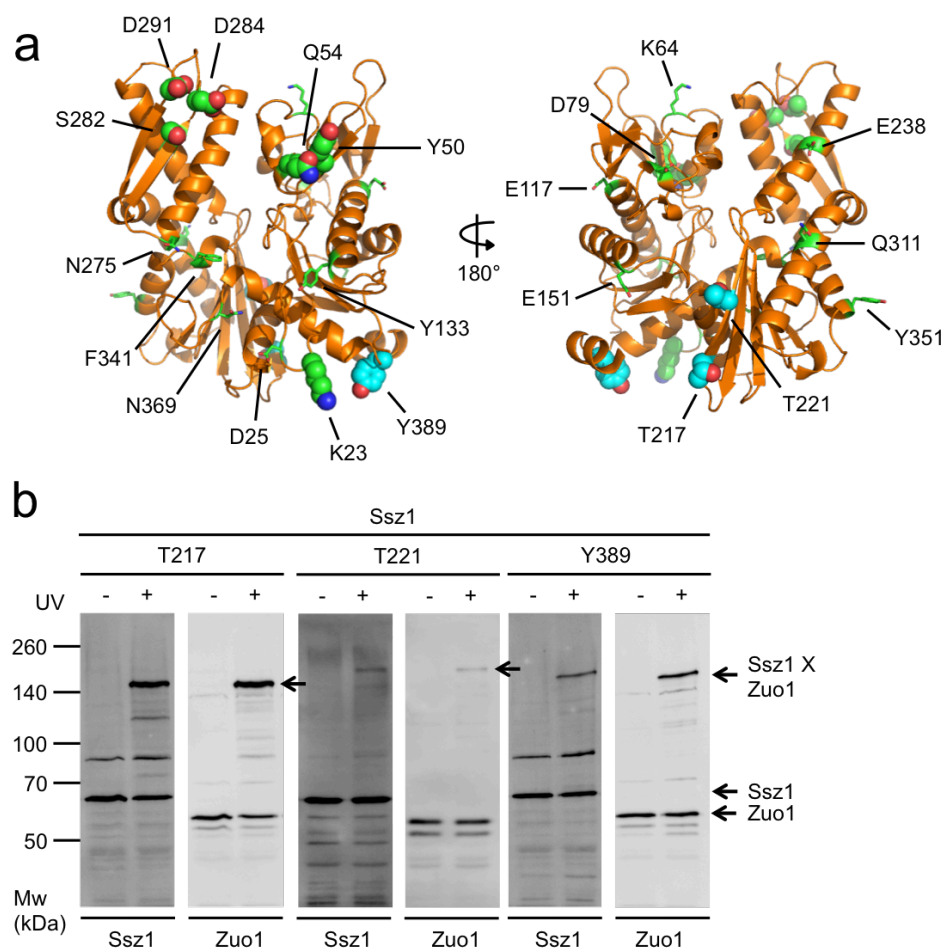
Figure 3-7. Model of the interaction network of the chaperone triad on the ribosome, implying the function of Ssz1. Zuo1 binds to both subunits of the ribosome directly. The N-terminal segment (N) next to the J-domain (J) of Zuo1 tethers Ssz1 to the ribosome. The ADP-bound state of Ssb binds to the ribosome near the polypeptide exit tunnel. Exchange of ADP to ATP alters conformation of Ssb, allowing dimerization with the ATPase domain of Ssz1. The interaction between Ssz1 and Ssb promotes the interaction of Ssb with nascent chains, coordinated by the J-domain of Zuo1.

Figure 3-7



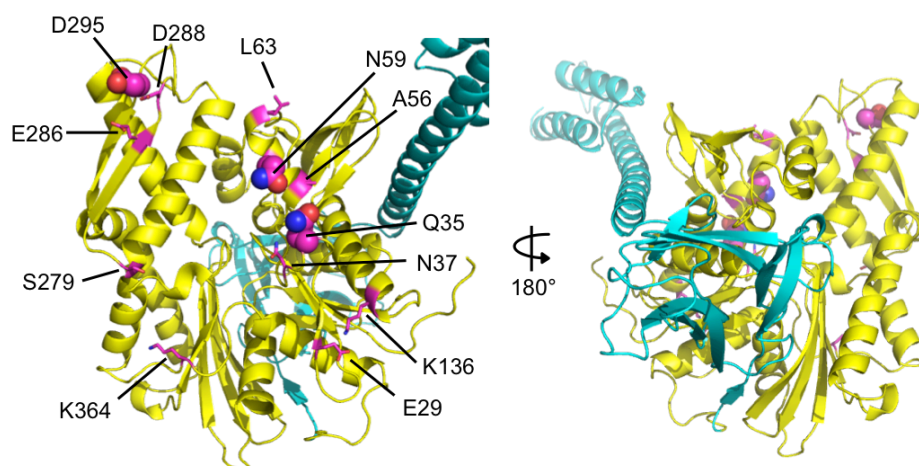
Supplementary Figure 3-1. Crosslinking of the ATPase domain of Ssz1. (a) Ribbon diagram of model structure of the ATPase domain of *S. cerevisiae* Ssz1. Crosslinked sites were highlighted with sphere or sites did not crosslink with stick representation. Green was used for sites crosslinked to Ssb1 and cyan as to Zuo1. (b) Site-specific crosslinking results between Ssz1 and Zuo1. Cells expressing Ssz1 variants containing Bpa at the indicated sites were exposed to UV (+) or unexposed (-) as a control. Immunoblotting was conducted after SDS-PAGE against Ssz1 or Zuo1 specific antibodies. Mw, molecular weight. Ssz1 and Zuo1 bands are indicated with arrows.

Supplementary Figure 3-1



Supplementary Figure 3-2. Crosslinking of the ATPase domain of Ssb1. Ribbon diagram of model structure of the ATPase domain of *S. cerevisiae* Ssb1. Crosslinked sites were highlighted with sphere or sites that did not crosslink with stick representation.

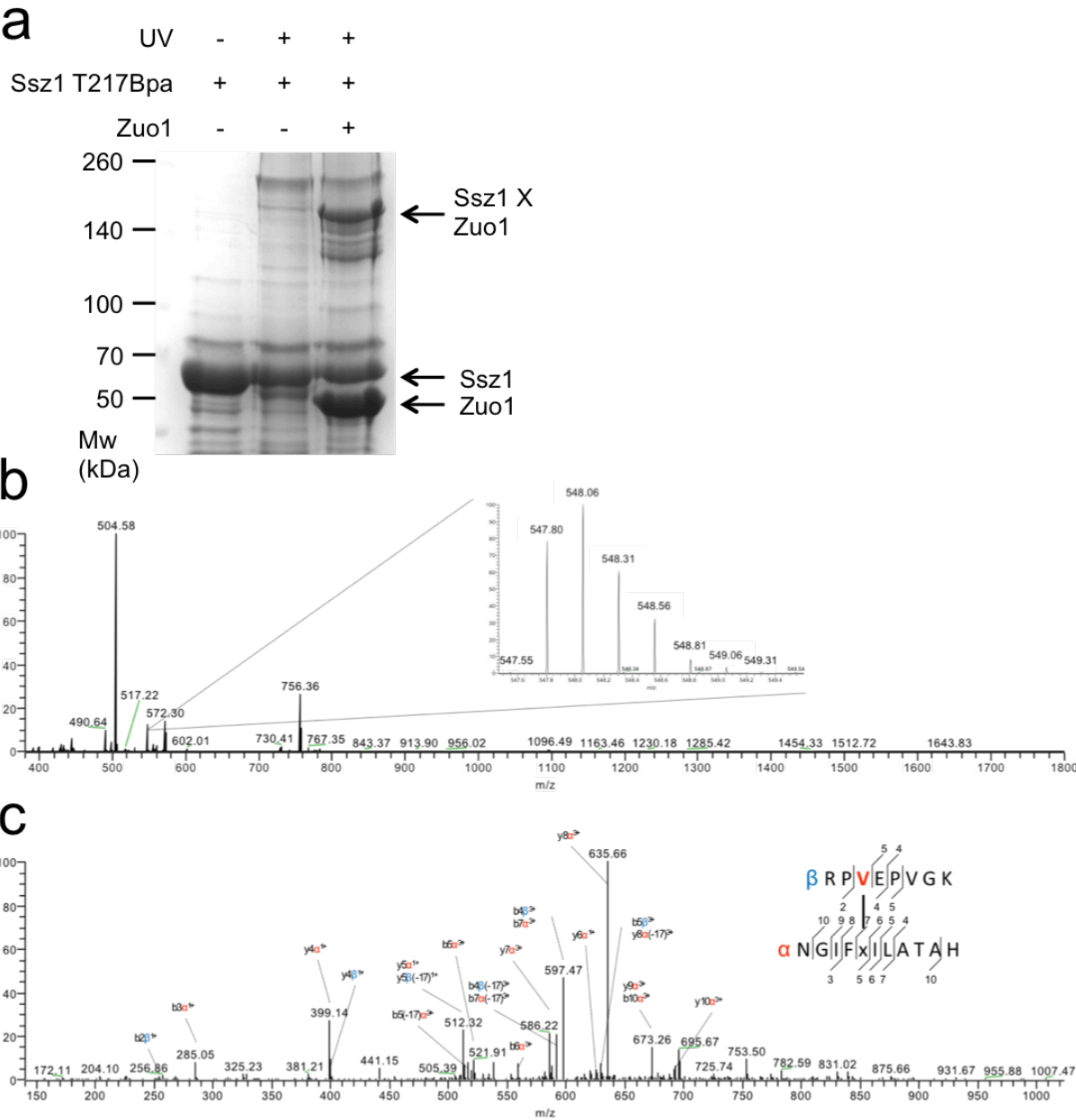
Supplementary Figure 3-2



Supplementary Figure 3-3. The crystal structure between Sse1 and the ATPase domain of Hsp70. Sse1 binds to the ATPase domain of Hsp70 with its ATPase domain and SBD α . Interaction of the SBD α of Sse1 with the subdomain IIb leads to “opening” of the ATP binding pocket between two lobes (I and II) of Hsp70. The ATPase domain of Sse1, green; the SBD of Sse1, red; the ATPase domain of Hsp70 (Hsp70 N), yellow. (PDB 3D2F)

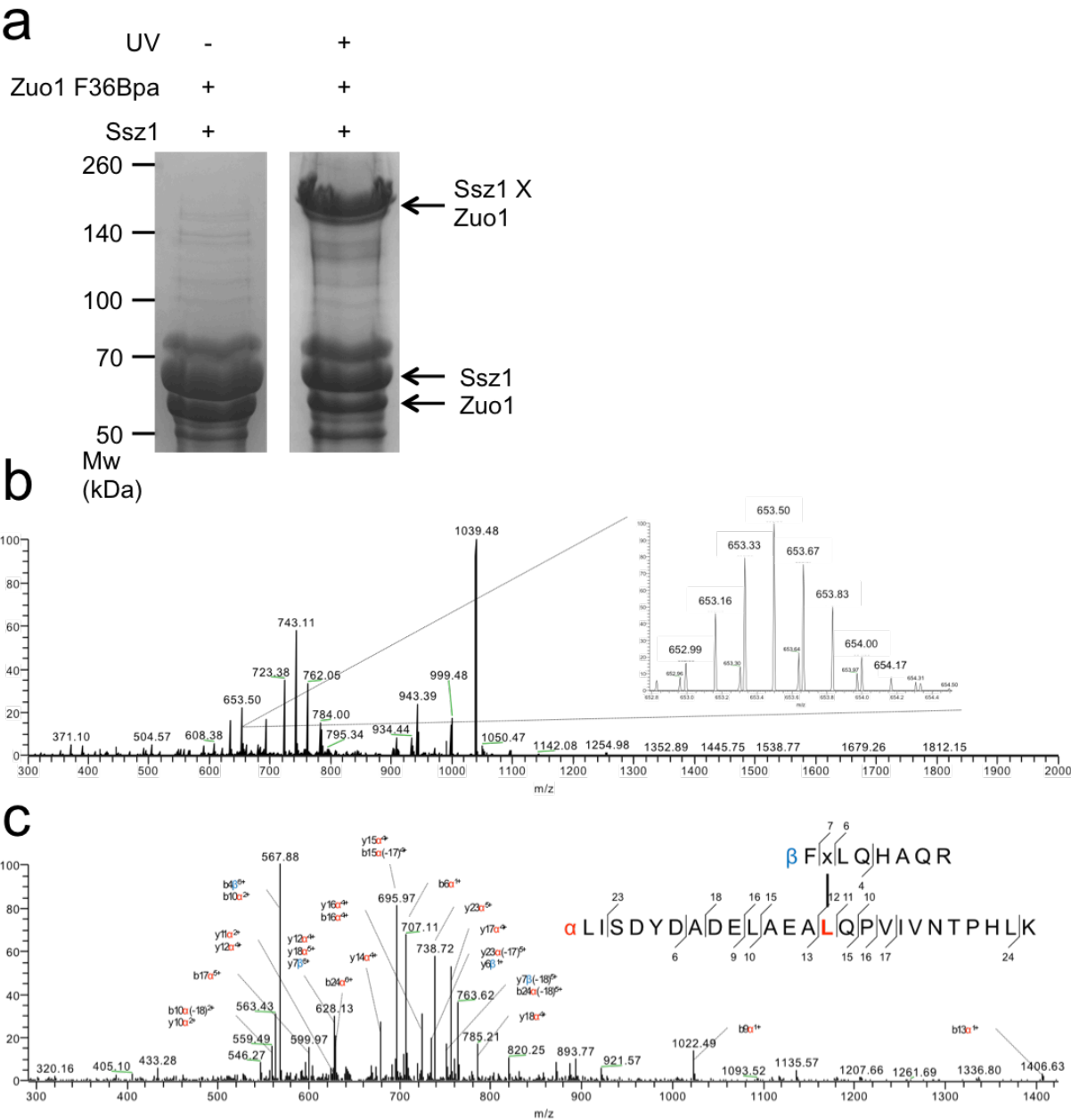
Supplementary Figure 3-4. Crosslinking between Ssz1 T217Bpa and Zuo1. (a) Ssz1 containing Bpa at position 217 and Zuo1 were expressed and purified from *E. coli*. Ssz1 T217Bpa were exposed to UV with or without Zuo1 or unexposed as a control. Proteins were then subjected to SDS-PAGE. The gel containing unique and the most abundant crosslinking product between Ssz1 T217Bpa and Zuo1 was excised to be digested with trypsin and Asp-N for mass spectrometry analysis. Mw, molecular weight. Ssz1 and Zuo1 bands are indicated with arrows. (b) Mass spectrum (MS) containing a 4+ charged ion at m/z 547.805 with a zoom-in view which was selected for fragmentation. (c) Fragment ion mass spectrum (MS/MS) of crosslinked peptides between Zuo1 (β peptide, in blue; amino acids 27-34) and Bpa containing Ssz1 (α peptide, in red; amino acids 213-223). Valine at position 29 of Zuo1 was identified to be crosslinked to Bpa at position 217 of Ssz1.

Supplementary Figure 3-4



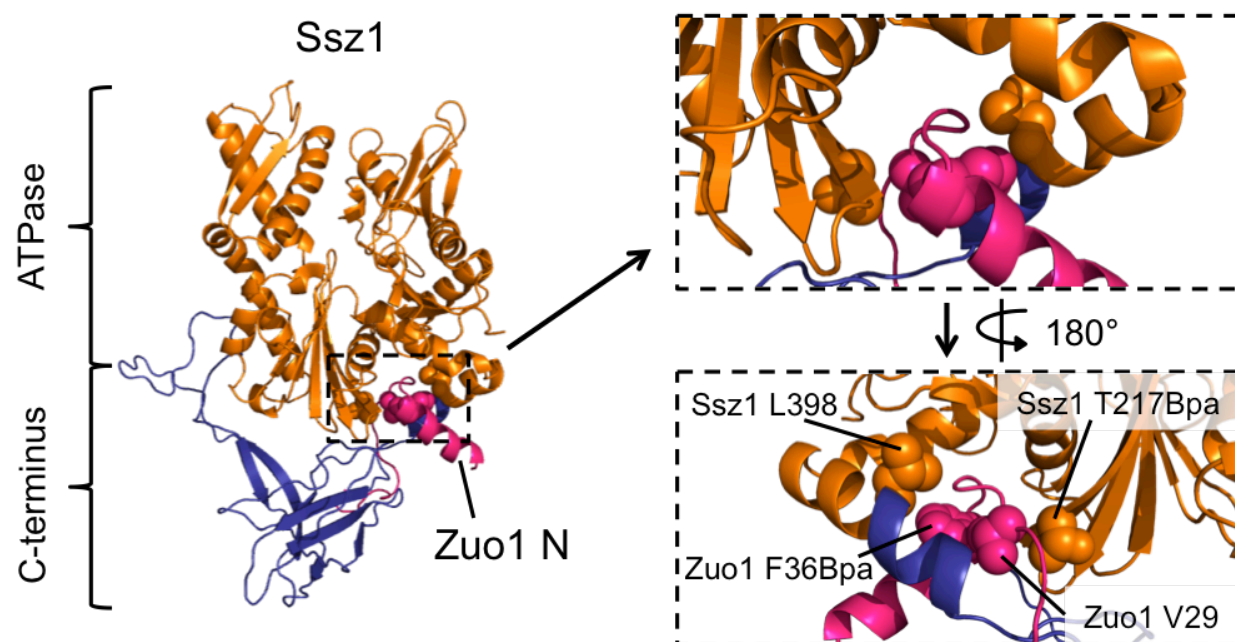
Supplementary Figure 3-5. Crosslinking between Zuo1 F36Bpa and Ssz1. (a) Zuo1 containing Bpa at position 36 and Ssz1 were expressed and purified from *E. coli*. Zuo1 F36Bpa and Ssz1 were exposed to UV or unexposed as a control. Proteins were then subjected to SDS-PAGE. The gel containing unique and the most abundant crosslinking product between Zuo1 F36Bpa and Ssz1 was excised to be digested with trypsin for mass spectrometry analysis. Mw, molecular weight. Ssz1 and Zuo1 bands are indicated with arrows. (b) Mass spectrum (MS) containing a 6+ charged ion at m/z 653.163 with a zoom-in view which was selected for fragmentation. (c) Fragment ion mass spectrum (MS/MS) of crosslinked peptides between Bpa containing Zuo1 (β peptide, in blue; amino acids 35-42) and Ssz1 (α peptide, in red; amino acids 385-409). Leucin at position 398 of Ssz1 was identified to be crosslinked to Bpa at position 36 of Zuo1.

Supplementary Figure 3-5

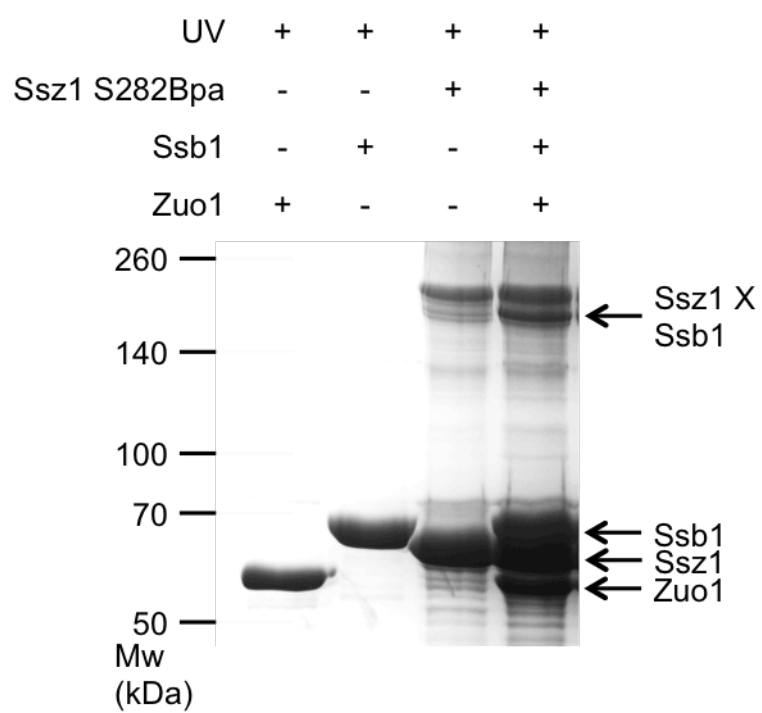


Supplementary Figure 3-6. Fidelity of mass spectrometry analysis. Left, ribbon diagram of the model structure of *S. cerevisiae* Ssz1 and Zuo1 N-terminus (Zuo1 N) complex based on the crystal structure of *C. thermophilum* Ssz1 and Zuo1 N-terminus complex (PDB 5MB9). Right, sites where Bpa were incorporated and residues crosslinked to Bpa (Ssz1 T217Bpa-Zuo1 V29 and Zuo1 F36Bpa-Ssz1 L398) were highlighted in sphere representation.

Supplementary Figure 3-6

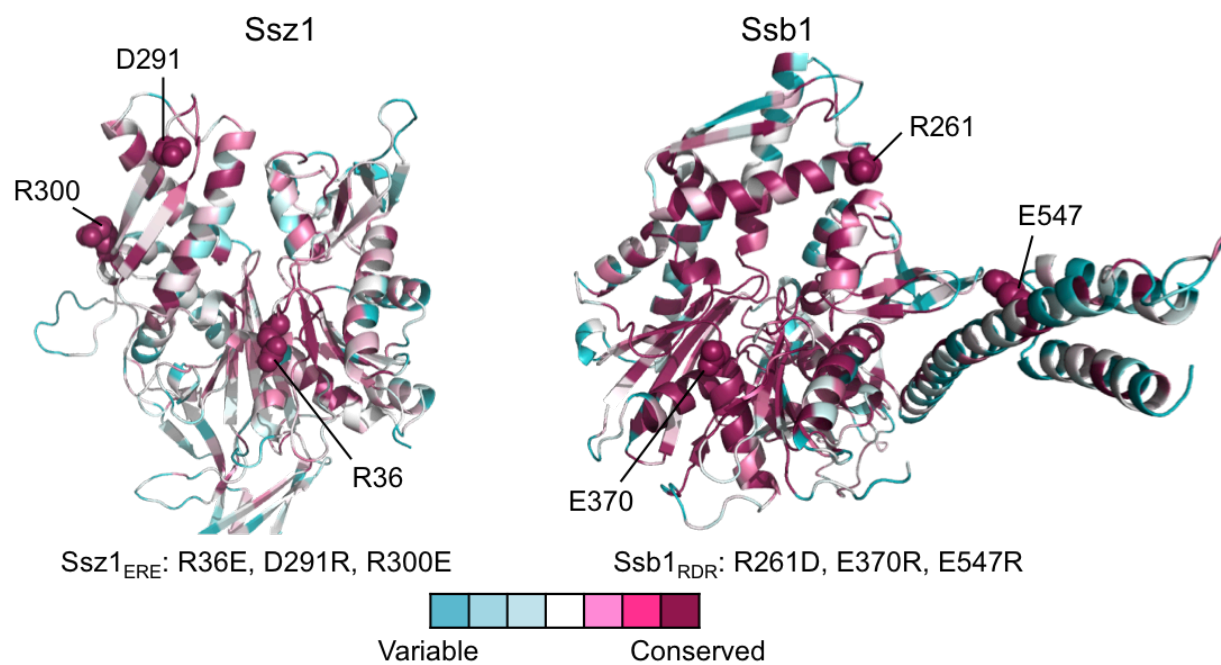


Supplementary Figure 3-7. Crosslinking between Ssz1 S282Bpa and Ssb1. Ssb1 containing Bpa at position 282, Ssz1 and Zuo1 were expressed and purified from *E. coli*. Individual or all protein(s) were exposed to UV and then subjected to SDS-PAGE. The gel containing unique and the most abundant crosslinking product between Ssz1 S282Bpa and Ssb1 was excised to be digested with trypsin and Asp-N for mass spectrometry analysis. Ssz1, Ssb1 and Zuo1 bands are indicated with arrows.

Supplementary Figure 3-7

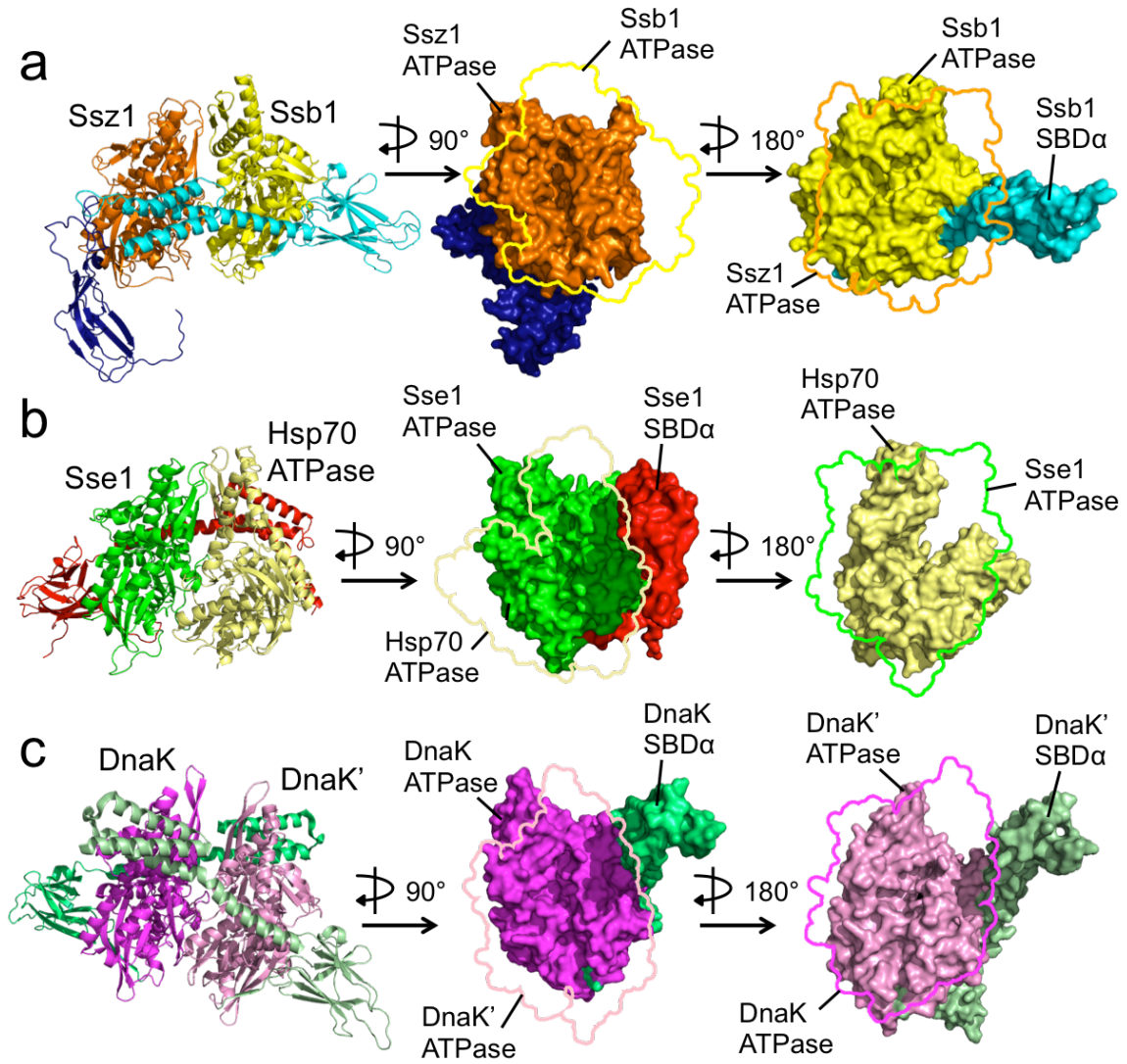
Supplementary Figure 3-8. Highly conserved residues important for the interaction between Ssz1 and Ssb1. Protein sequences of Ssz1 or Ssb1 in different fungal species were aligned and represented according to its conservation in the model structures of Ssz1 and Ssb1 in Fig. 3-3. using Consurf. Notably Ssb1 residues forming the ATP binding pocket and the cleft together with residues located at the interface between the ATPase domain and SBD displayed high conservation.

Supplementary Figure 3-8



Supplement Figure 3-9. Comparison of the interactions between Hsp70-type molecular chaperones. The crystal structures of Sse1 and Hsp70 complex (PDB 3D2F) or DnaK dimer (4JNE) was superimposed to the docking model between Ssz1 and Ssb1 based on the ATPase domains of Ssz1, Sse1 and DnaK. (a) Ribbon diagram of the docking model between Ssz1 and Ssb1 from this study. Either outline of the ATPase domain of Ssb1 or Ssz1 was shown on top of surface representation of Ssz1 or Ssb1 (b) Ribbon diagram of the crystal structure of Sse1 and Hsp70 ATPase domain. Either outline of the ATPase domain of Hsp70 or Sse1 was shown on top of surface representation of Sse1 or Hsp70 ATPase domain. (c) Ribbon diagram of the crystal structure of DnaK dimer. Either outline of the ATPase domain of DnaK' or DnaK was shown on top of surface representation of DnaK or DnaK'.

Supplement Figure 3-9



Supplementary Figure 3-10. Interaction between Ssz1_{ERE} and His-Zuo1. Ssz1 or a Ssz1 variant containing charge reverse mutations at position R36E, D291R and R300E, Ssb1 and Zuo1 containing His-SUMO tag at the N-terminus (His-Zuo1) were used. Ni-NTA resins were incubated with mixture of Ssz1 and Ssb1 or mixture of Ssz1_{ERE} and Ssb1 alone as a control or those with His-Zuo1. Bound proteins were eluted with imidazole and subjected to SDS-PAGE. Mw. Molecular weight. His-Zuo1, Ssb1 and Ssz1 bands are indicated with arrows.

Supplementary Figure 3-10

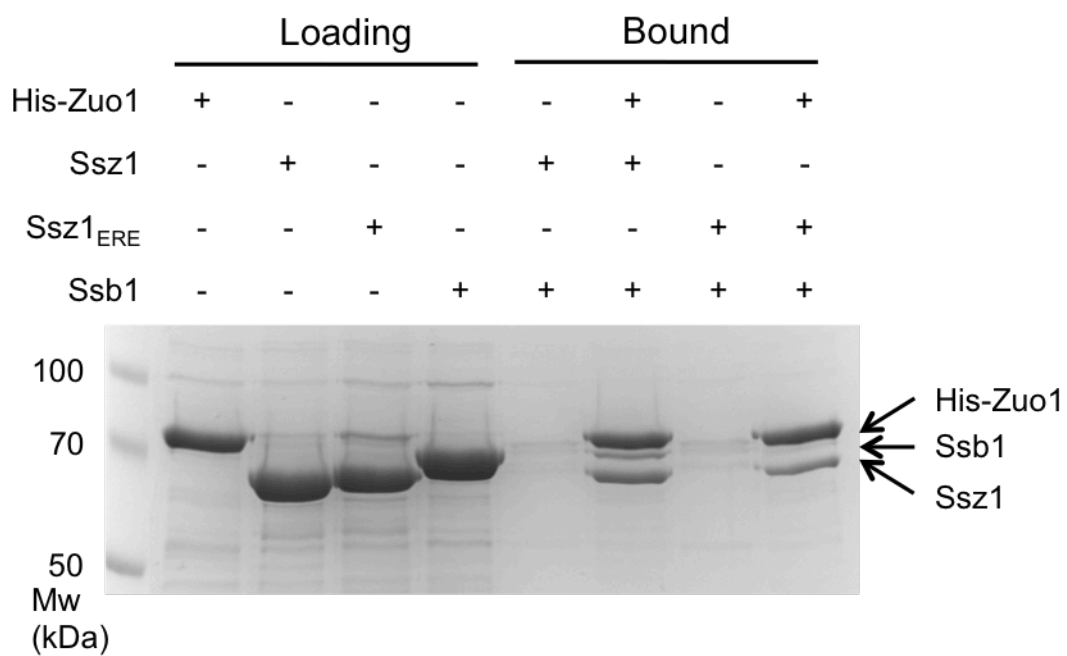


Table 3-1. StavroX analysis results of the crosslinking products between Ssz1 T217Bpa and Zuo1 shown in Supplementary Figure 3-3. Top ten candidates of crosslinked peptides and sites were shown. All candidates passed false discovery rate of 5%. (Meas.: Measured; Calc.: Calculated; Dev.: Deviation; Site: crosslinked to Bpa)

Table 3-1

Score	m/z	Charge	Mass (Meas.)	Mass (Calc.)	Dev. (ppm)	Zuo1 Peptide	From	To	Ssz1 Peptide	From	To	Site
180	730.069	3	2188.193	2188.191	0.80	[R PVEPVGK]	27	34	[NGIFxILATAH]	213	223	R27
173	547.805	4	2188.198	2188.191	2.89	[R P VPEPVGK]	27	34	[NGIFxILATAH]	213	223	V29
170	547.803	4	2188.192	2188.191	0.10	[R P VPEPVGK]	27	34	[NGIFxILATAH]	213	223	V29
166	730.069	3	2188.193	2188.191	0.80	[R P VPEPVGK]	27	34	[NGIFxILATAH]	213	223	P31
165	730.071	3	2188.198	2188.191	3.23	[R PVEPVGK]	27	34	[NGIFxILATAH]	213	223	R27
164	730.070	3	2188.195	2188.191	1.81	[R PVEPVGK]	27	34	[NGIFxILATAH]	213	223	R27
160	547.805	4	2188.200	2188.191	3.78	[R P VPEPVGK]	27	34	[NGIFxILATAH]	213	223	V29
158	547.805	4	2188.196	2188.191	2.33	[R P VPEPVGK]	27	34	[NGIFxILATAH]	213	223	V29
157	730.070	3	2188.194	2188.191	1.39	[R PVEPVGK]	27	34	[NGIFxILATAH]	213	223	R27
156	730.070	3	2188.195	2188.191	1.89	[R P VPEPVGK]	27	34	[NGIFxILATAH]	213	223	V29

Table 3-2. StavroX analysis results of crosslinking products between Zuo1 F36Bpa and Ssz1 shown in Supplementary Figure 3-5. Top ten candidates of crosslinked peptides and sites were shown. All candidates passed false discovery rate of 5%. (Meas.: Measured; Calc.: Calculated; Dev.: Deviation; Site: crosslinked to Bpa)

Table 3-2

Score	m/z	Charge	Mass (Meas.)	Mass (Calc.)	Dev. (ppm)	Zuo1 Peptide	From	To	Ssz1 Peptide	From	To	Site
163	979.240	4	3913.938	3914.012	-18.94	[FxLQHAQR]	35	42	[LISDYDADELAELQPVIIVNTPHLK]	385	409	I402
158	783.600	5	3913.971	3914.012	-10.58	[FxLQHAQR]	35	42	[LISDYDADELAELQPVIIVNTPHLK]	385	409	L398
148	653.163	6	3913.943	3914.012	-17.65	[FxLQHAQR]	35	42	[LISDYDADELAELQPVIIVNTPHLK]	385	409	L398
146	653.164	6	3913.947	3914.012	-16.62	[FxLQHAQR]	35	42	[LISDYDADELAELQPVIIVNTPHLK]	385	409	L398
139	653.165	6	3913.951	3914.012	-15.59	[FxLQHAQR]	35	42	[LISDYDADELAELQPVIIVNTPHLK]	385	409	E386
136	783.596	5	3913.953	3914.012	-15.21	[FxLQHAQR]	35	42	[LISDYDADELAELQPVIIVNTPHLK]	385	409	L398
136	653.164	6	3913.950	3914.012	-15.87	[FxLQHAQR]	35	42	[LISDYDADELAELQPVIIVNTPHLK]	385	409	L398
134	653.164	6	3913.945	3914.012	-17.09	[FxLQHAQR]	35	42	[LISDYDADELAELQPVIIVNTPHLK]	385	409	V403
128	683.210	7	4776.426	4776.515	-18.52	[RPVEPVGKFxLQHAQR]	27	42	[LISDYDADELAELQPVIIVNTPHLK]	385	409	E386
120	653.165	6	3913.951	3914.012	-15.59	[FxLQHAQR]	35	42	[LISDYDADELAELQPVIIVNTPHLK]	385	409	L398

Table 3-3. StavroX analysis results of crosslinking products between Ssz1 S282Bpa and Ssb1 shown in Fig. 3-4. Top ten candidates of crosslinked peptides and sites were shown. All candidates passed false discovery rate of 5%. (Meas.: Measured; Calc.: Calculated; Dev.: Deviation; Site: crosslinked to Bpa)

Table 3-3

Score	m/z	Charge	Mass (Meas.)	Mass (Calc.)	Dev. (ppm)	Ssb1 Peptide	From	To	Ssz1 Peptide	From	To	Site
195	742.394	3	2225.168	2225.156	5.50	[NQAA ^u LNPR]	59	66	[TL ^u SNATSATixI]	272	283	L63
194	785.092	3	2353.261	2353.251	4.40	[NQAA ^u LNPR]	59	66	[KTLSNATSATixI]	271	283	L63
174	871.123	3	2611.353	2611.336	6.47	[NQAA ^u LNPR]	59	66	[TL ^u SNATSATixIDSLA]	272	287	L63
173	742.394	3	2225.168	2225.156	5.42	[NQAA ^u LNPR]	59	66	[TL ^u SNATSATixI]	272	283	L63
169	785.092	3	2353.261	2353.251	4.32	[NQAA ^u LNPR]	59	66	[KTLSNATSATixI]	271	283	L63
167	742.394	3	2225.168	2225.156	5.50	[NQAA ^u LNPR]	59	66	[TL ^u SNATSATixI]	272	283	L63
165	589.072	4	2353.265	2353.251	5.74	[NQAA ^u LNPR]	59	66	[KTLSNATSATixI]	271	283	P65
157	742.392	3	2225.161	2225.156	2.04	[NQAA ^u LNPR]	59	66	[TL ^u SNATSATixI]	272	283	L63
157	589.071	4	2353.263	2353.251	4.91	[NQAA ^u LNPR]	59	66	[KTLSNATSATixI]	271	283	P65
150	685.617	4	2739.445	2739.431	4.94	[NQAA ^u LNPR]	59	66	[KTLSNATSATixIDSLA]	271	287	Q60

CHAPTER FOUR: Conclusion and future direction

1. CONCLUSION

In Chapter Two, I determined the interaction between Zuo1 and the ribosome, which provided insight into Zuo1 function. My results suggested that the ZHD binds near the ribosome tunnel exit. From crosslinking experiments, I identified interactions between the C-terminal region of helix III of the ZHD and a surface exposed loop of eL31. Ribosomal RNA mutagenesis and sucrose cushion centrifugation experiments suggested that two arginine residues of the ZHD at the tip of helix III interact with rRNA H24. A rigid-body docking model between the ZHD and the ribosome also supported my crosslinking and mutagenesis results.

We also verified an interaction between the C-terminus of Zuo1 and the 40S subunit that is important for translational fidelity. Deletion of either the C-terminal four-helix bundle of Zuo1 or ES12 of ribosomal RNA helix 44, which originates at the decoding center, destabilized ribosome association of Zuo1. These deletions resulted in a decrease in -1 frame shifting and increased stop codon readthrough, indicating that the interaction is important for maintaining translational fidelity. Moreover, we tested the junction between the ZHD and the middle domain connecting the C-terminus on 40S. We found that the junction is important not only for association of Zuo1 with the ribosome, but also for maintaining translational fidelity.

Our study showed how Zuo1 coordinates the folding of nascent chains at the ribosome tunnel exit with the decoding of mRNA at the decoding center by binding both subunits of the ribosome. I hypothesized that Zuo1 senses the folding state of nascent chains to regulate the rate of decoding, coordinating folding with translation. Future work is needed to understand how Zuo1 regulates the rate of translation based on the folding state of nascent chains. I will discuss several possible directions for future studies below.

In Chapter Three, I proposed that Ssz1 is a scaffold that positions Ssb on the ribosome. Direct interactions between Ssz1 and Ssb1 were identified from Bpa site-specific crosslinking. Computer based docking was performed to understand the mode of interaction between Ssz1 and Ssb1. In the docking model, the ATPase domains of both Ssz1 and Ssb1 interacted with each other. Mass spectrometry analysis of crosslinked products between Ssz1 and Ssb1 confirmed the docking model.

In my docking model, Ssz1 and Ssb1 interacted via salt bridges between highly conserved residues. I found that reverse charge substitutions of these residues destabilized the interaction between Ssz1 and Ssb1 in pull-down assays. Yeast strains with either Ssz1 or Ssb1 variants exhibited slow growth phenotypes. However, the presence of both variants complemented the growth defect, strongly supporting that this specific interaction is critical for wild-type growth *in vivo*.

I hypothesize that Ssz1 positions Ssb on the ribosome through ATPase domain dimerization, which facilitates the interaction between Ssb and nascent chains. This function might be much more significant for metazoans that do not contain ribosome-associated Ssb orthologs. Future work should confirm that Ssz1 orthologs in higher eukaryotes directly interact with cytosolic Hsp70s to facilitate the interaction between Hsp70s and nascent chains by localizing Hsp70s to the ribosome.

2. FUTURE DIRECTION

2.1. Chapter Two: Dual interaction of the Hsp70 J-protein cochaperone Zuotin with the 40S and 60S ribosomal subunits

2.1.1. Examining the function of Zuo1 in translation regulation

Zuo1 may sense the folding state of nascent chains at the ribosome tunnel exit and regulate peptide-bond formation through the interaction of its C-terminal four-helix bundle with rRNA H44. Cryo-EM data showed that binding of Zuo1 preferentially stabilizes ribosomes in their non-rotated state. Zuo1 might regulate translation by controlling the rotational state of the ribosome during peptide-bond formation.

To test whether binding of Zuo1 on the ribosome affects the rate of translation, *in vitro* translation assays can be conducted using yeast ribosomes isolated by centrifugation. These can be washed with salt to obtain intact ribosomes without ribosome-associated proteins such as Zuo1. Intact ribosomes can be incubated with or without purified Zuo1 and then used in translation assays to test whether the presence of Zuo1 affects translation rate. The C-terminal deletion variant of Zuo1 described in Chapter Two can be used as a negative control to exclude potential indirect effects of addition of Zuo1 on translation. This variant can also provide information on whether the C-terminal four-helix bundle of Zuo1 is required for regulating translation.

If the isolated ribosomes are non-functional after multiple purification steps, similar translation assays can be performed with lysates of strains with *zuo1* deleted or with the C-terminal deletion variant of Zuo1. However, lysates from different strain backgrounds can cause changes in translation rates that would confound the results, e.g., the number of functional ribosomes could be different. To overcome this potential problem, purified Zuo1, or its variants,

could be added to lysates of the *zuo1* deletion strain to make sure translation rate differences are caused solely by Zuo1.

The translation rate differences caused by Zuo1 variants could be below the limit of detection of conventional translation assays. To enhance the signal, the reporter protein can be codon optimized, or deoptimized, to speed up or slow down translation, which might result in more sensitivity to the function of Zuo1 (Yu et al., 2015). The ratchet-like motion of ribosomes also can be directly monitored by single molecule FRET assays to examine the effects of Zuo1 on translation.

2.1.2. Sensing of folding states of nascent chains by Zuo1 to regulate translation rate of the ribosome

If Zuo1 affects translation rate, one could test whether Zuo1 senses the folding states of nascent chains and relays that information to the peptidyl transferase center to regulate the rate of translation. The translation rates of nascent chains either bearing or lacking mutations that cause misfolding can be compared. Without Zuo1, the translation rate should be similar for both the wildtype and the folding defective variant. However, addition of Zuo1 might slow down the translation rate of the variant.

Zuo1 does not contain a domain that directly binds to nascent chains. Thus, Zuo1 might need to form a complex with Ssz1 to sense the folding state of nascent chains through the cleft of Ssz1. Alternatively, Ssb may be required for Zuo1 to sense nascent chains. To test these possibilities, the translation rates in wildtype or the nascent chain variants in the presence of Zuo1 with Ssz1 or both Ssz1 and Ssb1 could be monitored. In addition, the amino acids forming the cleft of Ssz1 or Ssb1 could be altered to block interaction with nascent chains. These

experiments will test the direct involvement of either the Ssz1 or the Ssb cleft in sensing the folding states of nascent chains.

The interaction between a nascent chain and Ssb (or Ssz1) could also trigger an overall conformational change in Zuo1 that affects translation, especially at the junction between the ZHD and MD. Comparing cryo-EM structures of the Zuo1/Ssz1/ribosome complex with wildtype or the misfolded nascent chain could be used to identify structural differences at this junction.

2.1.3. Sensing mRNA decoding by Zuo1 to regulate the ATPase activity of Hsp70

It is possible that Zuo1 senses mRNA decoding at the ribosome decoding center through the interaction between its C-terminal domain and rRNA H44. This may cause a conformational change in Zuo1 on the 60S subunit that activates the ATPase, Ssb1. The necessary structural information to confirm this regulatory mechanism is lacking. In particular, location of the J-domain in the Zuo1/Ssz1 complex is unknown. Obtaining a complete structure of the complex is likely difficult because the MD and the C-terminal domain are tethered to the ZHD of Zuo1 through a flexible junction. Thus, deletion of the MD and the C-terminal domain of Zuo1, leaving only domains of the complex on the 60S subunit, may increase the chance of getting the structure either by X-ray crystallography or cryo-EM.

Once the structure is determined, the interaction sites among Zuo1, Ssz1 and Ssb1 can be identified and used to test for translation-dependent conformational changes in Zuo1. However, this may still be hard because of the potential flexibility of the N-terminus of Zuo1, which consists of the N-terminal segment complexed with Ssz1, the J-domain, and the ZHD. If this is the case, the interaction sites between the J-domain of Zuo1 and Ssb1 could be predicted from a

recent crystal structure of the complex between DnaK (a *E. coli*. Hsp70) and the J-domain of DnaJ (a *E. coli*. J-protein). The J-domain of Zuo1 can be screened to identify Ssb1 binding sites using Bpa crosslinking.

After screening, *in vitro* crosslinking experiments can be conducted with Bpa containing Zuo1 purified from *E. coli*, and the isolated and salt washed ribosomes mentioned in the previous section can be used to test whether crosslinking between Zuo1 and Ssb1 depends on translation. In the absence of mRNA for translation, the crosslinking efficiency between the J-domain of Zuo1 and Ssb1 should be low. On the other hand, we expect that adding mRNA to initiate translation will increase the crosslinking efficiency if our working model is correct.

To test if the crosslinking efficiency depends on the interaction between the C-terminal domain and ribosomal RNA H44, a Zuo1 variant lacking the C-terminal domain can be used. However, deleting the C-terminal domain introduces a problem because the C-terminal domain of Zuo1 is required for the interaction between Zuo1 and the ribosome. To prevent this potential problem, one could use mutations that disrupt the junction between the ZHD and MD without affecting ribosome association of Zuo1. This kind of variant would allow us to test whether a connection between the C-terminal domain and ZHD of Zuo1 is required for transmitting a signal that regulates the interaction between the J-domain of Zuo1 and Ssb.

All of the experiments mentioned above can be carried out with FRET analysis instead of crosslinking. As mentioned earlier, the J-domain of Zuo1 interacts with the base of the ATPase domain of Ssb1. A donor and an acceptor can be incorporated in the J-domain of Zuo1 and the base of the ATPase domain of Ssb1, respectively. FRET efficiency will then depend on the translation states of ribosomes with wildtype Zuo1 or variants containing mutations at the ZHD/MD junction.

2.1.4. Sensing the transit of nascent chains at the ribosome exit tunnel by Zuo1 through ul22

The two arginine residues located at the tip of helix III of the ZHD of Zuo1 interact with rRNA H24. H24 contacts ul22, which contains a patch that forms a constriction site within the ribosome exit tunnel. It has been suggested that ul22 senses the transit of nascent chains at the tunnel and signals this to the outside of the ribosomes (Zhang et al., 2013). Because Zuo1 is indirectly connected to ul22 via H24, Zuo1 might receive the signal to regulate function of Ssb or the ribosome through ul22.

To identify whether Zuo1 function relies on ul22, several mutations can be introduced to ul22, Zuo1, or nascent chains. The effects of these mutations on the conformation of the J-domain of Zuo1 can be monitored with either crosslinking or FRET experiments described in the previous sections. The patch of ul22 that forms part of the tunnel could be altered to disrupt its recognition of nascent chains transiting the tunnel. Translation efficiency of nascent chains can be measured to examine whether mutations in ul22 affect folding of nascent chains. A mutation can be introduced to the two arginine residues of Zuo1 that interact with ul22. Although altering just one arginine does not exhibit growth defect phenotypes, it is possible that the mutation could hamper transmission of the signaling from ul22, resulting in a decrease in correct translation of nascent chains.

2.2. Chapter Three: The interaction between a typical and an atypical Hsp70s by ATPase domain dimerization at the ribosome

2.2.1. Interaction of Ssb with the ribosomes through Ssz1.

Ssz1 binds to Ssb1 directly through ATPase domain dimerization *in vitro*. This result implies that Ssz1 positions Ssb on the ribosome *in vivo*. However, it has not been tested whether the interaction is important for the ribosome-association of Ssb. It is difficult to examine importance of such an interaction because Ssb associates with the ribosome through Ssz1 and through the nascent chain after sucrose centrifugation. To exclude ribosome association of Ssb through the nascent chain, a Zuo1 variant that is defective for ATPase activation can be used. This variant would help to test the importance of the interaction between Ssz1 and Ssb using either the Ssz1 or Ssb1 variant described in Chapter Three.

2.2.2. Direct interaction of Ssb with the ribosomes.

I presented results suggesting that Ssz1 positions Ssb on the ribosome. However, localization of Ssb on the ribosome is more complex because Ssb also binds to the ribosome directly. In addition, the interaction of Ssb with the ribosome was suggested to be dependent on its nucleotide-bound states.

It has been implicated that all three domains of Ssb are involved in ribosome association (James et al., 1997). Here we report that the ATPase domain of Ssb interacts with Ssz1, potentially positioning Ssb on the ribosome near the ribosome tunnel exit. It was also shown that SBD α and SBD β of Ssb are involved in ribosome association (Gumiero et al., 2016; Hanebuth et al., 2016). Mutations in positively charged regions in these domains increased the soluble fraction of Ssb after sucrose centrifugation, indicating their importance for ribosome association.

In particular, it was suggested that C-terminal end of SBD α interacts with ES41 or ul29/el39 (also called Rpl35/Rpl39) depending on the ATP- or ADP-bound state of Ssb, respectively.

The interaction between Ssb and Ssz1 is also dependent on the nucleotide-bound states of Ssb. Thomas Ziegelhoffer recently found that adding ATP to the crosslinking reaction increased the crosslinking efficiency between Ssz1 Y351Bpa and Ssb by two-fold *in vitro*. But the addition of ADP decreased crosslinking efficiency, supporting the idea that the ATP-bound state of Ssb interacts with Ssz1. Thomas also recently identified crosslinking products between Ssz1 Y351Bpa and Ssb. Using mass spectrometry, he found Ssz1 Y351Bpa crosslinked to the C-terminal end of Ssb, which is consistent with the docking model between Ssz1 and the ATP-bound state of Ssb.

Based on the mass spectrometry results I reevaluated our docking model more precisely. I generated multiple model structures of *S. cerevisiae* Ssb based on the crystal structure of *C. thermophilum* Ssb. The overall model structures were similar to each other in that the ATPase domain was rigid. But, the C-terminal end structures of Ssb deviated, reflecting its flexibility. Previously, I selected the model with the highest score. But, the mass spectrometry results using Ssz1 Y351Bpa allow a more accurate selection of the model structure. The current model structure of Ssb1 better reflects all mass spectrometry results, indicating that both Bpa at S282 and Y351 of Ssz1 are located close to the cross-linked residues in the docking model.

Our results suggest that Ssb interacts with Ssz1 not only by ATPase domain dimerization but also through an interaction between the C-terminal SBD α of Ssb and the ATPase domain of Ssz1. Pull-down assays can be conducted to test whether the C-terminus of Ssb is required for stable interaction between Ssz1 and Ssb. These results might account for previously observed phenotypes of C-terminal deletion variants of Ssb. These variants might not form a stable dimer

with Ssz1, destabilizing its ribosome association. Alternatively, the C-terminal SBD α of Ssb may be flexible, as suggested by modeling, even though the interaction between ATPase domains is relatively rigid. This might allow the C-terminal SBD α of Ssb to toggle between the ATPase domain of Ssz1 and the previously suggested ribosomal contacts. Or the positively charged region at the C-terminus of Ssb in the ATP-bound state might directly contact ribosomal RNA ES41 when Zuo1 is absent, as was previously proposed (Gumiero et al., 2016). This hypothesis is consistent with the result that the C-terminal deletion variant of Ssb was mostly found in the soluble fraction in sucrose gradient experiments, which do not depend on the presence of Zuo1/Ssz1 complex (Hanebuth et al., 2016).

Addition of ADP led to a decrease in pull-down and crosslinking efficiency between Ssb1 and Ssz1. These results suggest that activating Ssb ATPase activity by the nascent chain triggers the dissociation of Ssb from Ssz1. To test this hypothesis, substrates of Ssb can be added to pull-down assays. The results may show that the ADP-bound state of Ssb dissociates from Ssz1 and remains bound with growing nascent chains during translation. It is also possible that nascent chain-bound Ssb stays on the ribosome through previously suggested direct contacts with ul29/el39 (Gumiero et al., 2016). These direct interactions may not only protect a segment of a nascent chain domain by Ssb, but also keep the segment near the tunnel exit until the domain synthesis is complete, promoting efficient folding.

Future work is needed to better understand the interaction dynamics of Ssb with the ribosome depending on its nucleotide-bound states and the presence of nascent chain. First, the proposed contacts between Ssb and the ribosome should be investigated more precisely with site-specific crosslinking experiments. This approach will exclude potential non-specific crosslinking products. In addition, the crosslinking experiments can be conducted with Ssb1 variants that

preferentially adopt either the ATP or ADP-bound state. This will help verify which components of the ribosome are responsible for the interaction with different nucleotide-bound states of Ssb.

In addition, sucrose centrifugation can be used to study mutations that disrupt particular interactions between Ssz1 and Ssb, and between Ssb and the ribosome, and the dependence of these interactions on the ATP- or ADP-bound state of Ssb1. Moreover, the effects of the nascent chain on these results can be examined using an *in vitro* translation system. These experiments may allow us to better understand the dynamics of Ssb/ribosome binding, providing insight into the functional mechanism of Ssb in the folding of nascent chains.

2.2.3. Mechanism of ATPase activation in Ssb1 by the Zuo1/Ssz1 complex

Zuo1 must form a complex with Ssz1 to activate the ATPase activity of Ssb. It is unknown why complex formation is required for Zuo1 to activate Ssb ATPase activity. Our findings suggest a mechanistic reason for forming the complex and ATPase activation. The correct orientation of Ssb1 with respect to the J-domain of Zuo1 is key, and is guided by the interaction with Ssz1. The interaction may correctly position the J-domain on the base of the ATPase domain of Ssb1 for activation. If this is the case, the complex between Zuo1 and Ssz1 variants which are defective for interaction with Ssb1 will not activate the ATPase activity of Ssb1 effectively. Or if activation solely relies on a conformational change of the J-domain of Zuo1 induced by complex formation, the Zuo1/Ssz1 variant complex should still activate the ATPase activity of Ssb1. There are some key prerequisites for these experiments. The Ssz1 variant needs to form a complex with Zuo1 so that it can lead to conformational changes in Zuo1 similar to wildtype Ssz1. The Ssb1 variant can also be used for these experiments, but the

mutations must not disrupt the interaction between Ssb1 and Zuo1 nor disrupt the ATPase activity of Ssb1.

ATPase assays can be utilized to test whether combinations of Ssz1 and Ssb1 variants complement the defects caused by individual variants. If the interaction between Ssz1 and Ssb1 is required for activation of the ATPase activity of Ssb1, complementary mutations in both proteins, as described in Chapter Three, could restore the function of Zuo1. This complementary ATPase assay could also ensure that ATPase activity defects caused by either variant are not due to structural impairment, but stem from the defects directly related to the Ssb/Ssz1 interaction.

2.2.4. Interaction between the cleft of Ssz1 and the nascent chain

The recent crystal structure revealed that Ssz1 contains a C-terminal cleft. Deleting the entire C-terminus of Ssz1 did not affect yeast cell growth, but it is still possible that interaction between the cleft of Ssz1 and nascent chain could be important under certain physiological conditions or for other cell types (for HspA14, among metazoans).

To test whether the cleft of Ssz1 interacts with nascent chain, the amount of Ssz1 in the cells can be reduced to check for the sensitivity of cell growth to cleft defects. If cleft mutations cause growth defects, it might suggest direct interaction between the cleft and nascent chain that help folding. To test this idea, *in vitro* translation systems can be used to investigate whether nascent chains directly interact with the cleft. Bpa can be incorporated into, or near the cleft, to test whether Bpa crosslinks to nascent chain. Nascent chain could also be trapped on ribosomes by introducing a nonsense stop codon in an open reading frame to increase the chance of obtaining crosslinking products.

Cleft mutants could also be used to test the importance of the cleft for folding nascent chains. If the interaction between the cleft and nascent chain is required for correct folding, the amount of functional translation products might be decreased upon alteration of the cleft of Ssz1. The sensitivity of the assays could be enhanced by the addition of misfolded proteins or denaturants that increase misfolding of nascent chains due to nonnative inter- or intra-molecular interaction.

2.2.5. Interaction between HspA14 and cytosolic Hsp70 in human cells

Metazoans do not contain ribosome-specific Hsp70s. Thus, recruiting cytosolic Hsp70s to the ribosomes might be critical for folding of nascent chains. To test whether HspA14 (the human ortholog of Ssz1), is involved in positioning cytosolic Hsp70 on the ribosome, the following experiments can be conducted. First, complex formation between HspA14 and DnaJC2 purified from *E. coli* can be tested to ensure that they have functional structures. Then, the HspA14/ DnaJC2 complex or HspA14 alone can be used in pull-down assays to examine whether it interacts with Hsp70 directly.

If the complex or HspA14 alone directly interacts with Hsp70, the amino acids of HspA14 and Hsp70 important for the interaction could be identified and altered to validate the interaction. Docking between the model structures of HspA14 and Hsp70 can be conducted because the crystal structures of both orthologs in *C. thermophilum* are available. Also, amino acid sequence conservation can be examined to identify key residues for the interaction. A variant that contains mutations in key residues can be constructed and used in pull-down assays. The results from these assays could verify that the residues are important for the interaction and that the mode of interaction is conserved between the human and yeast orthologs.

Sucrose centrifugation experiments can be conducted as previously described for yeast orthologs to test whether the interaction is important for association of Hsp70 with the ribosomes *in vivo*. For cells carrying either HspA14 or Hsp70 variant that are unable to interact with Hsp70 or HspA14, respectively, the amount of Hsp70 associated with the ribosomes may be decreased. These results would address the importance of the interaction between HspA14 and Hsp70 for the association of Hsp70 with the ribosome.

2.2.6. Function of Ssb1 in degradation of polylysine proteins

Deleting any component of the chaperone triad causes defects in the degradation of polylysine proteins, which are the translational products of nonstop mRNA. Polylysine segments might be trapped at the tunnel because of electrostatic interaction within the tunnel. It could be that Ssb1 binds to a polylysine protein to extract it from the ribosome tunnel to facilitate degradation. This mode of action might resemble the translocation of polypeptides across both ER and mitochondrial membranes, where Hsp70 binds polypeptides and aids their translocation.

To test this idea, an *in vitro* translation system could be used. In the absence of Ssb1, degradation of polylysine proteins might be reduced, with restoration of this process upon addition of Ssb1. The requirement of the interaction between Ssz1 and Ssb1 for this process could then be tested. For this, a variant of Ssz1 that is defective for interaction can be used to test whether the interaction between Ssz1 and Ssb1 is important for degradation of polylysine proteins. In addition, a Zuo1 variant that is defective for activation of the ATPase activity of Ssb1 could be used to examine whether Zuo1 is also required for degradation of polylysine proteins.

BIBLIOGRAPHY

Adams, P.D., Afonine, P.V., Bunkoczi, G., Chen, V.B., Davis, I.W., Echols, N., Headd, J.J., Hung, L.W., Kapral, G.J., Grosse-Kunstleve, R.W., *et al.* (2010). PHENIX: a comprehensive Python-based system for macromolecular structure solution. *Acta Crystallogr D Biol Crystallogr* **66**, 213-221.

Albanese, V., Reissmann, S., and Frydman, J. (2010). A ribosome-anchored chaperone network that facilitates eukaryotic ribosome biogenesis. *J Cell Biol* **189**, 69-81.

Blommel, P.G., Becker, K.J., Duvnjak, P., and Fox, B.G. (2007). Enhanced bacterial protein expression during auto-induction obtained by alteration of lac repressor dosage and medium composition. *Biotechnol Prog* **23**, 585-598.

Caliskan, N., Peske, F., and Rodnina, M.V. (2015). Changed in translation: mRNA recoding by -1 programmed ribosomal frameshifting. *Trends Biochem Sci* **40**, 265-274.

Carter, A.P., Clemons, W.M., Brodersen, D.E., Morgan-Warren, R.J., Wimberly, B.T., and Ramakrishnan, V. (2000). Functional insights from the structure of the 30S ribosomal subunit and its interactions with antibiotics. *Nature* **407**, 340-348.

Chen, V.B., Arendall, W.B., 3rd, Headd, J.J., Keedy, D.A., Immormino, R.M., Kapral, G.J., Murray, L.W., Richardson, J.S., and Richardson, D.C. (2010). MolProbity: all-atom structure validation for macromolecular crystallography. *Acta Crystallogr D Biol Crystallogr* **66**, 12-21.

Chiabudini, M., Conz, C., Reckmann, F., and Rospert, S. (2012). Ribosome-associated complex and Ssb are required for translational repression induced by polylysine segments within nascent chains. *Mol Cell Biol* **32**, 4769-4779.

Chiabudini, M., Tais, A., Zhang, Y., Hayashi, S., Wolfle, T., Fitzke, E., and Rospert, S. (2014). Release factor eRF3 mediates premature translation termination on polylysine-stalled ribosomes in *Saccharomyces cerevisiae*. *Mol Cell Biol* **34**, 4062-4076.

Clerico, E.M., Tilitsky, J.M., Meng, W., and Gierasch, L.M. (2015). How hsp70 molecular machines interact with their substrates to mediate diverse physiological functions. *Journal of molecular biology* **427**, 1575-1588.

Conz, C., Otto, H., Peisker, K., Gautschi, M., Wolfle, T., Mayer, M.P., and Rospert, S. (2007). Functional characterization of the atypical Hsp70 subunit of yeast ribosome-associated complex. *J Biol Chem* **282**, 33977-33984.

Craig, E.A., Eisenman, H.C., and Hundley, H.A. (2003). Ribosome-tethered molecular chaperones: the first line of defense against protein misfolding? *Curr Opin Microbiol* 6, 157-162.

Craig, E.A., and Marszalek, J. (2017). How Do J-Proteins Get Hsp70 to Do So Many Different Things? *Trends Biochem Sci* 42, 355-368.

Deuerling, E., Schulze-Specking, A., Tomoyasu, T., Mogk, A., and Bukau, B. (1999). Trigger factor and DnaK cooperate in folding of newly synthesized proteins. *Nature* 400, 693-696.

Doring, K., Ahmed, N., Riemer, T., Suresh, H.G., Vainshtein, Y., Habich, M., Riemer, J., Mayer, M.P., O'Brien, E.P., Kramer, G., *et al.* (2017). Profiling Ssb-Nascent Chain Interactions Reveals Principles of Hsp70-Assisted Folding. *Cell* 170, 298-311 e220.

Dragovic, Z., Broadley, S.A., Shomura, Y., Bracher, A., and Hartl, F.U. (2006). Molecular chaperones of the Hsp110 family act as nucleotide exchange factors of Hsp70s. *EMBO J* 25, 2519-2528.

Ducett, J.K., Peterson, F.C., Hoover, L.A., Prunuske, A.J., Volkman, B.F., and Craig, E.A. (2013). Unfolding of the C-terminal domain of the J-protein Zuo1 releases autoinhibition and activates Pdr1-dependent transcription. *J Mol Biol* 425, 19-31.

Eisenman, H.C., and Craig, E.A. (2004). Activation of pleiotropic drug resistance by the J-protein and Hsp70-related proteins, Zuo1 and Ssz1. *Mol Microbiol* 53, 335-344.

Elvekrog, M.M., and Walter, P. (2015). Dynamics of co-translational protein targeting. *Curr Opin Chem Biol* 29, 79-86.

Emsley, P., and Cowtan, K. (2004). Coot: model-building tools for molecular graphics. *Acta Crystallogr D Biol Crystallogr* 60, 2126-2132.

Ferbitz, L., Maier, T., Patzelt, H., Bukau, B., Deuerling, E., and Ban, N. (2004). Trigger factor in complex with the ribosome forms a molecular cradle for nascent proteins. *Nature* 431, 590-596.

Fiaux, J., Horst, J., Scior, A., Preissler, S., Koplin, A., Bukau, B., and Deuerling, E. (2010). Structural analysis of the ribosome-associated complex (RAC) reveals an unusual Hsp70/Hsp40 interaction. *The Journal of biological chemistry* 285, 3227-3234.

Fluitt, A., Pienaar, E., and Viljoen, H. (2007). Ribosome kinetics and aa-tRNA competition determine rate and fidelity of peptide synthesis. *Comput Biol Chem* 31, 335-346.

Frydman, J., Nimmesgern, E., Ohtsuka, K., and Hartl, F.U. (1994). Folding of nascent polypeptide chains in a high molecular mass assembly with molecular chaperones. *Nature* 370, 111-117.

Fulle, S., and Gohlke, H. (2009). Statics of the ribosomal exit tunnel: implications for cotranslational peptide folding, elongation regulation, and antibiotics binding. *Journal of molecular biology* 387, 502-517.

Gautschi, M., Lilie, H., Funfschilling, U., Mun, A., Ross, S., Lithgow, T., Rucknagel, P., and Rospert, S. (2001). RAC, a stable ribosome-associated complex in yeast formed by the DnaK-DnaJ homologs Ssz1p and zuotin. *Proc Natl Acad Sci U S A* 98, 3762-3767.

Gautschi, M., Mun, A., Ross, S., and Rospert, S. (2002). A functional chaperone triad on the yeast ribosome. *Proceedings of the National Academy of Sciences of the United States of America* 99, 4209-4214.

Gloge, F., Becker, A.H., Kramer, G., and Bukau, B. (2014). Co-translational mechanisms of protein maturation. *Current opinion in structural biology* 24, 24-33.

Gracheva, E., Chitale, S., Wilhelm, T., Rapp, A., Byrne, J., Stadler, J., Medina, R., Cardoso, M.C., and Richly, H. (2016). ZRF1 mediates remodeling of E3 ligases at DNA lesion sites during nucleotide excision repair. *The Journal of cell biology* 213, 185-200.

Greber, B.J., Boehringer, D., Montellese, C., and Ban, N. (2012). Cryo-EM structures of Arx1 and maturation factors Rei1 and Jjj1 bound to the 60S ribosomal subunit. *Nat Struct Mol Biol* 19, 1228-1233.

Gumiero, A., Conz, C., Gese, G.V., Zhang, Y., Weyer, F.A., Lapouge, K., Kappes, J., von Plehwe, U., Schermann, G., Fitzke, E., *et al.* (2016). Interaction of the cotranslational Hsp70 Ssb with ribosomal proteins and rRNA depends on its lid domain. *Nat Commun* 7, 13563.

Halladay, J.T., and Craig, E.A. (1995). A heat shock transcription factor with reduced activity suppresses a yeast HSP70 mutant. *Molecular and cellular biology* 15, 4890-4897.

Hanebuth, M.A., Kityk, R., Fries, S.J., Jain, A., Kriel, A., Albanese, V., Frickey, T., Peter, C., Mayer, M.P., Frydman, J., *et al.* (2016). Multivalent contacts of the Hsp70 Ssb contribute to its architecture on ribosomes and nascent chain interaction. *Nat Commun* 7, 13695.

Hartl, F.U., Bracher, A., and Hayer-Hartl, M. (2011). Molecular chaperones in protein folding and proteostasis. *Nature* 475, 324-332.

Hartl, F.U., and Hayer-Hartl, M. (2009). Converging concepts of protein folding in vitro and in vivo. *Nat Struct Mol Biol* 16, 574-581.

Hesterkamp, T., Hauser, S., Lutcke, H., and Bukau, B. (1996). Escherichia coli trigger factor is a prolyl isomerase that associates with nascent polypeptide chains. *Proc Natl Acad Sci U S A* 93, 4437-4441.

Hilal, T., and Spahn, C.M. (2015). Ribosome rescue and protein quality control in concert. *Molecular cell* 57, 389-390.

Hoffmann, A., Bukau, B., and Kramer, G. (2010). Structure and function of the molecular chaperone Trigger Factor. *Biochim Biophys Acta* 1803, 650-661.

Huang, P., Gautschi, M., Walter, W., Rospert, S., and Craig, E.A. (2005). The Hsp70 Ssz1 modulates the function of the ribosome-associated J-protein Zuo1. *Nat Struct Mol Biol* 12, 497-504.

Hundley, H., Eisenman, H., Walter, W., Evans, T., Hotokezaka, Y., Wiedmann, M., and Craig, E. (2002). The in vivo function of the ribosome-associated Hsp70, Ssz1, does not require its putative peptide-binding domain. *Proc Natl Acad Sci U S A* 99, 4203-4208.

Hundley, H.A., Walter, W., Bairstow, S., and Craig, E.A. (2005). Human Mpp11 J protein: ribosome-tethered molecular chaperones are ubiquitous. *Science* 308, 1032-1034.

Jaiswal, H., Conz, C., Otto, H., Wolfle, T., Fitzke, E., Mayer, M.P., and Rospert, S. (2011). The chaperone network connected to human ribosome-associated complex. *Mol Cell Biol* 31, 1160-1173.

James, P., Pfund, C., and Craig, E.A. (1997). Functional specificity among Hsp70 molecular chaperones. *Science* 275, 387-389.

- Jones, D.T., Taylor, W.R., and Thornton, J.M. (1992). The rapid generation of mutation data matrices from protein sequences. *Comput Appl Biosci* 8, 275-282.
- Kabsch, W. (2010). Xds. *Acta Crystallogr D Biol Crystallogr* 66, 125-132.
- Kampinga, H.H., and Craig, E.A. (2010). The HSP70 chaperone machinery: J proteins as drivers of functional specificity. *Nat Rev Mol Cell Biol* 11, 579-592.
- Kaschner, L.A., Sharma, R., Shrestha, O.K., Meyer, A.E., and Craig, E.A. (2015). A conserved domain important for association of eukaryotic J-protein co-chaperones Jjj1 and Zuo1 with the ribosome. *Biochimica et biophysica acta* 1853, 1035-1045.
- Kim, Y.E., Hipp, M.S., Bracher, A., Hayer-Hartl, M., and Hartl, F.U. (2013). Molecular chaperone functions in protein folding and proteostasis. *Annu Rev Biochem* 82, 323-355.
- Kityk, R., Kopp, J., and Mayer, M.P. (2018). Molecular Mechanism of J-Domain-Triggered ATP Hydrolysis by Hsp70 Chaperones. *Mol Cell* 69, 227-237 e224.
- Kityk, R., Vogel, M., Schlecht, R., Bukau, B., and Mayer, M.P. (2015). Pathways of allosteric regulation in Hsp70 chaperones. *Nat Commun* 6, 8308.
- Knowles, T.P., Vendruscolo, M., and Dobson, C.M. (2014). The amyloid state and its association with protein misfolding diseases. *Nat Rev Mol Cell Biol* 15, 384-396.
- Korennykh, A., and Walter, P. (2012). Structural basis of the unfolded protein response. *Annu Rev Cell Dev Biol* 28, 251-277.
- Kramer, E.B., Vallabhaneni, H., Mayer, L.M., and Farabaugh, P.J. (2010). A comprehensive analysis of translational missense errors in the yeast *Saccharomyces cerevisiae*. *Rna* 16, 1797-1808.
- Kramer, G., Boehringer, D., Ban, N., and Bukau, B. (2009). The ribosome as a platform for co-translational processing, folding and targeting of newly synthesized proteins. *Nat Struct Mol Biol* 16, 589-597.
- Krishnamurthy, M., Dugan, A., Nwokoye, A., Fung, Y.H., Lancia, J.K., Majmudar, C.Y., and Mapp, A.K. (2011). Caught in the act: covalent cross-linking captures activator-coactivator interactions in vivo. *ACS chemical biology* 6, 1321-1326.

- Kumar, S., Stecher, G. & Tamura, K. (2016). MEGA7: Molecular Evolutionary Genetics Analysis version 7.0 for bigger datasets. *Mol Biol Evol.*
- Lee, K., Sharma, R., Shrestha, O.K., Bingman, C.A., and Craig, E.A. (2016). Dual interaction of the Hsp70 J-protein cochaperone Zuo1 with the 40S and 60S ribosomal subunits. *Nat Struct Mol Biol* 23, 1003-1010.
- Leidig, C., Bange, G., Kopp, J., Amlacher, S., Aravind, A., Wickles, S., Witte, G., Hurt, E., Beckmann, R., and Sinning, I. (2013). Structural characterization of a eukaryotic chaperone--the ribosome-associated complex. *Nat Struct Mol Biol* 20, 23-28.
- Li, J., Qian, X., and Sha, B. (2003). The crystal structure of the yeast Hsp40 Ydj1 complexed with its peptide substrate. *Structure* 11, 1475-1483.
- Lin, P.J., Jongsma, C.G., Pool, M.R., and Johnson, A.E. (2011). Polytopic membrane protein folding at L17 in the ribosome tunnel initiates cyclical changes at the translocon. *The Journal of cell biology* 195, 55-70.
- Liu, Q., and Hendrickson, W.A. (2007). Insights into Hsp70 chaperone activity from a crystal structure of the yeast Hsp110 Sse1. *Cell* 131, 106-120.
- Meyer, A.E., Hung, N.J., Yang, P., Johnson, A.W., and Craig, E.A. (2007). The specialized cytosolic J-protein, Jjj1, functions in 60S ribosomal subunit biogenesis. *Proc Natl Acad Sci U S A* 104, 1558-1563.
- Michimoto, T., Aoki, T., Toh-e, A., and Kikuchi, Y. (2000). Yeast Pdr13p and Zuo1p molecular chaperones are new functional Hsp70 and Hsp40 partners. *Gene* 257, 131-137.
- Mountain, H.A., Byström, A.S., Larsen, J.T., Korch, C. (1991). Four major transcriptional responses in the methionine/threonine biosynthetic pathway of *Saccharomyces cerevisiae*. *Yeast* 7, 781-803.
- Muldoon-Jacobs, K.L., and Dinman, J.D. (2006). Specific effects of ribosome-tethered molecular chaperones on programmed -1 ribosomal frameshifting. *Eukaryot Cell* 5, 762-770.
- Mumberg, D., Muller, R., and Funk, M. (1995). Yeast vectors for the controlled expression of heterologous proteins in different genetic backgrounds. *Gene* 156, 119-122.

Nakatogawa, H., and Ito, K. (2002). The ribosomal exit tunnel functions as a discriminating gate. *Cell* 108, 629-636.

Namy, O., Hatin, I., and Rousset, J.P. (2001). Impact of the six nucleotides downstream of the stop codon on translation termination. *EMBO reports* 2, 787-793.

Nelson, R.J., Ziegelhoffer, T., Nicolet, C., Werner-Washburne, M., and Craig, E.A. (1992). The translation machinery and 70 kd heat shock protein cooperate in protein synthesis. *Cell* 71, 97-105.

Nemoto, N., Singh, C.R., Udagawa, T., Wang, S., Thorson, E., Winter, Z., Ohira, T., Ii, M., Valasek, L., Brown, S.J., *et al.* (2010). Yeast 18 S rRNA is directly involved in the ribosomal response to stringent AUG selection during translation initiation. *The Journal of biological chemistry* 285, 32200-32212.

Oh, H.J., Chen, X., and Subject, J.R. (1997). Hsp110 protects heat-denatured proteins and confers cellular thermoresistance. *J Biol Chem* 272, 31636-31640.

Oh, H.J., Easton, D., Murawski, M., Kaneko, Y., and Subject, J.R. (1999). The chaperoning activity of hsp110. Identification of functional domains by use of targeted deletions. *J Biol Chem* 274, 15712-15718.

Otto, H., Conz, C., Maier, P., Wolfle, T., Suzuki, C.K., Jenö, P., Rucknagel, P., Stahl, J., and Rospert, S. (2005). The chaperones MPP11 and Hsp70L1 form the mammalian ribosome-associated complex. *Proc Natl Acad Sci U S A* 102, 10064-10069.

Patzelt, H., Rudiger, S., Brehmer, D., Kramer, G., Vorderwulbecke, S., Schaffitzel, E., Waitz, A., Hesterkamp, T., Dong, L., Schneider-Mergener, J., *et al.* (2001). Binding specificity of *Escherichia coli* trigger factor. *Proc Natl Acad Sci U S A* 98, 14244-14249.

Pechmann, S., Willmund, F., and Frydman, J. (2013). The ribosome as a hub for protein quality control. *Molecular cell* 49, 411-421.

Peisker, K., Braun, D., Wolfle, T., Hentschel, J., Funfschilling, U., Fischer, G., Sickmann, A., and Rospert, S. (2008). Ribosome-associated complex binds to ribosomes in close proximity of Rpl31 at the exit of the polypeptide tunnel in yeast. *Mol Biol Cell* 19, 5279-5288.

Peisker, K., Chiabudini, M., and Rospert, S. (2010). The ribosome-bound Hsp70 homolog Ssb of *Saccharomyces cerevisiae*. *Biochim Biophys Acta* 1803, 662-672.

Pettersen, E.F., Goddard, T.D., Huang, C.C., Couch, G.S., Greenblatt, D.M., Meng, E.C., and Ferrin, T.E. (2004). UCSF Chimera--a visualization system for exploratory research and analysis. *J Comput Chem* 25, 1605-1612.

Pfund, C., Huang, P., Lopez-Hoyo, N., and Craig, E.A. (2001). Divergent functional properties of the ribosome-associated molecular chaperone Ssb compared with other Hsp70s. *Mol Biol Cell* 12, 3773-3782.

Pfund, C., Lopez-Hoyo, N., Ziegelhoffer, T., Schilke, B.A., Lopez-Buesa, P., Walter, W.A., Wiedmann, M., and Craig, E.A. (1998). The molecular chaperone Ssb from *Saccharomyces cerevisiae* is a component of the ribosome-nascent chain complex. *EMBO J* 17, 3981-3989.

Pierce, B.G., Wiehe, K., Hwang, H., Kim, B.H., Vreven, T., and Weng, Z. (2014). ZDOCK server: interactive docking prediction of protein-protein complexes and symmetric multimers. *Bioinformatics* 30, 1771-1773.

Polier, S., Dragovic, Z., Hartl, F.U., and Bracher, A. (2008). Structural basis for the cooperation of Hsp70 and Hsp110 chaperones in protein folding. *Cell* 133, 1068-1079.

Pool, M.R. (2009). A trans-membrane segment inside the ribosome exit tunnel triggers RAMP4 recruitment to the Sec61p translocase. *The Journal of cell biology* 185, 889-902.

Preissler, S., and Deuerling, E. (2012). Ribosome-associated chaperones as key players in proteostasis. *Trends in biochemical sciences* 37, 274-283.

Prunuske, A.J., Waltner, J.K., Kuhn, P., Gu, B., and Craig, E.A. (2012). Role for the molecular chaperones Zuo1 and Ssz1 in quorum sensing via activation of the transcription factor Pdr1. *Proceedings of the National Academy of Sciences of the United States of America* 109, 472-477.

Rakwalska, M., and Rospert, S. (2004). The ribosome-bound chaperones RAC and Ssb1/2p are required for accurate translation in *Saccharomyces cerevisiae*. *Mol Cell Biol* 24, 9186-9197.

Ramakrishnan, V. (2002). Ribosome structure and the mechanism of translation. *Cell* 108, 557-572.

Raviol, H., Sadlish, H., Rodriguez, F., Mayer, M.P., and Bukau, B. (2006). Chaperone network in the yeast cytosol: Hsp110 is revealed as an Hsp70 nucleotide exchange factor. *EMBO J* 25, 2510-2518.

Richly, H., Rocha-Viegas, L., Ribeiro, J.D., Demajo, S., Gundem, G., Lopez-Bigas, N., Nakagawa, T., Rospert, S., Ito, T., and Di Croce, L. (2010). Transcriptional activation of polycomb-repressed genes by ZRF1. *Nature* 468, 1124-1128.

Roy, A., Kucukural, A., and Zhang, Y. (2010). I-TASSER: a unified platform for automated protein structure and function prediction. *Nat Protoc* 5, 725-738.

Ryu, Y., and Schultz, P.G. (2006). Efficient incorporation of unnatural amino acids into proteins in *Escherichia coli*. *Nat Methods* 3, 263-265.

Sahi, C., Kominek, J., Ziegelhoffer, T., Yu, H.Y., Baranowski, M., Marszalek, J., and Craig, E.A. (2013). Sequential duplications of an ancient member of the DnaJ-family expanded the functional chaperone network in the eukaryotic cytosol. *Mol Biol Evol* 30, 985-998.

Salas-Marco, J., and Bedwell, D.M. (2005). Discrimination between defects in elongation fidelity and termination efficiency provides mechanistic insights into translational readthrough. *Journal of molecular biology* 348, 801-815.

Sali, A., and Blundell, T.L. (1993). Comparative protein modelling by satisfaction of spatial restraints. *J Mol Biol* 234, 779-815.

Schilke, B.A., Ciesielski, S.J., Ziegelhoffer, T., Kamiya, E., Tonelli, M., Lee, W., Cornilescu, G., Hines, J.K., Markley, J.L., and Craig, E.A. (2017). Broadening the functionality of a J-protein/Hsp70 molecular chaperone system. *PLoS Genet* 13, e1007084.

Schuermann, J.P., Jiang, J., Cuellar, J., Llorca, O., Wang, L., Gimenez, L.E., Jin, S., Taylor, A.B., Demeler, B., Morano, K.A., *et al.* (2008). Structure of the Hsp110:Hsc70 nucleotide exchange machine. *Mol Cell* 31, 232-243.

Sha, B., Lee, S., and Cyr, D.M. (2000). The crystal structure of the peptide-binding fragment from the yeast Hsp40 protein Sis1. *Structure* 8, 799-807.

Shaner, L., Trott, A., Goeckeler, J.L., Brodsky, J.L., and Morano, K.A. (2004). The function of the yeast molecular chaperone Sse1 is mechanistically distinct from the closely related hsp70 family. *J Biol Chem* 279, 21992-22001.

Shaner, L., Wegele, H., Buchner, J., and Morano, K.A. (2005). The yeast Hsp110 Sse1 functionally interacts with the Hsp70 chaperones Ssa and Ssb. *J Biol Chem* 280, 41262-41269.

Shen, P.S., Park, J., Qin, Y., Li, X., Parsawar, K., Larson, M.H., Cox, J., Cheng, Y., Lambowitz, A.M., Weissman, J.S., *et al.* (2015). Protein synthesis. Rqc2p and 60S ribosomal subunits mediate mRNA-independent elongation of nascent chains. *Science* 347, 75-78.

Sherman, M.Y., and Qian, S.B. (2013). Less is more: improving proteostasis by translation slow down. *Trends in biochemical sciences* 38, 585-591.

Sievers, F., Wilm, A., Dineen, D., Gibson, T.J., Karplus, K., Li, W., Lopez, R., McWilliam, H., Remmert, M., Soding, J., *et al.* (2011). Fast, scalable generation of high-quality protein multiple sequence alignments using Clustal Omega. *Mol Syst Biol* 7, 539.

Sikorski, R.S., and Hieter, P. (1989). A system of shuttle vectors and yeast host strains designed for efficient manipulation of DNA in *Saccharomyces cerevisiae*. *Genetics* 122, 19-27.

Steitz, T.A. (2008). A structural understanding of the dynamic ribosome machine. *Nat Rev Mol Cell Biol* 9, 242-253.

Stone, D.E., and Craig, E.A. (1990). Self-regulation of 70-kilodalton heat shock proteins in *Saccharomyces cerevisiae*. *Molecular and cellular biology* 10, 1622-1632.

Svidritskiy, E., Brilot, A.F., Koh, C.S., Grigorieff, N., and Korostelev, A.A. (2014). Structures of yeast 80S ribosome-tRNA complexes in the rotated and nonrotated conformations. *Structure* 22, 1210-1218.

Szyperski, T., Pellicchia, M., Wall, D., Georgopoulos, C., and Wuthrich, K. (1994). NMR structure determination of the *Escherichia coli* DnaJ molecular chaperone: secondary structure and backbone fold of the N-terminal region (residues 2-108) containing the highly conserved J domain. *Proc Natl Acad Sci U S A* 91, 11343-11347.

Ting, S.Y., Schilke, B.A., Hayashi, M., and Craig, E.A. (2014). Architecture of the TIM23 inner mitochondrial translocon and interactions with the matrix import motor. *J Biol Chem* 289, 28689-28696.

Tsai, J., and Douglas, M.G. (1996). A conserved HPD sequence of the J-domain is necessary for YDJ1 stimulation of Hsp70 ATPase activity at a site distinct from substrate binding. *J Biol Chem* 271, 9347-9354.

Vilardell, J., and Warner, J.R. (1997). Ribosomal protein L32 of *Saccharomyces cerevisiae* influences both the splicing of its own transcript and the processing of rRNA. *Molecular and cellular biology* 17, 1959-1965.

Voorhees, R.M., and Ramakrishnan, V. (2013). Structural basis of the translational elongation cycle. *Annu Rev Biochem* 82, 203-236.

Voss, N.R., Gerstein, M., Steitz, T.A., and Moore, P.B. (2006). The geometry of the ribosomal polypeptide exit tunnel. *J Mol Biol* 360, 893-906.

Wai, H.H., Vu, L., Oakes, M., and Nomura, M. (2000). Complete deletion of yeast chromosomal rDNA repeats and integration of a new rDNA repeat: use of rDNA deletion strains for functional analysis of rDNA promoter elements in vivo. *Nucleic acids research* 28, 3524-3534.

Wang, X., and Chen, X.J. (2015). A cytosolic network suppressing mitochondria-mediated proteostatic stress and cell death. *Nature* 524, 481-484.

Webb, B., and Sali, A. (2014). Comparative Protein Structure Modeling Using MODELLER. *Curr Protoc Bioinformatics* 47, 5 6 1-32.

Weyer, F.A., Gumiero, A., Gese, G.V., Lapouge, K., and Sinning, I. (2017). Structural insights into a unique Hsp70-Hsp40 interaction in the eukaryotic ribosome-associated complex. *Nat Struct Mol Biol* 24, 144-151.

Wild, K., Halic, M., Sinning, I., and Beckmann, R. (2004). SRP meets the ribosome. *Nature structural & molecular biology* 11, 1049-1053.

Willmund, F., del Alamo, M., Pechmann, S., Chen, T., Albanese, V., Dammer, E.B., Peng, J., and Frydman, J. (2013). The cotranslational function of ribosome-associated Hsp70 in eukaryotic protein homeostasis. *Cell* 152, 196-209.

Wilson, D.N., and Beckmann, R. (2011). The ribosomal tunnel as a functional environment for nascent polypeptide folding and translational stalling. *Current opinion in structural biology* 21, 274-282.

Winkelman, J.T., Winkelman, B.T., Boyce, J., Maloney, M.F., Chen, A.Y., Ross, W., and Gourse, R.L. (2015). Crosslink Mapping at Amino Acid-Base Resolution Reveals the Path of Scrunched DNA in Initial Transcribing Complexes. *Mol Cell* 59, 768-780.

Wrobel, L., Topf, U., Bragoszewski, P., Wiese, S., Sztolsztener, M.E., Oeljeklaus, S., Varabyova, A., Lirski, M., Chroscicki, P., Mroczek, S., *et al.* (2015). Mistargeted mitochondrial proteins activate a proteostatic response in the cytosol. *Nature* 524, 485-488.

Yan, W., Schilke, B., Pfund, C., Walter, W., Kim, S., and Craig, E.A. (1998). Zuotin, a ribosome-associated DnaJ molecular chaperone. *EMBO J* 17, 4809-4817.

Youngman, E.M., Cochella, L., Brunelle, J.L., He, S., and Green, R. (2006). Two distinct conformations of the conserved RNA-rich decoding center of the small ribosomal subunit are recognized by tRNAs and release factors. *Cold Spring Harb Symp Quant Biol* 71, 545-549.

Yu, C.H., Dang, Y., Zhou, Z., Wu, C., Zhao, F., Sachs, M.S., and Liu, Y. (2015). Codon Usage Influences the Local Rate of Translation Elongation to Regulate Co-translational Protein Folding. *Mol Cell* 59, 744-754.

Zaher, H.S., and Green, R. (2009). Fidelity at the molecular level: lessons from protein synthesis. *Cell* 136, 746-762.

Zhang, Y., Ma, C., Yuan, Y., Zhu, J., Li, N., Chen, C., Wu, S., Yu, L., Lei, J., and Gao, N. (2014). Structural basis for interaction of a cotranslational chaperone with the eukaryotic ribosome. *Nat Struct Mol Biol* 21, 1042-1046.

Zhang, Y., Wolfle, T., and Rospert, S. (2013). Interaction of nascent chains with the ribosomal tunnel proteins Rpl4, Rpl17, and Rpl39 of *Saccharomyces cerevisiae*. *J Biol Chem* 288, 33697-33707.